Morphological control of multifunctionalized mesoporous silica nanomaterials for catalysis applications

by

Seong Huh

A dissertation submitted to the graduate faculty

in partial fulfillment of the requirements for the degree of

DOCTOR OF PHILOSOPHY

Major: Inorganic Chemistry

Program of Study Committee:
Victor S. –Y. Lin, Major Professor
James H. Espenson
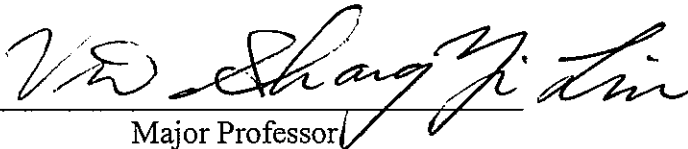Nenad M. Kostic
Nicola L. Pohl
Brent H. Shanks

Iowa State University

Ames, Iowa

2004

Graduate College
Iowa State University

This is to certify that the doctoral dissertation of

Seong Huh

has met the dissertation requirements of Iowa State University

_____
Major Professor

_____
For the Major Program

To my parents, and brothers Hyun and Hoon

TABLE OF CONTENTS

ABSTRACT

I found an efficient method to control the morphology of the organically
monofunctionalized mesoporous silica materials by introducing different types of
organoalkoxysilanes in a base-catalyzed co-condensation reaction. The monofunctionalized
materials exhibit different particle morphologies relative to the pure MCM-41 material. The
concentration dependence of the morphology is a critical factor to determine the final particle
shape. A proposed mechanism of the shape evolution is also offered. After understanding the
role of organoalkoxysilanes in producing various well-shaped nanomaterials, I also obtained
a series of bifunctional mesoporous silica materials with certain particle morphology. A
series of bifunctional mesoporous silica nanospheres (MSNs) whose physicochemical
properties was investigated *via* solid state NMR techniques and Cu^{2+} adsorption capacity
tests. The ratio of two different organic groups inside of mesopores of these MSNs could be
fine-tuned. These MSNs serve as a useful model system to study substrate selectivity in
catalytic reactions and sorption phenomena. For example, the Cu^{2+} adsorption capacity of
these materials was dictated by the chemical nature of the mesopores generated by the
different organic functional groups.

An investigation of the substrate selectivity of the bifunctionalized MSNs in a
competitive nitroaldol reaction using an equimolar amount of two competing 4-
nitrobenzaldehyde derivatives was performed. Shape-controlled bifunctional MSNs were
employed as the catalysts. The properties of the MSNs were investigated using various
spectroscopic methods and electron microscopy. The more hydrophobic the surface organic
groups are, the higher the ratio of hydrophobic final product. This is the first example to

demonstrate the selection of substrate using physicochemical nature of the mesopore surface other than the conventional shape selection in zeolite systems.

I also created a cooperative dual catalyst system that is capable of activating two different substrates in aldol reaction, Henry reaction and cyanosilylation. One catalytic group activates the nucleophile, another organic group simultaneously activates the electrophile to enhance the total reaction rate. I systematically varied the amount of two organic groups and performed the three model reactions to compare rate enhancements.

CHAPTER 1. GENERAL INTRODUCTION

Introduction

Since the first discovery of the mesoporous silica materials a decade ago, such as

MCM-41/48[1,2] and SBA-15,[3,4] numerous methods for the synthesis of mesostructured

siliceous and nonsiliceous materials have been reported.[5,6] These mesostructured materials

usually exhibit well-ordered hexagonal, cubic or lamellar phases according to their synthetic

conditions. In addition, highly disordered channel structures have been observed when

neutral amine templates were applied to give MSU type of materials.[7] The major synthetic

parameters include temperature, pH, aging time, stirring rate, types of templates and the

concentration of surfactant. Particle morphology of the mesostructured materials is also a

critical factor for various reasons.[8]

Dissertation Organization

This thesis is consisted of four main chapters with three published papers,[9-11] one

submitted paper, and two chapters including a general introduction and a general conclusion

chapter. Chapter 1 includes an overview about the synthesis and functionalization of

mesoporous materials. Chapter 2 describes the morphology control of the organically

monofunctionalized mesoporous silica materials by introducing different types of

organoalkoxysilanes in a base-catalyzed co-condensation reaction.[9] The monofunctionalized

materials exhibit different particle morphologies relative to the pure MCM-41 material. I also

observed concentration dependence of the morphology which is a critical factor to determine

the final particle shape. A proposed mechanism of the shape evolution is also offered in this chapter. After understanding the role of organoalkoxysilanes in producing various well-shaped nanomaterials, I also obtained a series of bifunctional mesoporous silica materials with certain particle morphology. Chapter 3 deals with a series of bifunctional mesoporous silica nanospheres (MSNs) whose physicochemical properties were investigated via solid state NMR techniques and Cu(II) adsorption capacity tests.[10] The ratio of two different organic groups inside of mesopores of these MSNs could be fine-tuned. These MSNs serve as a useful model system to study substrate selectivity in catalytic reactions and sorption phenomena. For example, the Cu(II) adsorption capacity of these materials was dictated by the chemical nature of the mesopores generated by the different organic functional groups.

Chapter 4 entails an investigation of the substrate selectivity of the bifunctionalized MSNs in a competitive nitroaldol reaction using an equimolar amount of two competing 4-nitrobenzaldehyde derivatives.[11] Shape-controlled bifunctional MSNs were employed as the catalysts. The properties of the MSNs were investigated using various spectroscopic methods and electron microscopy. The more hydrophobic the surface organic groups are, the higher the ratio of hydrophobic final product. This is the first example to demonstrate the selection of substrate using physicochemical nature of the mesopore surface other than conventional shape selection in zeolite systems.

In Chapter 5, I try to expand the basic concept developed in Chapter 4 to create a cooperative dual catalyst system that is capable of activating two different substrates in aldol reaction, Henry reaction and cyanosilylation. One catalytic group activates the nucleophile, the other organic groups simultaneously activate the electrophile to enhance the total reaction

rate. I systematically varied the amount of two organic groups systematically and performed the three model reactions to compare rate enhancements.

Literature Review

Mesoporous silica materials prepared by numerous templating approaches open a new era to exceed the pore size limit of zeolites. The hexagonal MCM-41 and cubic MCM-48 were synthesized using a traditional soft sol-gel chemistry using a quarternary ammonium surfactant as an ionic template, such as CTAB.[1,2] Charge-matching has been recognized as the most critical factor in governing the final phases and stability. Stucky introduced nonionic surfactants in acidic condition to produce thick-wall large pore size hexagonal mesoporous silica SBA-15.[3,4] The SBA-15 usually has mesopores and micropores together evidenced by BET isotherm and TEM study. In general, almost every organic molecule can be used as a soft template to lead hard inorganic porous materials in solution state. One is able to freely alter the pore organization (hexagonal, cubic or lamellar) and a pore size as well. Disordered mesostructured siliceous or nonsiliceous materials were also synthesized by Pinnavaia *et al.* through a neutral amine templating.[7]

These materials provide new research opportunities in catalysis,[11-13] delivery of biologically important molecules,[14,15] immobilizations of enzymes,[16,17] and remediation of toxic compounds.[18-20] Recent progress in preparation of mesoporous carbon materials takes advantage of the predefined silica structure as a template for replication by carbonaceous sources.[21-23] Mesoporous carbons are also important for their potential applications to sorption, fuel cells, and drug delivery.

Another novel class of mesoporous organic/inorganic hybrid materials is a periodic mesoporous organosilica (PMO) developed by three different independent research groups at the same time.[24-26] The PMOs have quite different physicochemical properties from typical mesoporous silicas because the surface wall is consisted of both organic and inorganic moieties. Different types of organoalkoxysilanes have been employed to form well structured PMOs.[27-29] The PMOs having an atomic scale periodicity have been also reported by Inagaki *et al.*[30-32] Recently 3D macroporous PMO materials bearing hybrid groups have been achieved using a polystyrene crystalline phase as a macroporous template.[33] Amine-functionalized PMOs have been prepared through a co-condensation method.[34]

Mesostructured films were successfully obtained via an evaporation-induced self assembly (EISA) process developed by Brinker *et al.*[35] In addition to the preparation of high quality mesoporous silica films, they demonstrated patterned mesoporous silica films using photolytically polymerizable diacetylenic surfactants.[36] Mesostructured silica thin films prepared in supercritical fluids are also important low dielectric materials with a strong mechanical strength.[37] A hierarchically arranged mesostructured silica film has been also realized by using a standard PDMS patterning method.[5] They applied a mesoporous silica precursor solution as an ink for the PDMS stamping.

The functionalization of the pore surface of the mesoporous materials has been intensively investigated.[38] There are two major ways to decorate the surface wall, a post-grafting and a co-condensation.[39] Although the post-grafting method is straightforward to introduce any organic functionalities using organoalkoxysilane or organosilyl chloride precursors in a refluxing toluene solution, the distribution of functional groups tends to be

inhomogeneous. Compared with the post-grafting method, the co-condensation is able to give homogeneously distributed organic groups on the entire inner pore surfaces and no pore-blockage or shrinkage problems have been reported. Even though bulky organoalkoxysilane precursors often perturb the original textural properties of the systems, we and others have been developing methods to decorate the surface wall efficiently while maintaining the mesoprous structure.[9, 10]

Recently, small shape-controlled mesoporous material particles have attracted much attention owing to their superior properties in a variety of applications.[10, 11, 14] Controlling of particle morphology as well as mesostructure is an emerging research area which is closely related to the biomineralization process in nature. If the mesostructure is a primary structure, the particle morphology is a hierarchical secondary structure. The complex forms of diatoms are good examples.[40] There are many sophisticated methods to prepare shape-controlled pure mesoporous siliceous materials. Ozin has demonstrated that the particle morphology of the surfactant micelle-templated mesoporous silica materials could be manipulated via an acid synthesis ($S^+X^-T^+$) route.[41] This synthetic method is based on different hierarchical orderings of individual micellar rods as mentioned by Ozin.[42] Several other synthetic strategies have also been reported in the literature for the morphological control of various mesoporous silica materials, including hollow tubular silica materials whose wall consists of MCM-41 type of mesoporous structure,[43] fluorine anion induced hierarchical ordering of SBA type of materials,[44] rod-shaped mesoporous materials obtained from rapid pH change of sodium metasilicate and cationic surfactant mixture,[45] bacterial thread-templated mesoporous silica rod,[46] mesoporous fibers from the rubbing treated polyimide film,[47] ultrastable mesoporous

silica vesicles prepared via a neutral gemini surfactant template method,[48] hydrothermal transformation of MCM-41 silica spheres into rod-shaped particles,[49] and hollow mesoporous fibers and spheres prepared by a spray drying.[50] Twisted mesoporous silica particles were prepared with the use of enantiopure templates having an amino acid head group.[51] Despite much inspiring progress in fine tuning the particle morphology of pure inorganic mesoporous silica materials, the quest for synthetic pathways that could combine the particle morphology control with surface functionalization to create uniformly shaped and sized mesoporous materials with various organic functionalities has just begun.[9-11]

During my research, two independent groups reported shape-controlled organically functionalized nanomaterials through a co-condensation method. Walcarius used a traditional Stöber method to synthesize mercaptopropyl- and aminopropyl-functionalized mesoporous silica spheres.[52] Detailed textural properties were also investigated. In fact, this method is an extension of the Unger's work[53, 54] to prepare micron-sized spherical mesoporous silicas based on the Stöber method.[55] Their internal channel structures were further investigated in detail by a transmission electron microscopy (TEM).[56] Mann *et al.* invented a method to produce organically functionalized spherical and rod-shaped particles.[57] They used a dilution/neutralization process to control the size of the final particles.[58] However, there are still remaining questions to be answered about the role of organic group (the starting form of organoalkoxysilane) during shape evolution and the effect of two or more different organic groups during the condensation.[10, 11]

Zhao *et al.* reported a very interesting observation during the preparation of bulk mercaptopropyl-functionalized materials.[59] In the presence of a certain amount of

mercaptopropyltrimethoxysilane (MPTMS), the original hexagonal phase of the material was partly transformed into a cubic phase. This phenomenon is relevant to my observation during my synthetic conditions.

The preparation method for micron-sized pure siliceous mesoporous materials via a low concentration of CTAB has been reported by Cai et al.[60] Because of the broad range of critical micelle concentration (CMC) of CTAB, they chose the lower limit of the CMC value and successfully obtained small hexagonally arranged mesoporous silicas. This approach is a similar way of preparing small mesoporous particles like the dilution/neutralization method proposed by Mann et al.[57] It is clear that low concentration of ammonium surfactants easily induces small size of micelle aggregates.

Because of their high surface area and large pore size, mesostructured materials frequently employed as catalyst support for immobilization of precious metal catalysts.[61] Highly crystalline polyethylene nanofibers were prepared by using covalently anchored Ti(IV) complexes on the inner surface of the fibrous mesoporous silica.[62] They proposed the polymerization/extrusion mechanism from the hexagonally aligned mesopores which is similar to the biosynthesis of crystalline cellulose. Conducting graphite-type carbon polymer encapsulated mesoporous silica nanocomposites were made through a pyrolysis of polymerized acrylonitrile inside of the mesopores by Bein et al.[63, 64] The periodic arrangement of mesopores manifested the role of a nanocontainer for an efficient nanocomposite formation. Jones et al. developed an ingenious way to graft the organic functional groups on the mesoporous silica surface by using a labile protecting group at the terminal aminopropyl groups.[65, 66] The resulting site-isolated organometallic catalyst is

known to be a very active catalytic system. Acid-labile surfactant has been synthesized and successfully employed as a template for the preparation of MCM-41 type of materials.[67] After hydrocarbon tail cleavage by a simple acid hydrolysis, the as-made materials were changed into amino acid functionalized mesoporous materials. Even though this approach always requires sophisticated design of template molecules, the resultant surface coverage is exceptionally high and functional groups are well defined.

References

1. Kresge, C. T.; Leonowicz, M. E.; Roth, W. J.; Vartuli, J. C.; Beck, J. S., *Nature (London)* **1992**, *359*, 710-712.

2. Beck, J. S.; Vartuli, J. C.; Roth, W. J.; Leonowicz, M. E.; Kresge, C. T.; Schmitt, K. D.; Chu, C. T. W.; Olson, D. H.; Sheppard, E. W., *J. Am. Chem. Soc.* **1992**, *114*, 10834-10843.

3. Zhao, D.; Feng, J.; Huo, Q.; Melosh, N.; Frederickson, G. H.; Chmelka, B. F.; Stucky, G. D., *Science (Washington, D. C.)* **1998**, *279*, 548-552.

4. Zhao, D.; Huo, Q.; Feng, J.; Chmelka, B. F.; Stucky, G. D., *J. Am. Chem. Soc.* **1998**, *120*, 6024-6036.

5. Yang, P.; Deng, T.; Zhao, D.; Feng, P.; Pine, D.; Chmelka, B. F.; Whitesides, G. M.; Stucky, G. D., *Science (Washington, D. C.)* **1998**, *282*, 2244-2247.

6. Yang, P.; Zhao, D.; Margolese, D. I.; Chmelka, B. F.; Stucky, G. D., *Nature (London)* **1998**, *396*, 152-155.

7. Bagshaw, S. A.; Prouzet, E.; Pinnavaia, T. J., *Science (Washington, D. C.)* **1995**, *269*, 1242-1244.

8. Ciesla, U.; Schuth, F., *Micropor. Mesopor. Mater.* **1999**, *27*, 131-149.

9. Huh, S.; Wiench, J. W.; Yoo, J.-C.; Pruski, M.; Lin, V. S. Y., *Chem. Mater.* **2003**, *15*, 4247-4256.

10. Huh, S.; Wiench, J. W.; Trewyn, B. G.; Song, S.; Pruski, M.; Lin, V. S. Y., *Chem. Commun.* **2003**, 2364-2365.

11. Huh, S.; Chen, H.-T.; Wiench, J. W.; Pruski, M.; Lin, V. S. Y., *J. Am. Chem. Soc.* **2004**, *126*, 1010-1011.

12. Tanev, P. T.; Chibwe, M.; Pinnavaia, T. J., *Nature (London)* **1994**, *368*, 321-323.

13. Xia, Y.; Mokaya, R., *Angew. Chem., Int. Ed.* **2003**, *42*, 2639-2644.

14. Lai, C.-Y.; Trewyn, B. G.; Jeftinija, D. M.; Jeftinija, K.; Xu, S.; Jeftinija, S.; Lin, V. S. Y., *J. Am. Chem. Soc.* **2003**, *125*, 4451-4459.

15. Han, Y.-J.; Stucky, G. D.; Butler, A., *J. Am. Chem. Soc.* **1999**, *121*, 9897-9898.

16. Lei, C.; Shin, Y.; Liu, J.; Ackerman Eric, J., *J. Am. Chem. Soc.* **2002**, *124*, 11242-11243.

17. Fan, J.; Yu, C.; Gao, F.; Lei, J.; Tian, B.; Wang, L.; Luo, Q.; Tu, B.; Zhou, W.; Zhao, D., *Angew. Chem. Int. Ed.* **2003**, *42*, 3146-3150.

18. Yoshitake, H.; Yokoi, T.; Tatsumi, T., *Chem. Mater.* **2003**, *15*, 1713-1721.

19. Yoshitake, H.; Yokoi, T.; Tatsumi, T., *Chem. Mater.* **2002**, *14*, 4603-4610.

20. Feng, X.; Fryxell, G. E.; Wang, L. Q.; Kim, A. Y.; Liu, J.; Kemner, K. M., *Science (Washington, D. C.)* **1997**, *276*, 923-926.

21. Ryoo, R.; Joo, S. H.; Kruk, M.; Jaroniec, M., *Adv. Mater.* **2001**, *13*, 677-681.

22. Lee, J.-S.; Joo, S. H.; Ryoo, R., *J. Am. Chem. Soc.* **2002**, *124*, 1156-1157.

23. Joo, S. H.; Choi, S. J.; Oh, I.; Kwak, J.; Liu, Z.; Terasaki, O.; Ryoo, R., *Nature (London)* **2001**, *414*, 169-172.

24. Asefa, T.; MacLachlan, M. J.; Coombs, N.; Ozin, G. A., *Nature (London)* **1999**, *402*, 867-871.

25. Inagaki, S.; Guan, S.; Fukushima, Y.; Ohsuna, T.; Terasaki, O., *J. Am. Chem. Soc.* **1999**, *121*, 9611-9614.

26. Melde, B. J.; Holland, B. T.; Blanford, C. F.; Stein, A., *Chem. Mater.* **1999**, *11*, 3302-3308.

27. Kapoor, M. P.; Yang, Q.; Inagaki, S., *Chem. Mater.* **2004**, *16*, 1209-1213.

28. Landskron, K.; Hatton Benjamin, D.; Perovic Doug, D.; Ozin Geoffrey, A., *Science (Washington, D. C.)* **2003**, *302*, 266-269.

29. Temtsin, G.; Asefa, T.; Bittner, S.; Ozin, G. A., *J. Mater. Chem.* **2001**, *11*, 3202-3206.

30. Inagaki, S.; Guan, S.; Ohsuna, T.; Terasaki, O., *Nature (London)* **2002**, *416*, 304-307.

31. Kapoor Mahendra, P.; Yang, Q.; Inagaki, S., *J. Am. Chem. Soc.* **2002**, *124*, 15176-15177.

32. Yang, Q.; Kapoor Mahendra, P.; Inagaki, S., *J. Am. Chem. Soc.* **2002**, *124*, 9694-9695.

33. Zhou, Z.; Bao, X.; Zhao, X. S., *Chem. Commun.* **2004**, 1376-1377.

34. Burleigh, M. C.; Markowitz, M. A.; Spector, M. S.; Gaber, B. P., *Chem. Mater.* **2001,** *13,* 4760-4766.

35. Lu, Y.; Ganguli, R.; Drewien, C. A.; Anderson, M. T.; Brinker, C. J.; Gong, W.; Guo, Y.; Soyez, H.; Dunn, B.; Huang, M. H.; Zink, J. I., *Nature (London)* **1997,** *389,* 364-368.

36. Lu, Y.; Yang, Y.; Sellinger, A.; Lu, M.; Huang, J.; Fan, H.; Haddad, R.; Lopez, G.; Burns, A. R.; Sasaki, D. Y.; Shelnutt, J.; Brinker, C. J., *Nature (London)* **2001,** *410,* 913-917.

37. Pai, R. A.; Humayun, R.; Schulberg, M. T.; Sengupta, A.; Sun, J.-N.; Watkins, J. J., *Science (Washington, D. C.)* **2004,** *303,* 507-511.

38. Stein, A.; Melde, B. J.; Schroden, R. C., *Adv. Mater.* **2000,** *12,* 1403-1419.

39. Lim, M. H.; Stein, A., *Chem. Mater.* **1999,** *11,* 3285-3295.

40. Mann, S.; Ozin, G., *Nature (London)* **1996,** *382,* 313-318.

41. Yang, H.; Coombs, N.; Ozin, G. A., *Nature (London)* **1997,** *386,* 692-695.

42. Ozin, G. A., *Chem. Commun.* **2000,** 419-432.

43. Lin, H.-P.; Mou, C.-Y., *Science (Washington, D. C.)* **1996,** *273,* 765-768.

44. Schmidt-Winkel, P.; Yang, P.; Margolese, D. I.; Chmelka, B. F.; Stucky, G. D., *Adv. Mater.* **1999,** *11,* 303-307.

45. Shio, S.; Kimura, A.; Yamaguchi, M.; Yoshida, K.; Kuroda, K., *Chem. Commun.* **1998,** 2461-2462.

46. Davis, S. A.; Burkett, S. L.; Mendelson, N. H.; Mann, S., *Nature (London)* **1997,** *385,* 420-423.

47.   Miyata, H.; Kuroda, K., *Adv. Mater.* **2001**, *13*, 558-561.

48.   Kim, S. S.; Zhang, W.; Pinnavaia, T. J., *Science (Washington, D. C.)* **1998**, *282*, 1302-1305.

49.   Mokaya, R., *Chem. Commun.* **2001**, 933-934.

50.   Lu, Y.; Fan, H.; Stump, A.; Ward, T. L.; Rieker, T.; Brinker, C. J., *Nature (London)* **1999**, *398*, 223-226.

51.   Che, S.; Liu, Z.; Ohsuna, T.; Sakamoto, K.; Terasaki, O.; Tatsumi, T., *Nature (London)* **2004**, *429*, 281-284.

52.   Etienne, M.; Lebeau, B.; Walcarius, A., *New J. Chem.* **2002**, *26*, 384-386.

53.   Gruen, M.; Lauer, I.; Unger, K. K., *Adv. Mater.* **1997**, *9*, 254-257.

54.   Schumacher, K.; Du Fresne von Hohenesche, C.; Unger, K. K.; Ulrich, R.; Du Chesne, A.; Wiesner, U.; Spiess, H. W., *Adv. Mater.* **1999**, *11*, 1194-1198.

55.   Stoeber, W.; Fink, A.; Bohn, E., *J. Colloid Interface Sci.* **1968**, *26*, 62-69.

56.   Pauwels, B.; Van Tendeloo, G.; Thoelen, C.; Van Rhijn, W.; Jacobs, P. A., *Adv. Mater.* **2001**, *13*, 1317-1320.

57.   Sadasivan, S.; Khushalani, D.; Mann, S., *J. Mater. Chem.* **2003**, *13*, 1023-1029.

58.   Fowler, C. E.; Khushalani, D.; Lebeau, B.; Mann, S., *Adv. Mater.* **2001**, *13*, 649-652.

59.   Che, S.; Garcia-Bennett, A. E.; Liu, X.; Hodgkins, R. P.; Wright, P. A.; Zhao, D.; Terasaki, O.; Tatsumi, T., *Angew. Chem. Int. Ed.* **2003**, *42*, 3930-3934.

60.   Cai, Q.; Luo, Z.-S.; Pang, W.-Q.; Fan, Y.-W.; Chen, X.-H.; Cui, F.-Z., *Chem. Mater.* **2001**, *13*, 258-263.

61.   Clark, J. H., *Acc. Chem. Res.* **2002**, *35*, 791-797.

62.   Kageyama, K.; Tamazawa, J.-I.; Aida, T., *Science (Washington, D. C.)* **1999**, *285*, 2113-2115.

63.   Wu, C. G.; Bein, T., *Science (Washington, D. C.)* **1994**, *264*, 1757-1759.

64.   Wu, C.-G.; Bein, T., *Science (Washington, D. C.)* **1994**, *266*, 1013-1015.

65.   McKittrick, M. W.; Jones, C. W., *J. Am. Chem. Soc.* **2004**, *126*, 3052-3053.

66.   Yu, K.; McKittrick, M. W.; Jones, C. W., *Organometallics* **2004**, *23*, 4089-4096.

67.   Zhang, Q.; Ariga, K.; Okabe, A.; Aida, T., *J. Am. Chem. Soc.* **2004**, *126*, 988-989.

CHAPTER 2. ORGANIC FUNCTIONALIZATION AND MORPHOLOGY CONTROL OF MESOPOROUS SILICAS VIA A CO-CONDENSATION SYNTHESIS METHOD

A paper published in *Chemistry of Materials*[1]

Seong Huh, Jerzy W. Wiench, Ji-Chul Yoo, Marek Pruski and Victor S. –Y. Lin

Abstract

A series of new mesoporous silica materials with MCM-41 type of structure containing a homogeneous layer of organic functional groups inside the pores was prepared using a co-condensation method under low surfactant concentration condition. This reproducible synthetic approach resulted in high surface coverage with several functional groups such as a primary amine, secondary amine, urea, isocyanate, vinyl, and nitrile. In addition, the presence of organoalkoxysilane precursors during the base catalyzed condensation greatly influenced the final particle shape. By changing the precursor or its concentration, the particle morphology was tuned to various shapes, including spheres, tubes, and rods of various dimensions. The synthetic procedures that gave rise to the specific particle morphologies were investigated and the mechanism responsible for shape control was postulated. The structure and functionality of these materials were characterized by the field-emission scanning electron microscopy, transmission scanning microscopy, solid state

---

NMR spectroscopy, thermogravimetric analysis, and nitrogen adsorption and desorption studies (BET isotherms and BJH pore size distribution measurements).

Introduction

Ever since the discovery of surfactant micelle-templated synthesis of mesoporous silica materials, such as MCM-41/48,[1,2] SBA-15,[3] MSU-n,[4] KIT-1,[5] and FSM-16,[6] many research efforts have focused on (i) preparing the organic/inorganic hybrids through *functionalization* of the exterior and/or interior surfaces and (ii) controlling the *particle morphology*. The success of such investigations will prompt the utilization of these materials in separation,[7] sensor design,[8] catalysis,[9] and drug delivery.[10]

Although numerous synthetic approaches have been pursued and significant progress has been made in *functionalization* of the MCM silicas with various organic groups, the current state-of-the-art methods, such as *post synthesis grafting*[11] and *organosiloxane/siloxane co-condensation*,[12] need to be improved in order to control the amount and location of the incorporated functional groups. For example, the post synthesis grafting method typically results in inhomogeneous surface coverage because the introduced organic moieties congregate near the entries to the mesoporous channels and on the exterior surfaces.[13] While many organically functionalized mesoporous materials were prepared via co-condensation,[13-27] only few very recent investigations reported that spherical or tubular MCM-41 type silicas could be synthesized via incorporation of either mercaptopropyl, allyl, or aminopropyl functional groups.[28] Also, the previously reported co-condensation methods usually result in breakup of the structural integrity and long-range periodicity at surface coverages exceeding 25%.

Herein, we report and analyze a new synthetic method that could combine efficient organic functionalization of mesoporous silicas with the control of particle morphology. The degree of functionalization and particle morphology were dictated by the concentration, molecular size and hydrophilicity/hydrophobicity of the organoalkoxysilane precursors. Our strategy involved a co-condensation method based on sodium hydroxide-catalyzed reactions of tetraethoxysilane (TEOS) with various organoalkoxysilanes in the presence of a low concentration of cetyltrimethylammonium bromide (CTAB) surfactant. The organoalkoxysilanes included 3-aminopropyltrimethoxysilane (APTMS), *N*-(2-aminoethyl)-3-aminopropyltrimethoxysilane (AAPTMS), 3-[2-(2-aminoethylamino)ethylamino]propyl-trimethoxysilane (AEPTMS), ureidopropyltrimethoxysilane (UDPTMS), 3-isocyanatopropyltriethoxy-silane (ICPTES), 3-cyanopropyltriethoxysilane (CPTES), and allyltrimethoxysilane (ALTMS). In contrast to the Stöber process[29] or the recently reported controlled quenching method,[28] our approach did not involve any organic co-solvents or instantaneous neutralization of alkaline solutions during the co-condensation reaction, respectively. By systematically varying the type and the amount of organoalkoxysilanes, we obtained a series of nanoparticles in form of spheres, rods, and hexagonal tubes. Throughout this paper, we will refer to these materials as X-MP, where X describes the organoalkoxysilane precursor and MP stands for mesoporous particle. To examine the different mechanistic effects of the organoalkoxysilane-induced shape transformation, we analyzed the structures of these mesoporous organic/inorganic hybrid materials by powder X-ray diffraction (XRD) spectroscopy, field-emission scanning electron microscopy (FE-SEM), nitrogen adsorption-desorption surface analysis (BET isotherms and BJH pore size distributions), and thermogravimetric analysis (TGA). The incorporation of the organic

functional groups was quantitatively studied by solid state NMR spectroscopy of ^{13}C and ^{29}Si. Based on the observations of the morphological structures and the degree of organic functionalization, we proposed a formation mechanism of mesoporous silica nanoparticles with different morphologies that relies on the interaction between organoalkoxysilanes and CTAB micelles.

Experimental Section

The organoalkoxysilane precursors used for our co-condensation reactions contain a common trimethoxysilyl or triethoxysilyl terminal group and different organic functional groups, as depicted in Scheme 1. APTMS, AAPTMS, AEPTMS, UDPTMS, ICPTES, CPTES, ALTMS, TEOS and CTAB were purchased from Aldrich and used as received. The reaction mixture contained 1.0 CTAB : 8.16 TEOS : 1.05 organotrialkoxysilane of choice (unless specified otherwise): 2.55 NaOH : 4857 H_2O based on the molar ratio. For example, in the case of AP-MP, the mixture of CTAB (2.0 g, 5.49 mmol), 2.0 M of NaOH(aq) (7.0 mL, 14.0 mmol) and H_2O (480 g, 26.67 mol) was heated at 80 °C for 30 min to reach pH 12.3. To this clear solution, TEOS (9.34 g, 44.8 mmol) and APTMS (1.03 g, 5.75 mmol) were added sequentially and rapidly via injection. Following the injection, a white precipitation was observed after 3 min of stirring at *ca.* 550 rpm. The reaction temperature was maintained at 80 °C for 2 h. The products were isolated by a hot filtration, washed with copious amount of water and methanol and dried under vacuum. The reaction yields of as-made products varied with respect to the choice of organoalkoxysilane and ranged from 38% to 65% of the starting weight of TEOS. An acid extraction was performed in methanol (100 mL) mixture of concentrated hydrochloric acid (1.0 mL) and as-made materials (1.0 g) at 60

°C for 6 h. Resulting surfactant-removed solid products were filtered and washed with water and methanol and then dried under vacuum. Pure MCM-41 samples were prepared as reference using the same experimental conditions. The as-synthesized sample containing the surfactant will be referred to as s-MCM-41, while the sample with CTAB removed will be simply denoted as MCM-41.

Particle morphology of these materials was determined by scanning electron microscopy (SEM) using a Hitachi S4700 FE-SEM system with 10 kV accelerating voltage and 0.005 nA of beam current for imaging. For transmission electron microscopy (TEM) studies, a small aliquot was taken from a suspension of methanol and placed in a lacey carbon coat TEM grid, which was pulled through the suspension and allowed to dry in air. Thin sections of samples embedded in epoxy resin were obtained with ultramicrotomy (60-80 nm). The resulting sample was examined with a Philips model CM-30 TEM operated at 300 kV. The specimen was given no further treatment, as it appeared stable under beam bombardment.

Powder XRD experiments were performed on a Scintag XDS 2000 diffractometer using a Cu Kα radiation source. Low angle diffraction with a 2θ range of 1 to 10° was used to investigate the long-range order of the materials. The surface area and median pore diameter were measured using N_2 adsorption/desorption measurements in a Micromeritics ASAP 2000 BET surface analyzer system. The data were evaluated using the Brunauer-Emmett-Teller (BET) and Barrett-Joyner-Halenda (BJH) methods to calculate the surface area and pore volumes/pore size distributions, respectively. Samples were prepared by degassing at 90 °C for 1 h and then at 150 °C for 4h. TGA curves were recorded using a TA

Instruments TGA 2950 thermogravimetric analyzer with a temperature ramp of 5 °C/min under continuous flow of nitrogen (100 mL/min).

Solid-state nuclear magnetic resonance (NMR) experiments were performed on a Varian/Chemagnetics Infinity spectrometer at the frequencies of 79.5, 100.6 and 400.0 MHz for ^{29}Si, ^{13}C and ^{1}H nuclei, respectively. ^{13}C and ^{29}Si nuclei were observed using direct polarization (DP) or by cross polarization[30] (CP) from the neighboring ^{1}H nuclei. The samples were placed in 5 mm zirconia rotors and spun at 10 kHz in a doubly tuned Chemagnetics probe. The saturation recovery experiment, carried out for AL-MP and ICP-MP samples, yielded the ^{29}Si longitudinal relaxation times in the range of 30 to 65 s. In spite of slow relaxation, ^{29}Si DPMAS measurements were performed to obtain quantitative spectra for all samples. These experiments used excitation with a single 90° pulse of 2.1 μs followed by data acquisition under continuous wave (CW) ^{1}H decoupling at 65 kHz. Typically 270 scans were completed using pulse delay of 300 s.

The variable amplitude CPMAS scheme[31] was used to enhance the polarization of observed nuclei and increase the repetition rate of data acquisition. During each cross polarization period, the ^{1}H rf field was ramped between 16 and 40 kHz using 2.4 kHz increments, whereas the ^{29}Si (or ^{13}C) rf field was maintained at a constant level of approximately 36 kHz. The maximum ^{1}H→^{29}Si polarization transfer was achieved using a contact time of approximately 10 ms, which is in agreement with previous studies performed for silicas.[32] For ^{13}C nuclei, shorter contact times of 0.4 ~ 1.5 ms were used. The ^{1}H rf magnetic fields of 90 kHz and 65 kHz were used for initial excitation and decoupling, respectively. The values of ^{1}H longitudinal relaxation time encountered in all mesoporous samples examined in this study did not exceed 1 s, which allowed for repetition time of 1.2 s

to be used in the CPMAS experiments. Typically, 4K scans were accumulated for $^1H\rightarrow^{29}Si$ CPMAS, whereas $^1H\rightarrow^{13}C$ experiments required between 1K and 10K scans per spectrum. All chemical shifts were referenced to $SiMe_4$.

Results and Discussion

Organic functionalization. To simplify the analysis, we initially prepared a series of samples in which the amount of organoalkoxysilane used for the preparation was fixed at 12.8 mol % of the amount of TEOS. The $^1H\rightarrow^{13}C$ CPMAS spectra of these samples, shown in Figure 1, provide clear evidence that they were indeed functionalized as intended. The observed chemical shifts, listed in Table 1, agreed well with those observed in homogeneous solutions of the corresponding precursors and were easily assigned. For example, the resonances at 6.5, and 45.3 ppm in the spectrum of APTMS dissolved in $CDCl_3$ (not shown) corresponded to those at 9.1 ppm (C1) and 42.3 ppm (C3) observed in AP-MP. The resonance at 28 ppm representing C2 exhibited a larger shift change toward higher field relative to the liquid state (20.6 ppm). The CPMAS spectrum of s-MCM-41 sample (Figure 1h) consisted of several resonances due to CTAB, among which the peak at around 30 ppm, corresponding to carbons C3 through C14, is most intense. Two samples, CP-MP and AL-MP, contained detectable resonances from CTAB (marked with asterisks in spectra f and g), which comprised just a few % of the total ^{13}C intensity.

The functionalization of silicas was further studied by TGA and solid state NMR of ^{29}Si (Figure 2 and Table 2). In general, three or four distinct weight loss TGA profiles were found, including methanol, organic functional groups, and a small weight loss due to the dehydration of the surface hydroxyl groups. While the TGA data provided evidence of the

existence of organic functional groups inside the pores, a direct, quantitative measure of the organic functionalization was provided by [29]Si DPMAS spectra shown in the left column of Figure 2. The resonances at around -59 and -68 ppm represented silicon atoms in positions $(\equiv SiO)_2Si(OH)R$ and $(\equiv SiO)_3SiR$, which are denoted T^2 and T^3, respectively.[33-36] These silicon species were better observed using the ^{29}Si CP-MAS NMR method (see Figure 2, right column), which detected only the nuclei located within 2-3 bond lengths from the nearest hydrogen atoms. Note that the presence of T^3 and T^2 functionalities confirmed the existence of the covalent linkage between the organic groups and the silica surface. The resonance lines representing Q^4 (siloxane, $(\equiv SiO)_4Si$), Q^3 (single silanol, $(\equiv SiO)_3SiOH$) and Q^2 (geminal silanol, $(\equiv SiO)_2Si(OH)_2$) silicons were also observed in their usual spectral positions.[32-36] The relative concentrations of all silicon sites were obtained by deconvolution of DPMAS spectra (see Table 2). Assuming that all Q^3 and Q^2 sites decorated the interior walls of mesoporous silicas, the surface coverage (SC) of the mesopores with organic moieties could be estimated as SC = $(T^2 + T^3)/(Q^2 + Q^3 + T^2 + T^3)$. As shown in Table 2, the SC values varied between 13% for UDP-MP and 33% for AL-MP. The measured loading efficiencies of the MP's synthesized with the organoalkoxysilanes containing hydrophobic functional groups, such as CPTES and ALTMS, were higher than those that contained the hydrophilic precursors, such as AAPTMS and AEPTMS. These results suggested that the organoalkoxysilanes with hydrophobic functional groups could better orient themselves around the water/micelle interface and intercalate these groups to the hydrophobic regions of the CTAB micelles during the co-condensation reactions.

Morphology control. The morphology and mesoporous structure of the organically functionalized MP materials were studied using FE-SEM and powder X-ray diffraction. The

FE-SEM micrographs demonstrated a variety of particle shapes and sizes. For example, the AP-MP material showed a curved hexagonal shaped tubular morphology, as depicted in Figure 3a. Interestingly, upon replacing the APTMS with other structurally similar organoalkoxysilanes, such as AAPTMS and AEPTMS (Figure 3b, c), the shapes transformed into twisted columns and micrometer-sized spheres, respectively. In contrast to smooth particle surface of AEP-MP, UDP-MP (Figure 3d) exhibited micron-sized spherical particles with raspberry-like bumpy rough surfaces. The ICP-MP material (Figure 3e) consisted of smallest spherical particles with diameters ranging from 100 to 500 nm. In the synthesis of CP-MP (Figure 3f) and AL-MP materials (Figure 3g), hexagonal rod-shaped particles of different lengths and diameters were observed. The average particle size of CP-MP (1 μm in length and 500 nm in diameter) is larger than that of AL-MP (500 nm and 50 nm, respectively). As a rule, the particle sizes of materials prepared with the hydrophobic organoalkoxysilane precursors, such as ICPTES, CPTES, and ALTMS, appear significantly smaller than pure MCM-41 (Figure 3h), whereas the materials synthesized using more hydrophilic organoalkoxysilanes, such as AAPTMS, AEPTMS, and UDPTMS, yielded larger particles. Note that the co-condensation reactions took place in a basic aqueous solution (pH = 12.3), therefore the trialkoxysilyl groups of these organoalkoxysilanes were hydrolyzed and converted to the trihydroxysilyl group, which is always hydrophilic. The other end of the molecule can be either hydrophilic or hydrophobic depending on the water solubility of the organic functional group involved.

The surface areas, pore volumes and pore size distributions of the MP materials were analyzed by the nitrogen adsorption-desorption techniques. As shown in Figure 4, all silicas exhibited characteristic Type IV BET isotherms consistent with the presence of cylindrical

meso-scale pores. However, as outlined in Table 3, the BJH average pore diameters were different depending on the types of the incorporated organic functional groups. Again, utilization of the hydrophobic precursors yielded smaller pores. The powder XRD spectra of these materials (Figure 5) featured an intense (100) reflection peak corresponding to lattice spacings in the range of 33.7 to 43.7 Å. Even though (210) peaks were not observed, the well resolved diffraction patterns characteristic of hexagonal MCM-41 silicas,[37] including (100), (110), and (200) peaks with the spacing ratio of $1 : \sqrt{3} : \sqrt{4}$, were observed in AP-MP, AAP-MP, CP-MP, ICP-MP and AL-MP. On the other hand, AEP-MP and UDP-MP (Figure 5c, d) appeared to be disordered as evidenced by a broad peak at 4.52° and 4.10°, respectively, representing superimposed (110), and (200) patterns. The TEM micrographs of these samples shown in Figures 6a and 6d are consistent with this observation. In contrast, the TEM micrographs of materials prepared with hydrophobic organoalkoxysilanes, such as CPTES, showed well-organized mesopores packed in hexagonal symmetry as evidenced in Figure 6b, c.

Mechanism responsible for the shape formation. As discussed earlier, similar organic precursors can yield very different particle morphologies, e.g., AAP-MP showed tubular-shaped particles (Figure 3b) while the AEP-MP exhibited exclusively spherical particles (Figure 3c). Clearly, several different interactions, such as electrostatic attraction/repulsion, hydrogen bonding, and hydrophobic interaction, between the organoalkoxysilanes and surfactant molecules at the micelle/water interface could contribute cooperatively to the observed drastic changes in particle morphology. We undertook an approach of deconvoluting some of these factors by investigating how the concentration of a selected organoalkoxysilane (AEPTMS) could influence the resulting particle shape and size.

The molar ratio of AEPTMS/TEOS was systematically varied from 1.28 to 12.8 mol%, while the concentrations of all the other chemicals introduced to the co-condensation reaction were fixed at the previously described levels. The incorporation of AEP was quantitatively determined by DPMAS and CPMAS ^{29}Si NMR (Figure 7a,b). As discussed earlier, the DPMAS spectra provided quantitative measure of the relative concentrations of Q^n and T^n functionalities. However, due to low concentration of T^n species the SC values were not directly measured in this series of samples. Instead, we used the CPMAS spectra to evaluate the relative change of T^n intensities versus the concentration of AEPTMS. The results, plotted in Figure 7c in reference to the sample with 1.28 mol% of AEPTMS, showed that the concentration of AEP increased almost linearly as the initial AEPTMS/TEOS molar ratio changed from 1.28 to 12.8 mol%. The particle morphology and mesoporous structure of the resulting materials were analyzed by FE-SEM and TEM. The FE-SEM micrographs of Figure 8 showed a concurrent transformation of the particle morphology from small kidney bean shaped rods to spheres, with elongated rods and ellipsoidal particles being observed at intermediate concentrations of AEPTMS. Furthermore, a noticeable increase of the average particle sizes of these materials could be observed at higher concentrations of AEPTMS. The TEM micrographs (Figure 9a,b) of the AEP-MP materials with low degrees of functionalization (1.28 and 6.43 mol%, respectively) revealed that the mesopores are uniformly aligned along the long axes of MP's despite of their different particle sizes. This is in contrast to the randomly oriented mesopores observed in the spherical AEP-MP's with the higher degree of functionalization (Figure 6a).

Based on these results, the following mechanism is proposed to account for the formation of different particle shapes and sizes. To facilitate the ensuing discussion, we

present Scheme 2 where R_1 and R_2 represent the hydrophilic and hydrophobic functional groups, respectively. In the case of the more hydrophobic organoalkoxysilane precursors, such as CPTES and ALTMS, the aforementioned strong interaction between their non-polar groups (R_2) and the hydrophobic hydrocarbon tails of the CTAB molecules could likely stabilize the formation of long individual cylindrical micelles by intercalating their hydrophobic groups to the micelles, as shown in Scheme 2b. The uniform organization of the trialkoxysilyl group at the Gouy-Chapman region of the surface of micelles and their increased length would assist in the rapid cross-linking/condensation between the "micelle-oriented" trialkoxysilyl groups in the basic NaOH aqueous solution, as depicted in Scheme 2c. The resulting "side-on" packing of the silicate-coated cylindrical micelles would give rise to small rod-like nanoparticles. Similar phenomenon has been observed by Cai et al.[38] while utilizing NaOH and NH_4OH as catalysts to manipulate the particle morphology of the MCM-41 silicas without organic functional groups. The above mechanism would not be operable for more hydrophilic organoalkoxysilane precursors, such as AAPTMS, AEPTMS, and UDPTMS, because their R_1 functional groups are not favored by the interaction with the surfactant molecules (Scheme 2a). This would inhibit the formation of long micelles and reduce their tendency toward side-on condensation. The difference in rate of condensation between silicate-coated micelles versus that of the free silicate (TEOS) molecules would be small. Due to the lack of thermodynamic incentives for the silicate-coated micelles to pack in an ordered fashion, such co-condensation reactions should yield particles with randomly oriented pore structures. This hypothesis was supported by our study of synthesizing AEP-MP's with different concentrations of AEPTMS. The fact that the spherical-shaped AEP-MP obtained with 12.8 mol% AEPTMS showed disordered mesoporous structure indicated that

the amount of hydrophilic precursors introduced was perhaps high enough to disturb the side-on growth mechanism. A similar phenomenon was recently reported by Mann and co-workers,[28] who observed the growth of the mesoporous silica particle in the direction that is perpendicular to the pore-alignment upon the introduction of amine-containing organoalkoxysilanes. At lower concentrations of AEPTMS, rod-shaped materials were generated with small average particle sizes, which indicated that the disruption of the packing mechanism was indeed minimized.

Conclusions

In this study, we have demonstrated that a series of organically functionalized MCM-41 type mesoporous silicas with various particle morphologies could be synthesized by a co-condensation method. The co-condensation reactions used various amounts of organoalkoxysilanes with different functional groups as structure-directing reactants. The mechanism responsible for the observed changes in particle morphology and pore alignment has been proposed. Further studies of this mechanism, which will also include the size effect of the organoalkoxysilane precursors, will be performed. Better understanding of such synthetic strategies and the underlying mechanisms of functionalization and morphology control will lead to construction of various sophisticated organic/inorganic hybrid nanomaterials for heterogeneous sensors and/or catalysts with high selectivity and efficiency.

Acknowledgement

Figure 1. $^1H \rightarrow ^{13}C$ CPMAS spectra of AP-MP (a), AAP-MP (b), AEP-MP (c), UDP-MP (d), ICP-MP (e), CP-MP (f), AL-MP (g), and s-MCM-41 (h) using CP contact time of 0.4 (spectra a-c and h) or 1.5 ms (spectra d-g). Asterisks mark positions of residual surfactant carbons present in spectra f, and g. Note that spectrum (e) represents the propyl-carbamic acid group formed during the synthesis of ICP-MP by base-catalyzed hydrolysis of isocyanopropyl group.
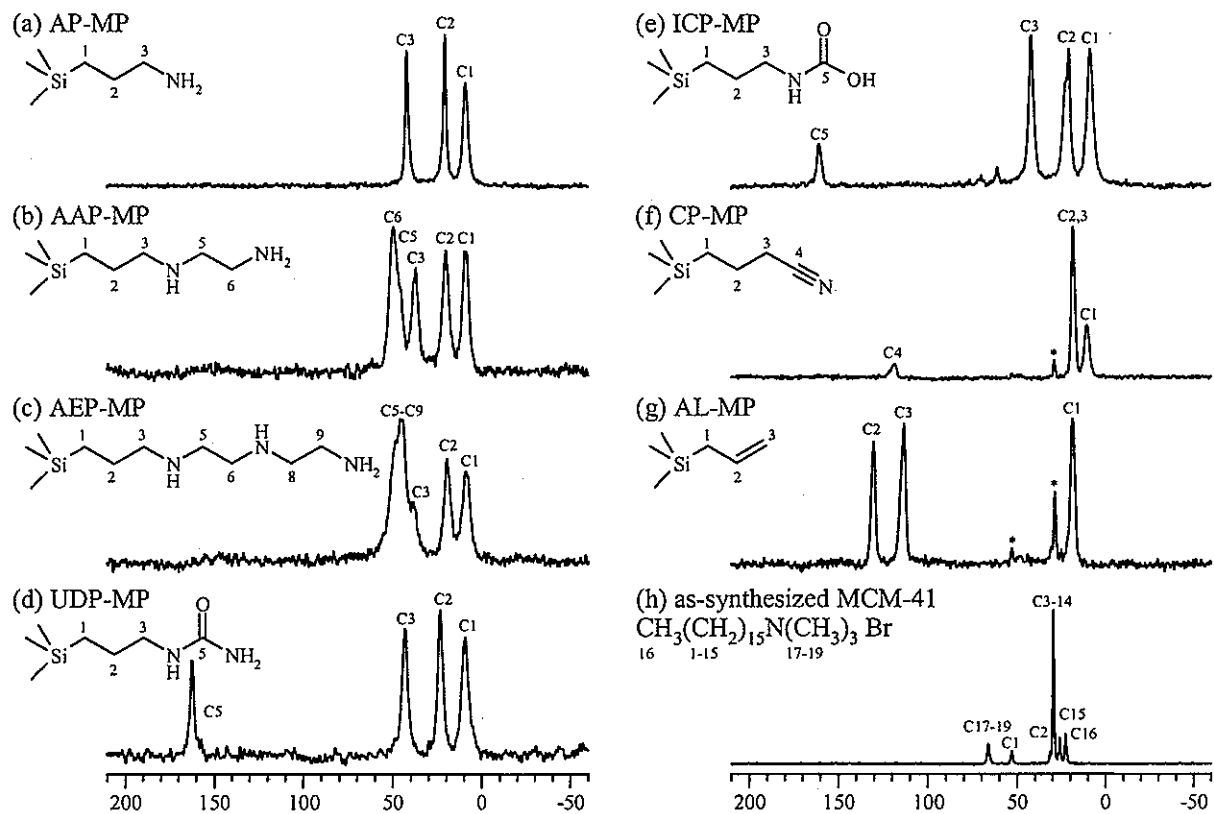
Figure 2. ^{29}Si DPMAS (left) and ^{1}H→^{29}Si CPMAS (right) spectra of AP-MP (a), AAP-MP (b), AEP-MP (c), UDP-MP (d), ICP-MP (e), CP-MP (f), AL-MP (g), s-MCM-41 (h), and MCM-41 after the extraction of surfactant (i).
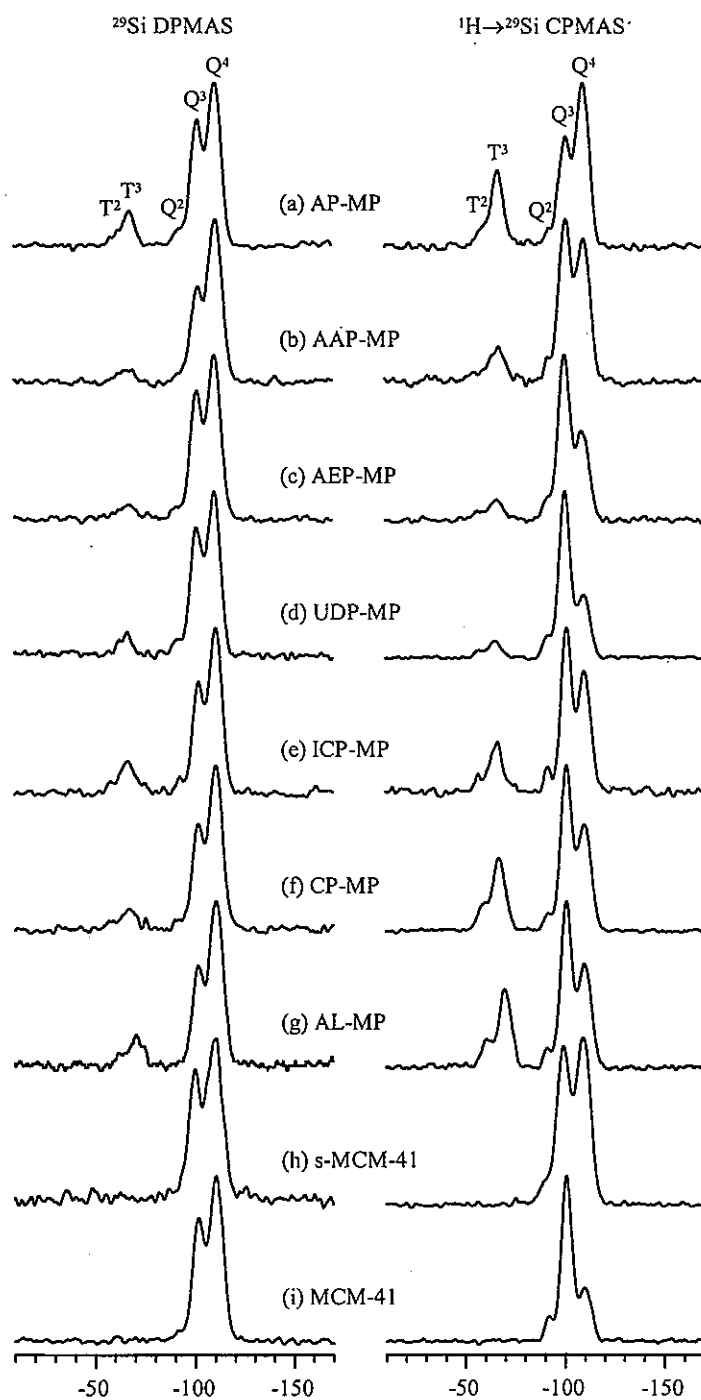
Figure 3. FE-SEM Images of AP-MP (a), AAP-MP (b), AEP-MP (c), UDP-MP (d), ICP-MP (e), CP-MP (f), AL-MP (g), and pure MCM-41 silica (h) synthesized via our condensation reaction condition without adding any organic functional group. All images are presented using the same scale, with the scale bar = 3 μm.
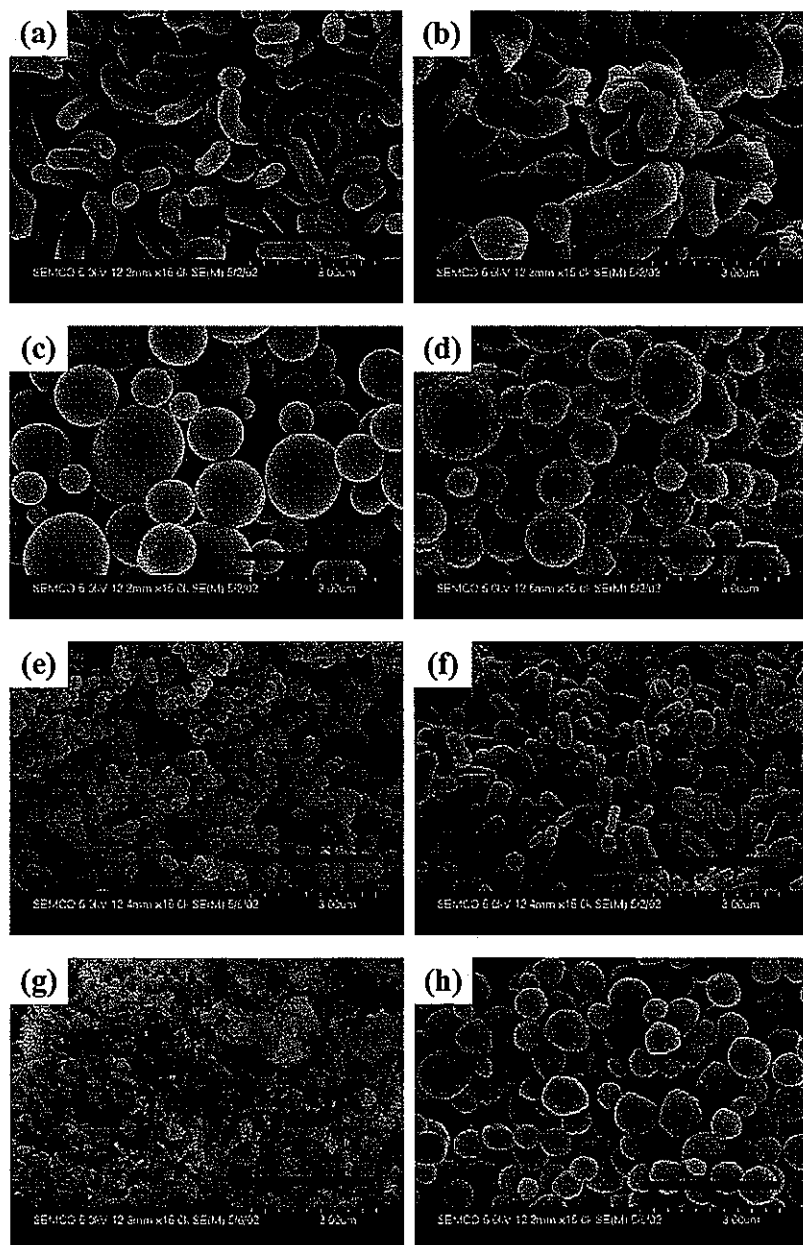
Figure 4. BET isotherms and BJH pore size distributions (insets) of AP-MP (a), AAP-MP (b), AEP-MP (c), UDP-MP (d), ICP-MP (e), CP-MP (f), AL-MP (g) and pure MCM-41 silica (h) materials.
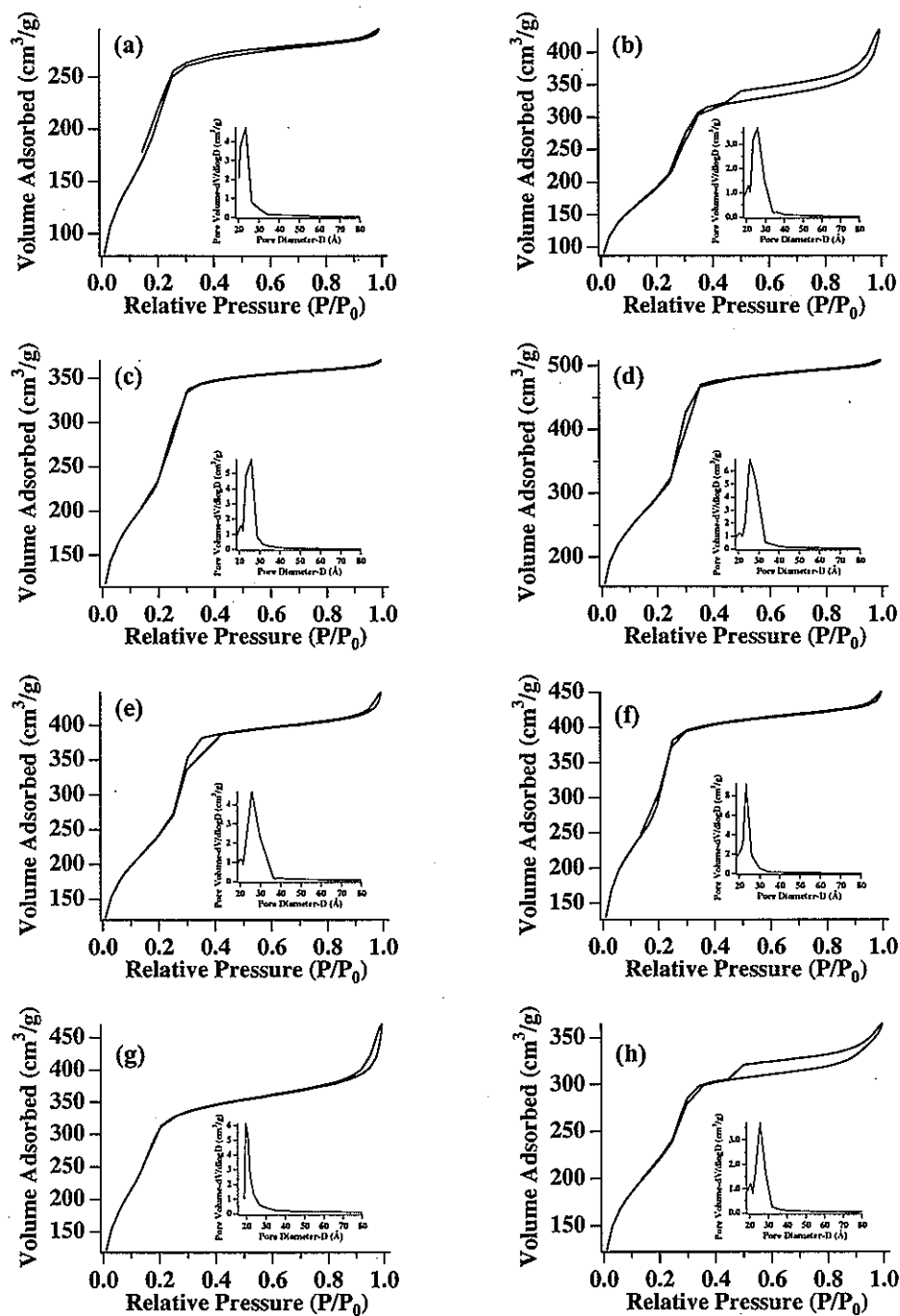
Figure 5. XRD spectra of the surfactant-removed AP-MP (a), AAP-MP (b), AEP-MP (c), UDP-MP (d), AL-MP (e), CP-MP (f) and ICP-MP (g).
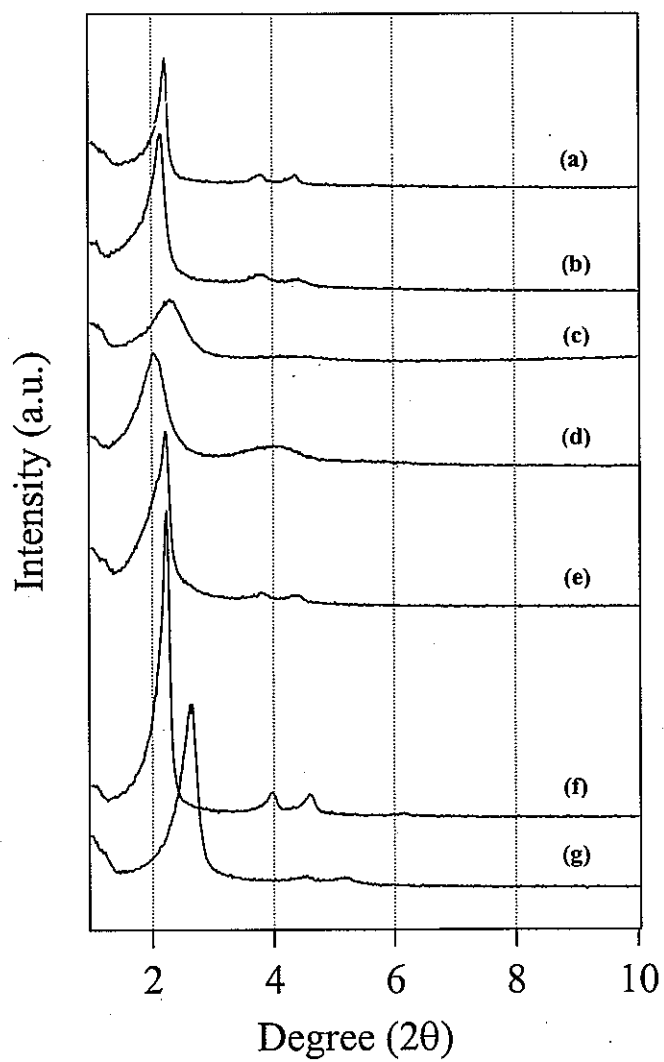
Figure 6. TEM micrographs of AEP-MP (a), CP-MP (b, c), and UDP-MP (d) materials. Images (a) and (b) represent ultramicrotomed samples (scale bar = 100 nm).

34
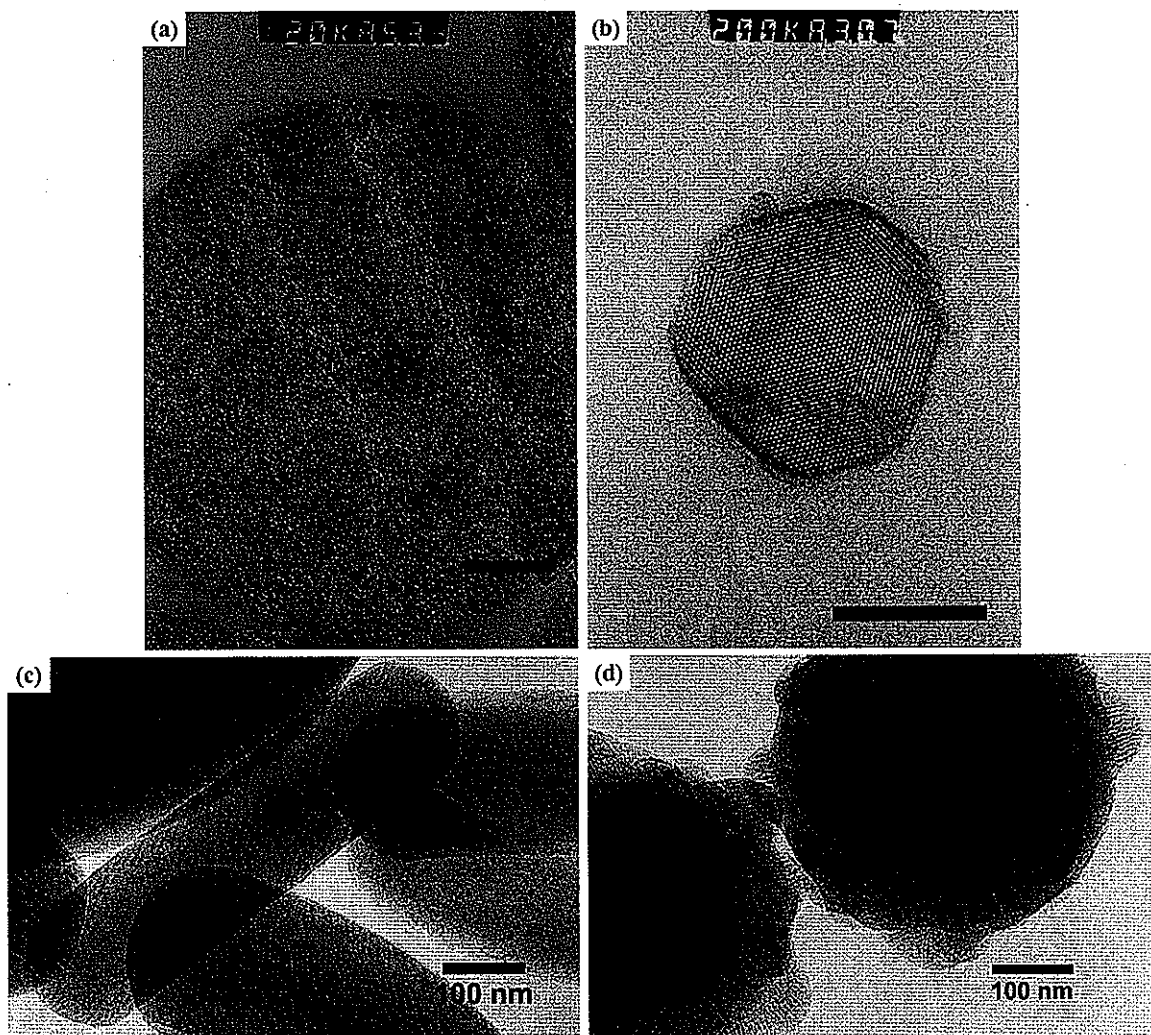
Figure 7. ^{29}Si DPMAS (a) and ^{1}H→^{29}Si CPMAS (b) spectra of functionalized mesoporous materials with various amounts of AEPTMS. A contact time of 1 ms was used during cross polarization period. (c) The relative increase of functionalization versus the concentration of AEPTMS estimated from CPMAS.
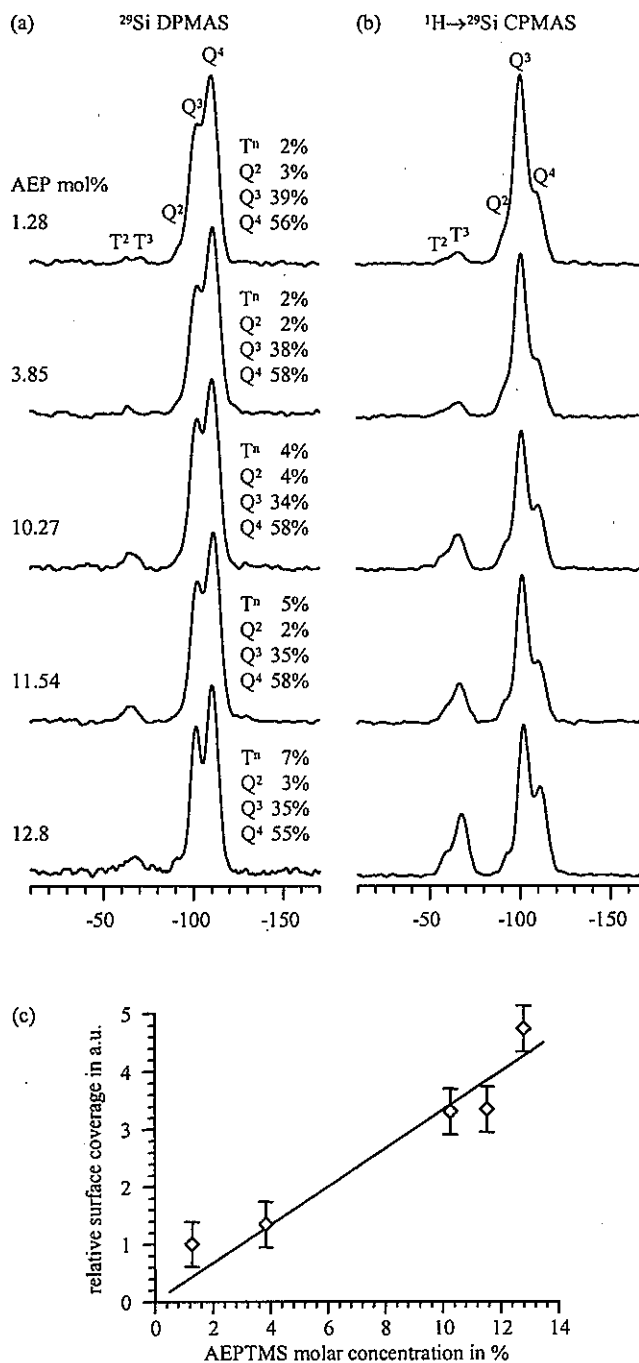
Figure 8. FE-SEM Images of AEP-MP's with different initial loadings of AEPTMS: 1.28 mol% (a), 3.85 mol% (b), 6.43 mol% (c), 10.27 mol% (d), 11.54 mol% (e), and 12.80 mol% (f). All images are presented using the same scale, with the scale bar = 3 μm.
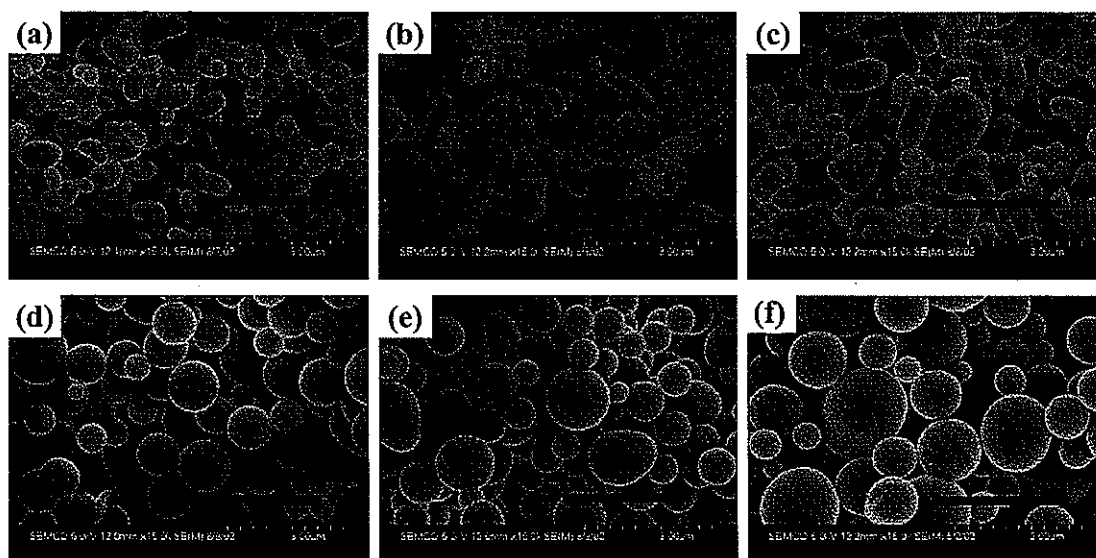
Figure 9. TEM images of ultramicrotomed AEP-MP's with 1.28 mol% (a) and 6.43 mol% (b) AEPTMS (scale bar = 100 nm).
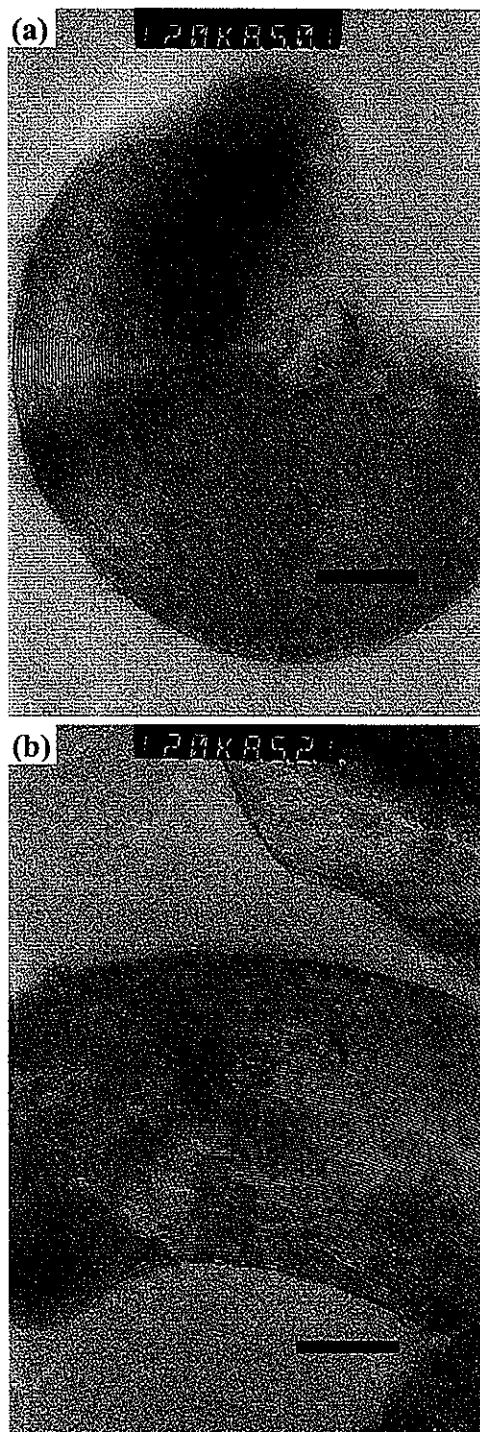
Table 1. ^{13}C chemical shifts (δ_C, in ppm from TMS) of organic groups obtained from $^1H \rightarrow {}^{13}C$ CPMAS spectra.

AP-MP		AAP-MP		AEP-MP		UDP-MP		ICP-MP		CP-MP		AL-MP		s-MCM-41	
	δ_C		δ_C		δ_C		δ_C		δ_C		δ_C		δ_C		δ_C
C1	9.1	C1	8.5	C1	8.7	C1	9.0	C1	8.8	C1	10.5	C1	18.8	C16	22.7
C2	20.6	C2	19.8	C2	19.4	C2	23.1	C2	20.7	C2	18.3	C2	130.8	C15	26.1
C3	42.3	C3	37.2	C3	38.5	C3	42.9	C3	42.2	C3	18.3	C3	114.2	C3-14	29.8
		C5[a]	49.8	C5[b]	49.1	C5	162.2	C5	160.4	C4	118.4			C2	31.8
		C6[a]	45.0	C6[b]	44.5									C1	66.4
				C8[c]	56.1									NCH_3	53.4
				C9[c]	52.2										

[a], [b], [c] The assignments are somewhat ambiguous for these three pairs of carbons (they may be reversed).

Table 2. ^{29}Si chemical shifts (δ_{Si}, in ppm from TMS) and relative concentrations of T^n and Q^n groups obtained from ^{29}Si DPMAS spectra.

	AP-MP		AAP-MP		AEP-MP		UDP-MP		ICP-MP		CP-MP		AL-MP		s-MCM-41		MCM-41	
	δ_{Si}	%	δ_{Si}	%	δ_{Si}	%	δ_{Si}	%	δ_{Si}	%	δ_{Si}	%	δ_{Si}	%	δ_{Si}	%	δ_{Si}	%
T^2	-59	4	-65	4	-56	1	-62	2	-57	1	-58	2	-64	3				
T^3	-68	8	-69	1	-67	6	-66	4	-66	13	-67	8	-71	8				
Q^2	-93	3	-94	3	-91	3	-91	4	-92	3	-92	2	-97	1	-93	2	-92	3
Q^3	-102	26	-101	28	-101	35	-101	38	-102	29	-101	29	-101	24	-99	34	-101	37
Q^4	-111	59	-111	64	-110	55	-110	52	-111	54	-111	59	-111	64	-110	64	-110	60
T_{surf}		29		14		16		13		30		24		33				

Table 3. Structural properties of the organically functionalized mesoporous silica materials.

Sample	d_{100} (Å)[a]	a_0 (Å)[a]	S_{BET} (m²/g)[a]	V_p (cm³/g)[a]	W_{BJH} (Å)[a]	$d_{pore wall}$ (Å)[a]	Amount of organic groups (mmol/g)[b]
AP-MP	39.8	46.0	721.7	0.45	23.7	22.3	1.7
AAP-MP	41.3	47.7	664.6	0.48	25.9	21.8	0.7
AEP-MP	38.4	44.4	805.8	0.57	26.0	18.4	1.0
UDP-MP	43.7	50.5	1022.4	0.78	28.6	21.9	0.9
ICP-MP	39.8	46.0	840.1	0.66	25.8	20.2	1.5
CP-MP	39.4	45.5	1012.5	0.68	23.5	22.0	1.4
AL-MP	33.7	38.9	1080.5	0.65	19.7	19.2	1.7
MCM-41	38.1	44.0	767.1	0.55	25.5	18.5	—

[a] The BET surface area (S_{BET}), the mesopore volume (V_p), and the mean mesopore width (W_{BJH}) were obtained from the nitrogen adsorption/desorption data. The d_{100} numbers represent the d-spacing corresponding to the main (100) XRD peak. The unit cell size (a_0) is calculated from the d_{100} data using the formula $a_0 = 2d_{100}/3^{1/2}$. The pore wall thickness $d_{pore wall} = a_0 - W_{BJH}$. [b] The amounts of organic functional groups incorporated to the silica materials were estimated from the ^{29}Si DPMAS.

Scheme 1

APTMS   (MeO)$_3$Si$\diagdown\diagup\diagdown$NH$_2$

AAPTMS   (MeO)$_3$Si$\diagdown\diagup\diagdown$N$\diagup\diagdown$NH$_2$
                                H

AEPTMS   (MeO)$_3$Si$\diagdown\diagup\diagdown$N$\diagup\diagdown$N$\diagup\diagdown$NH$_2$

UDPTMS (MeO)$_3$Si$\diagdown\diagup\diagdown$N$\overset{\displaystyle O}{\underset{H}{\diagup}}NH_2$

ICPTES   (EtO)$_3$Si$\diagdown\diagup\diagdown$NCO

CPTES   (EtO)$_3$Si$\diagdown\diagup\diagdown$CN

ALTMS   (MeO)$_3$Si$\diagdown\diagup\diagup$
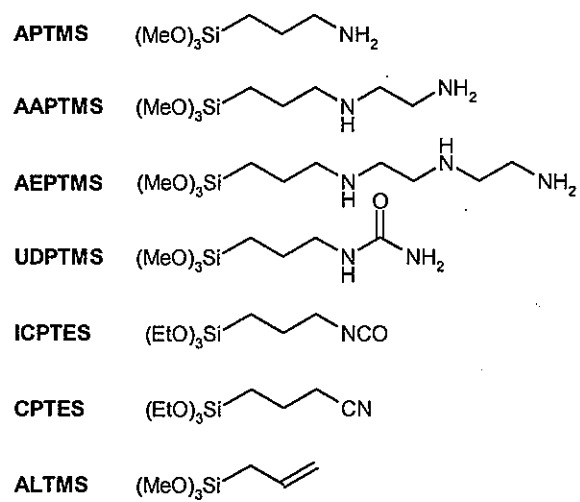
Scheme 2
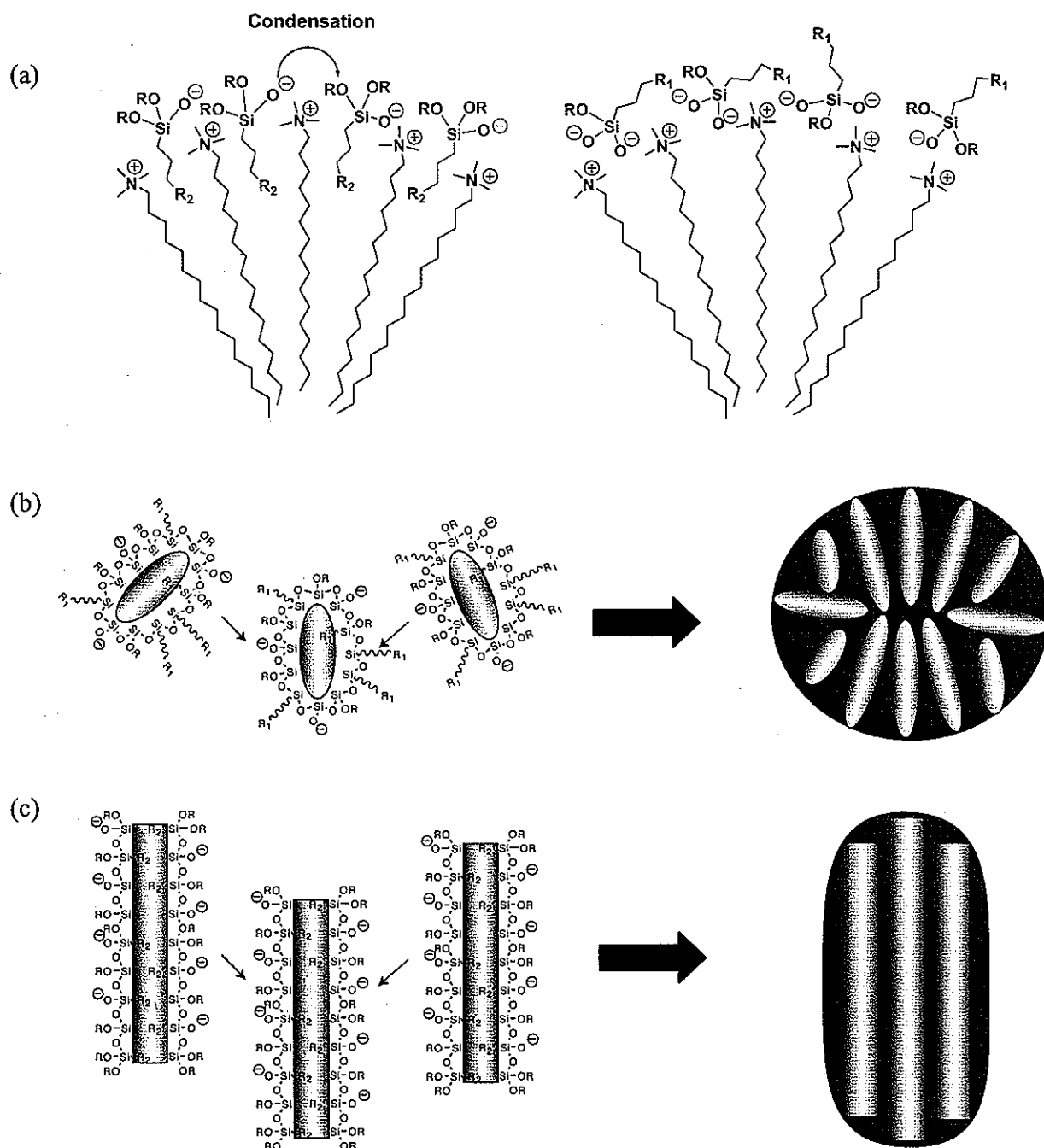
References

1. Beck, J. S.; Vartuli, J. C.; Roth, W. J.; Leonowicz, M. E.; Kresge, C. T.; Schmitt, K. D.; Chu, C. T. W.; Olson, D. H.; Sheppard, E. W.; et al. *J. Am. Chem. Soc.* **1992**, *114*, 10834-10843.

2. Kresge, C. T.; Leonowicz, M. E.; Roth, W. J.; Vartuli, J. C.; Beck, J. S. *Nature (London)* **1992**, *359*, 710-712.

3. Zhao, D.; Feng, J.; Huo, Q.; Melosh, N.; Frederickson, G. H.; Chmelka, B. F.; Stucky, G. D. *Science (Washington, D. C.)* **1998**, *279*, 548-552.

4. Bagshaw, S. A.; Prouzet, E.; Pinnavaia, T. J. *Science (Washington, D. C.)* **1995**, *269*, 1242-1244.

5. Ryoo, R.; Kim, J. M.; Ko, C. H.; Shin, C. H. *J. Phys. Chem.* **1996**, *100*, 17718-17721.

6. Inagaki, S.; Koiwai, A.; Suzuki, N.; Fukushima, Y.; Kuroda, K. *Bull. Chem. Soc. Jpn.* **1996**, *69*, 1449-1457.

7. (a) Dai, S.; Burleigh, M. C.; Shin, Y.; Morrow, C. C.; Barnes, C. E.; Xue, Z. *Angew. Chem., Int. Ed. Engl.* **1999**, *38*, 1235-1239. (b) Lin, Y.; Fryxell, G. E.; Wu, H.; Engelhard, M. *Environ. Sci. Technol.* **2001**, *35*, 3962-3966. (c) Yoshitake, H.; Yokoi, T.; Tatsumi, T. *Chem. Mater.* **2003**, *15*, 1713-1721. (d) Yoshitake, H.; Yokoi, T.; Tatsumi, T. *Bull. Chem. Soc. Jpn.* **2003**, *76*, 847-852. (e) Hossain, K. Z.; Mercier, L. *Adv. Mater. (Weinheim, Ger.)* **2002**, *14*, 1053-1056.

8. (a) Lin, V. S. Y.; Lai, C.-Y.; Huang, J.; Song, S.-A.; Xu, S. *J. Am. Chem. Soc.* **2001**, *123*, 11510-11511. (b) Burleigh, M. C.; Dai, S.; Hagaman, E. W.; Lin, J. S. *Chem. Mater.* **2001**, *13*, 2537-2546.

9. (a) Soler-Illia Galo, J. d. A. A.; Sanchez, C.; Lebeau, B.; Patarin, J. *Chem. Rev.* **2002,** *102,* 4093-4138. (b) Stein, A. *Adv. Mater. (Weinheim, Ger.)* **2003,** *15,* 763-775. (c) Davis, M. E. *Nature (London)* **2002,** *417,* 813-821. (d) Corma, A. *Chem. Rev.* **1997,** *97,* 2373-2419. (e) Price, P. M.; Clark, J. H.; Macquarrie, D. J. *Dalton* **2000,** 101-110. (f) Ying, J. Y.; Mehnert, C. P.; Wong, M. S. *Angew. Chem., Int. Ed. Engl.* **1999,** *38,* 56-77. (g) Sayari, A. *Chem. Mater.* **1996,** *8,* 1840-1852. (h) Moller, K.; Bein, T. *Chem. Mater.* **1998,** *10,* 2950-2963.

10. Lai, C.-Y.; Trewyn, B. G.; Jeftinija, D. M.; Jeftinija, K.; Xu, S.; Jeftinija, S.; Lin, V. S. Y. *J. Am. Chem. Soc.* **2003,** *125,* 4451-4459.

11. Liu, J.; Shin, Y.; Nie, Z.; Chang, J. H.; Wang, L.-Q.; Fryxell, G. E.; Samuels, W. D.; Exarhos, G. J. *J. Phys. Chem. A* **2000,** *104,* 8328-8339.

12. Stein, A.; Melde, B. J.; Schroden, R. C. *Adv. Mater. (Weinheim, Ger.)* **2000,** *12,* 1403-1419.

13. Lim, M. H.; Stein, A. *Chem. Mater.* **1999,** *11,* 3285-3295.

14 Fowler, C. E.; Khushalani, D.; Lebeau, B.; Mann, S. *Adv. Mater. (Weinheim, Ger.)* **2001,** *13,* 649-652.

15. MacLachlan, M. J.; Asefa, T.; Ozin, G. A. *Chem.-Eur. J.* **2000,** *6,* 2507-2511.

16. Fowler, C. E.; Burkett, S. L.; Mann, S. *Chem. Commun.* **1997,** 1769-1770.

17. Fowler, C. E.; Mann, S.; Lebeau, B. *Chem. Commun.* **1998,** 1825-1826.

18. Hall, S. R.; Fowler, C. E.; Mann, S.; Lebeau, B. *Chem. Commun.* **1999,** 201-202.

19. Zub, Y. L.; Seredyuk, I. V.; Chuiko, A. A.; Jaroniec, M.; Jones, M. O.; Parish, R. V.; Mann, S. *Mendeleev Commun.* **2001,** 208-210.

20. Lim, M. H.; Blanford, C. F.; Stein, A. *Chem. Mater.* **1998,** *10,* 467-470.

21. Lim, M. H.; Blanford, C. F.; Stein, A. *J. Am. Chem. Soc.* **1997**, *119*, 4090-4091.

22. Babonneau, F.; Leite, L.; Fontlupt, S. *J. Mater. Chem.* **1999**, *9*, 175-178.

23. Moller, K.; Bein, T.; Fischer, R. X. *Chem. Mater.* **1999**, *11*, 665-673.

24. Sayari, A.; Hamoudi, S. *Chem. Mater.* **2001**, *13*, 3151-3168.

25. Inagaki, S.; Guan, S.; Ohsuna, T.; Terasaki, O. *Nature (London)* **2002**, *416*, 304-307.

26. Burleigh, M. C.; Markowitz, M. A.; Spector, M. S.; Gaber, B. P. *J. Phys. Chem. B* **2001**, *105*, 9935-9942.

27. Burleigh, M. C.; Markowitz, M. A.; Spector, M. S.; Gaber, B. P. *Chem. Mater.* **2001**, *13*, 4760-4766.

28. Sadasivan, S.; Khushalani, D.; Mann, S. *J. Mater. Chem.* **2003**, *13*, 1023-1029.

29. Stoeber, W.; Fink, A.; Bohn, E. *J. Colloid Interface Sci.* **1968**, *26*, 62-69.

30. Pines, A.; Gibby, M. G.; Waugh, J. S. *J. Chem. Phys.* **1973**, *59*, 569-590.

31. Peersen, O. B.; Wu, X.; Kustanovich, I.; Smith, S. O. *J. Magn. Reson. A* **1993**, *104*, 334-339.

32. Maciel, G. E.; Sindorf, D. W. *J. Am. Chem. Soc.* **1980**, *102*, 7606-7607.

33. Sindorf, D. W.; Maciel, G. E. *J. Am. Chem. Soc.* **1983**, 105, 3767-3776.

34. Maciel, G. E. In *Encyclopedia of Nuclear Magnetic Resonance*; Grant, D. M., Harris, R. K., Eds.; John Wiley & Sons Ltd: Chichester, 1996; Vol. 7, pp 4370-4386.

35. Engelhardt, G.; Michel, D. *High-Resolution Solid-State NMR of Silicates and Zeolites*; John Wiley & Sons: Chichester, 1987.

36. Lindner, E.; Schneller, T.; Auer, F.; Mayer, H. A. *Angew. Chem., Int. Ed. Engl.* **1999**, *38*, 2155-2174.

37. Gulik, A.; Delacroix, H.; Krischner, G.; Luzzati, V. *J. de Physique II* **1995**, *5*, 445-464.

38. Cai, Q.; Luo, Z.-S.; Pang, W.-Q.; Fan, Y.-W.; Chen, X.-H.; Cui, F.-Z. *Chem. Mater.* **2001**, *13*, 258-263.

CHAPTER 3. TUNING OF PARTICLE MORPHOLOGY AND PORE PROPERTIES IN MESOPOROUS SILICAS WITH MULTIPLE ORGANIC FUNCTIONAL GROUPS

Seong Huh, Jerzy W. Wiench, Brian G. Trewyn, Seahn Song, Marek Pruski, and Victor S.-Y. Lin

Abstract

A synthetic method has been developed that can control both multifunctionalization and morphology of the mesoporous organic/inorganic hybrid materials by introducing different molar ratios of organoalkoxysilane precursors to a base-catalyzed co-condensation of silicate.

Introduction

Recent advances in synthesizing organically functionalized mesoporous silica materials[1] have highlighted the promising potential of utilizing these materials as building blocks to construct multifunctional microdevices for selective catalysis,[1b,2] adsorption,[3] and sensor[4] applications. Further progress in such applications will rely on the ability to tune the extent of functionalization with multiple organic moieties and to control the particle morphology in order to direct the mass-transport properties of the resulting *organic/inorganic* hybrid materials. Morphology control of inorganic mesoporous silicas has

---

been studied intensively ever since the first report of MCMs family a decade ago. The desired particle shapes were prepared via pH control,[5] utilization of base catalysts,[7] and by the use of co-solvents,[6] e.g. in a modified Stoeber process.[6c,d] We describe herein a new approach, in which various organoalkoxysilane precursors introduced during the co-condensation reactions, rather than the co-solvents, are used for morphology control. An added advantage of this method is that it results in simultaneous anchoring of multiple functional groups to the mesopores (multifunctionalization). The roles and quantities of these moieties may be tailored independently and/or cooperatively for various applications, such as gatekeeping. To the best of our knowledge, the synthetic pathway that controls both *multifunctionalization* and *morphology* of the mesoporous organic/inorganic hybrid material has not been reported prior to this communication.

Experimental Section

The FE-SEM images of two mesoporous silicas functionalized through the introduction of 3-[2-(2-aminoethylamino)ethylamino]propyl (AEP) and 3-cyanopropyl (CP) as organoalkoxysilane precursors, are shown in Figure 1a and b, respectively.[8] In contrast to the pure MCM-41 synthesized under the same conditions, which exhibits irregular spherical shape,[8] monofunctionalization with AEP or CP resulted in different particle shapes and sizes, i.e., spheres with an average particle diameter ~ 3 μm and rods with an average particle size: L × W = 1 × 0.2 μm. These materials were prepared by sodium hydroxide-catalyzed condensation reactions of tetraethoxysilane (TEOS) with AEP-trimethoxysilane (AEPTMS) or CP-triethoxysilane (CPTES), in the presence of a low concentration of cetyltrimethylammonium bromide (CTAB) surfactant, under stirring (550 rpm) at 80 °C for 2

h. The reaction mixture molar ratio was 1.00 CTAB : 8.16 TEOS : 1.05 total

organoalkoxysilanes : 2.55 NaOH : 4857 H_2O. Surfactant-free materials were obtained with

an acid extraction.[8] The observed difference in particle morphology prompted us to

synthesize a series of bifunctional materials in which the molar ratio between the AEPTMS

and CPTES was varied systematically from 100% AEPTMS to 100% CPTES. During the

synthesis, the total amount of the organoalkoxysilanes (AEPTMS + CPTES) relative to

TEOS was fixed at the level of 12.8 mol % in all samples. In this Communication, we will

refer to the monofunctionalized microparticle (MP) as AEP-MP (CP-MP) and to the

bifunctionalized materials as AEP/CP-MP.

Results and Discussion

As depicted in Figure 1c, d, and e, the FE-SEM micrographs of the bifunctional

AEP/CP-MP materials synthesized with different molar ratios of AEPTMS/CPTES showed

only spherical particles. In contrast to the micron-sized AEP-MP, the average particle

diameters of the bifunctional AEP/CP-MP spheres decreased as the relative ratio of

AEPTMS/CPTES changed from 5/5 to 1/9. It is interesting to note that even in the 1/9 case

(1.28 mol % of AEPTMS and 11.52 mol % of CPTES, Figure 1e), no rod-like particles were

observed, which is in stark contrast with CP-MP sample (12.8 mol % of CPTES, Figure 1b).

Evidently, the presence of AEPTMS precursor in the co-condensation reaction played a

crucial role in governing the particle shape of the resulting bifunctional materials.

To investigate the influence of the organoalkoxysilanes on the pore properties and

structure, we measured the powder XRD diffraction patterns of the bifunctional samples. As

shown in Figure 2a and in the Supporting Information, the observed patterns exhibited a

strong d_{100} peak and a broad peak derived from the combination of d_{110} and d_{200} diffractions, most likely due to a disordered wormhole-like porous structure. This observed diffraction pattern is very similar to that of the AEP-MP material. Also, the TEM micrographs[8] revealed the disordered, wormhole pore structure in both AEP-MP and AEP/CP-MP. Interestingly, the XRD (Figure 2a) and TEM measurements of the CP-MP rods showed a typical MCM-41 type of hexagonal symmetry of the mesopores packed in a parallel fashion along the long axis of the rod-shaped particles. These observations provided further evidence that the sample morphology is very sensitive to the presence of AEPTMS during co-condensation. ^{13}C solid-state NMR was used to (i) obtain spectroscopic evidence for the presence of the organic functional moieties in the mesopores, (ii) confirm their chemical structure, and (iii) measure their relative concentration in bifunctionalized samples. The spectra were obtained at 9.4 T on a Varian/Chemagnetics Infinity spectrometer, using [1]H-^{13}C cross polarization with magic angle spinning (CPMAS).[9] The spectra, shown in Figure 2b, demonstrated that the mesopores were indeed functionalized as intended.

Measurements of the "build-up" of carbon magnetization during cross-polarization revealed details about the molecular motions of both functional groups and allowed to measure their relative concentration in all samples.[8] In AEP-MP, all CH_2 carbons were polarized with a time constant τ_{CH} on the order of 60 µs, which is typical for such functional groups when they are sufficiently rigid (in this case, do not undergo motions on a kHz scale). A similar time constant has been found for the C1 carbon in CP-MP. However, the evolution of resonance at 19 ppm assigned to the C2 and C3 groups in this sample involved two time constants of approximately 100 and 700 µs. This result showed that the C2-H_2 and C3-H_2 groups in CP-MP experienced increasing mobility, which weakened the [1]H-^{13}C dipolar

coupling and inhibited the cross polarization process. The τ_{CH} value of 5 ms observed for carbon C4 was consistent with the nitrile end of CP-MP being the most mobile. Our measurements also showed that in the AEP/CP-MP samples the cross polarization dynamics was the same, within the experimental error, as for the corresponding carbon species in AEP-MP and CP-MP. This allowed us to use the physical mixture of AEP-MP with CP-MP in a known molar ratio as the intensity standard for quantitative analysis of the spectra of bifunctionalized samples, which are shown in Figure 3. Two unique resonances, at around 48 ppm in AEP (carbons C4-C7) and at 120 ppm in CP (carbon C4), offered best indicators of both functionalities. The exact procedure used for quantitative measurements is described in the Supporting Information.[8]

In order to investigate the *chemical accessibility* of the organic functional groups, we examined the Cu^{2+} adsorption capacity of representative samples.[10] Because of the chelate effect of the diethylene triamine moiety of the AEP group, we anticipated significantly higher Cu^{2+} adsorption capacities for the materials with higher amount of AEP. Indeed, our results indicated that the AEP-MP and CP-MP materials showed adsorptivities of 0.284 and 0.017 $\mu mol/m^2$, respectively (Figure 4). The corresponding values for bifunctional 5/5 and 1/9 AEP/CP-MP silicas were 0.073 and 0.028 $\mu mol/m^2$. We note, however, that the Cu^{2+} adsorption capacity increased by a factor of only 2.6 between the 1/9 to 5/5 AEP/CP-MP samples, whereas solid state NMR showed an 8-fold increase of the relative AEP/CP ratio in these materials. Given that the total loading of both organic groups was fixed at 12.8 mol %, these results indicated that the chemical accessibility of organic functional groups did not increase linearly with the amount of AEP groups in bifunctional silicas. The CP

functionality, which is hydrophobic in nature, might have played an active role in decreasing the adsorption capacity per AEP group.

Conclusions

In conclusion, we have prepared a series of bifunctional mesoporous silica materials with the ability to control the particle morphology and the degree of multifunctionalization. This new synthetic approach proved useful in preparation of other bifunctionalized mesoporous materials in our laboratory. We envision that these materials could be used in selective catalysis and other applications.

Acknowledgement

52

Figure 1. FE-SEM images of (a) AEP-MP, (b) CP-MP, (c) 5/5 AEP/CP-MP (d) 3/7 AEP/CP-MP, (e) 1/9 AEP/CP-MP. Scale bar = 1 μm for all the micrographs.
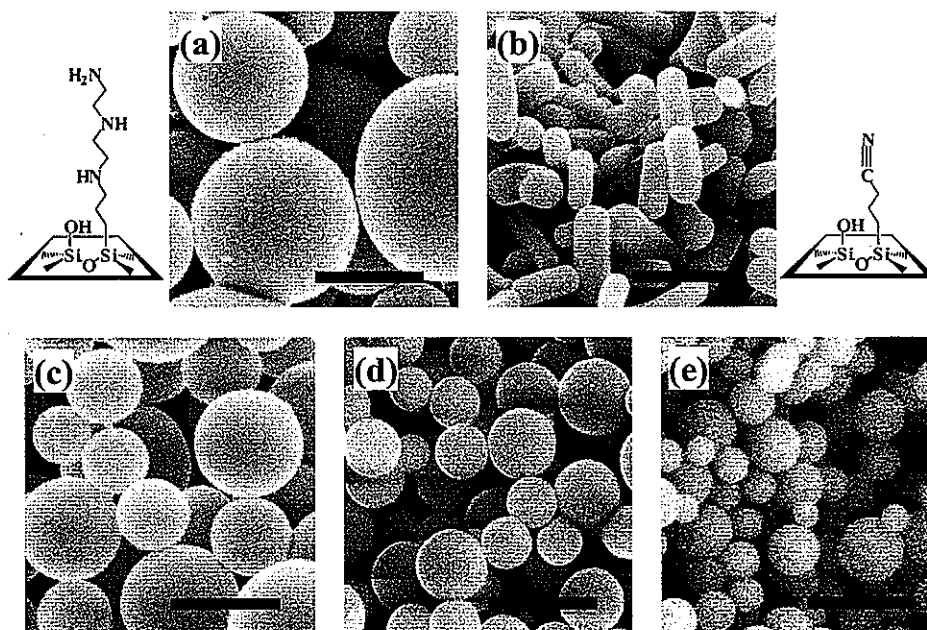
Figure 2. (a) Powder XRD diffraction patterns of bifunctional AEP/CP-MP materials synthesized with different molar ratios of AEPTMS/CPTES. (b) ^{13}C solid-state CPMAS NMR measurements of the AEP-MP (above) and CP-MP (below) materials.
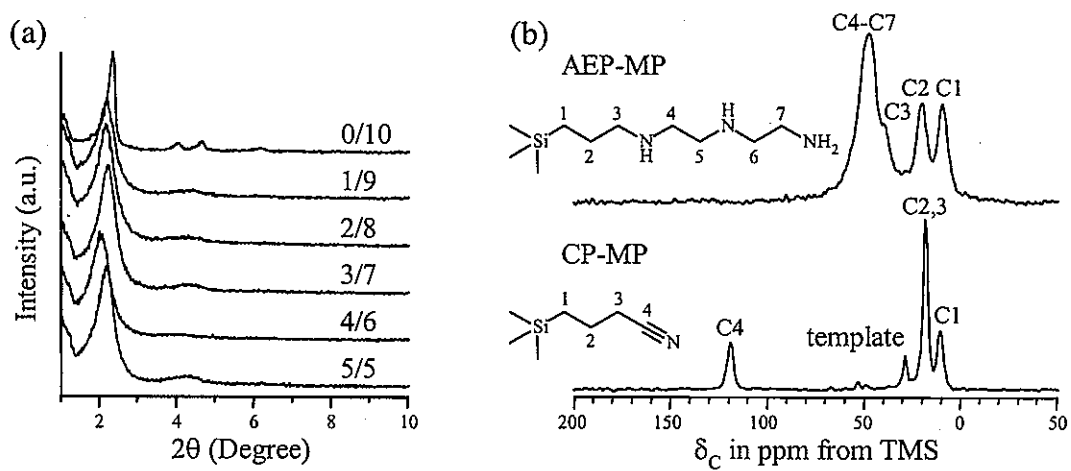
Figure 3. ^{13}C CPMAS spectra of monofunctionalized (top and bottom traces) and bifunctionalized (middle traces) AEP/CP-MP's. Arrows highlight the resonances that are unique for each species and thus were used for quantitative analysis. The numbers represent the molar ratio between two components used for preparation (left column) and obtained form analysis of NMR spectra (right column).

AEPTMS/CPTES	
prep.	NMR
0/10	0/10
1/9	1.1/8.9
2/8	1.9/8.1
3/7	2.8/7.2
4/6	4.7/5.3
5/5	4.9/5.1
10/0	10/0
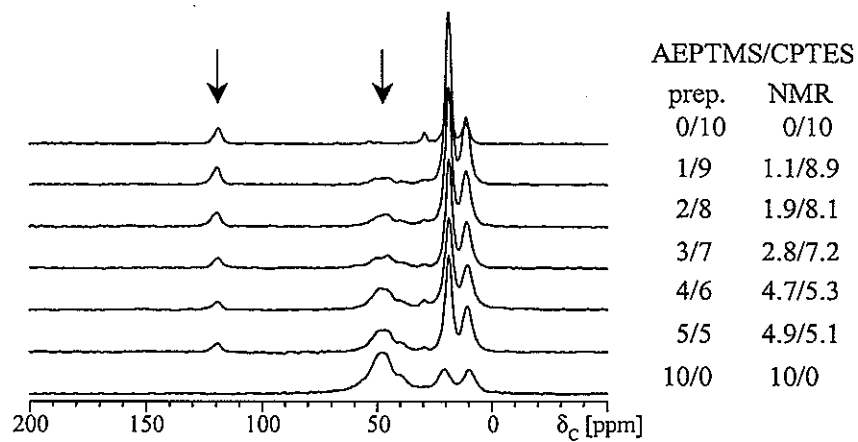
Figure 4. Diagram of Cu(II) adsorption capacity for selected samples.
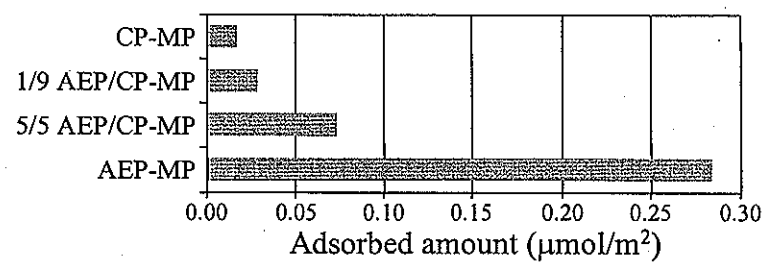
References

1. (a) M.H. Lim, C.F. Blanford and A. Stein, *J. Am. Chem. Soc.*, 1997, **119**, 4090; (b) A. Stein, B.J. Melde and R.C. Schroden, *Adv. Mater.*, 2000, **12**, 1403; (c) C.E. Fowler, S.L. Burkett and S. Mann, *Chem. Commun.*, 1997, 1769; (d) S.R. Hall, C.E. Fowler, S. Mann and B. Lebeau, *Chem. Commun.*, 1999, 201; (e) C.E. Fowler, S. Mann and B. Lebeau, *Chem. Commun.*, 1998, 1825; (f) Q. Yang, M.P. Kapoor and S. Inagaki, *J. Am. Chem. Soc.*, 2002, **124**, 9694; (g) S. Inagaki, S. Guan, T. Ohsuna and O. Terasaki, *Nature*, 2002, **416**, 304; (h) H. Fan, Y. Lu, A. Stump, S.T. Reed, T. Baer, R. Schunk, V. Perez-Luna, G.P. Lopez and C.J. Brinker, *Nature*, 2000, **405**, 56.

2. (a) V. S.-Y. Lin, D.R. Radu, M.-K. Han, W. Deng, S. Kuroki, B.H. Shanks and M. Pruski, *J. Am. Chem. Soc.*, 2002, **124**, 9040; (b) J.Y. Ying, C.P. Mehnert and M.S. Wong, *Angew. Chem., Int. Ed.*, 1999, **38**, 56; (c) A. Sayari, *Chem. Mater.*, 1996, **8**, 1840; (d) K. Moller and T. Bein, *Chem. Mater.*, 1998, **10**, 2950; (e) X. He and D. Antonelli, *Angew. Chem., Int. Ed.*, 2002, **41**, 214; (f) K. Kageyama, J.-I. Tamazawa and T. Aida, *Science*, 1999, **285**, 2113; (g) M.E. Davis, *Nature*, 2002, **417**, 813.

3. (a) S. Dai, M.C. Burleigh, Y. Shin, C.C. Morrow, C.E. Barnes and Z. Xue, *Angew. Chem., Int. Ed.*, 1999, **38**, 1235; (b) J. Brown, L. Mercier and T.J. Pinnavaia, *Chem. Commun.*, 1999, 69; (c) X. Feng, G.E. Fryxell, L.Q. Wang, A.Y. Kim, J. Liu, K.M. Kemner, *Science*, 1997, **276**, 923.

4. (a) V.S.-Y. Lin, C.-Y. Lai, J. Huang, S.-A. Song and S. Xu, *J. Am. Chem. Soc.*, 2001, **123**, 11510; (b) G. Wirnsberger, B.J. Scott and G.D. Stucky, *Chem. Commun.*, 2001, 119; (c) A.B. Descalzo, D. Jimenez, M.D. Marcos, R. Martinez-Manez, J. Soto, J. El

Haskouri, C. Guillem, D. Beltran, P. Amoros and M.V. Borrachero, *Adv. Mater.*, 2002, **14**, 966.

5. (a) H.-P. Lin and C.-Y. Mou, *Acc. Chem. Res.*, 2002, **35**, 927; (b) Q. Huo, D. Zhao, J. Feng, K. Weston, S.K. Buratto, G.D. Stucky, S. Schacht and F. Schuth, *Adv. Mater.*, 1997, **9**, 974; (c) G.A. Ozin, *Chem. Commun.*, 2000, 419.

6. (a) M.T. Anderson, J.E. Martin, J.G. Odinek and P.P. Newcomer, *Chem. Mater.*, 1998, **10**, 1490; (b) D. Zhao, J. Sun, Q. Li and G.D. Stucky, *Chem. Mater.*, 2000, **12**, 275; (c) M. Etienne, B. Lebeau and A. Walcarius, *New J. Chem.*, 2002, **26**, 384; (d) K. Schumacher, C. Du Fresne von Hohenesche, K.K. Unger, R. Ulrich, A. Du Chesne, U. Wiesner and H.W.Spiess, *Adv. Mater.*, 1999, **11**, 1194, and the references therein.

7. Q. Cai, Z.-S. Luo, W.-Q. Pang, Y.-W. Fan, X.-H. Chen and F.-Z. Cui, *Chem. Mater.*, 2001, **13**, 258.

8. See the Supporting Information for experimental details, SEM images, N_2 adsorption isotherms, pore size distributions, TEM images, and details of solid state ^{13}C and ^{29}Si NMR experiments (PDF).

9. A. Pines, M.G. Gibby and J.S. Waugh, *J. Chem. Phys.*, 1973, **59**, 569.

10. M.C. Burleigh, M.A. Markowitz, M.S. Spector and B.P. Gaber, *Chem. Mater.*, 2001, **13**, 4760.

Supporting Information of *Chem. Commun.* 2003, 2364-2365

1. Preparation of the materials

For example, 5/5 AEP/CP-MP was prepared by the following method: The mixture of CTAB (2.0 g, 5.49 mmol), 2.0 M of NaOH (aq) (7.0 mL, 14.0 mmol) and H_2O (480 g, 26.67 mol) was heated at 80 °C for 30 min. To this clear solution, TEOS (9.34 g, 44.8 mmol), AEPTMS (0.76 g, 2.88 mmol) and CPTES (0.67 g, 2.88 mmol) were added sequentially and rapidly via injection. The reaction mixture was allowed to be vigorously stirred (rpm *ca.* 550). White solids were observed within 2 min upon the mixing of the initial opaque emulsion. The reaction was further heated at 80 °C for 2 h then white solids were separated by hot filtration of the mixture giving rise to the as-made solid products. The products were washed with copious amount of water and methanol and then dried under vacuum. An acid extraction was performed in methanol (100 mL) mixture of concentrated hydrochloric acid (0.3 ~ 1.0 mL) and as-made materials (1.0 g) at 50 °C for 1.5 ~ 2 h. Resulting surfactant-removed solid products were filtered and washed with water and methanol and then dried under vacuum. The materials were dried under vacuum at 90 °C for 3 h before Cu(II) adsorption tests and solid state NMR study.

2. Cu(II) adsorption capacity test

The Cu(II) adsorption capacity tests were performed according to the literature method.[2] We used 0.01 M $Cu(NO_3)_2 \cdot 2.5H_2O$ in 0.1 M tris(hydroxymethyl)aminomethane (= Trizma, Aldrich) solution and the contact time was 1 h. The remaining amount of Cu(II) ions

---

[2] Burleigh, M. C. *et al. Chem. Mater.* **2001**, *13*, 4760-4766.

in the filtrate was measured using HP 8453 diode array UV/VIS spectrophotometer at λ_{max} = 601 nm after a centrifuge.

3. Summary of NMR measurements

3.1. Experimental

^{13}C solid-state nuclear magnetic resonance (NMR) was used to (i) obtain spectroscopic evidence for the presence of various organic functional moieties in the mesopores, (ii) confirm their structure, and (iii) measure the relative concentration of both moieties in bifunctionalized samples, whereas ^{29}Si NMR data (i) confirmed finctionalizaton of mesoporous materials with AEP and CP organic groups, (ii) provided relative concentration of T^n and Q^n groups, and (iii) imparted molecular formula of AEPMP and CP-MP samples as well as molar concentration of organic functionalities (AEP or CP) in the mesopores.

The spectra were obtained at 9.4 T on a Varian/Chemagnetics Infinity spectrometer, resonating at 100.59 (^{13}C), and 79.47 MHz (^{29}Si), equipped with a doubly tuned, 5 mm magic angle spinning (MAS) probe. ^{1}H→^{13}C variable amplitude cross polarization (CP) pulse sequence (**Fig. S1**) was used to enhance the carbon signal and the repetition rate of data acquisitions.[3] During each cross polarization period, the ^{1}H rf field was ramped between 16 and 40 kHz using 2.4 kHz increments, whereas the ^{13}C rf field was maintained at a constant level of 36 kHz. The ^{1}H rf magnetic fields of 83 kHz and 60 kHz were used for initial

---

[3] Pines, A.; Gibby, M. G.; Waugh, J. S. *J. Chem. Phys.* **1973**, *59*, 569-590; Peersen, O. B; Wu, X.; Kustanovich, I.; Smith, S. O. *J. Magn. Reson., Ser. A,* **1993**, *104*, 334-339.

excitation and decoupling, respectively. The values of ^{1}H longitudinal relaxation time T_1^H encountered in all mesoporous samples examined in this study did not exceed 1 s, which allowed for repetition time of 1.2 s to be used in the CPMAS experiments. Typically, 5 to 10K scans were accumulated using a sample rotation rate of 9 kHz.

Fig. S2 presents the ^{13}C CPMAS spectra acquired for the mesoporous materials functionalized with AEPTMS (spectrum a, AEP-MP) and CPTES (spectrum b, CP-MP). The NMR results demonstrate that the mesopores are indeed functionalized as intended. The specific resonances are assigned based on the chemical shifts found in the liquid state spectra of the analogous compounds. Carbons C1 and C2 in both samples are observed at around 10 and 20 ppm, respectively. In CP-MP, the C3 carbon resonates at 19 ppm, while in AEP-MP the corresponding line is shifted downfield to 39 ppm due to the influence of an adjacent nitrogen atom. The remaining carbon sites can serve as suitable fingerprints of both functional groups. In AEP-MP, the resonances from carbons C4-C7 are superimposed at around 48 ppm, whereas C4 carbon in CP-MP is found at 120 ppm.

For silicon measurements (see **Fig. S3**), direct polarization (DP) of ^{29}Si nuclei experiment at 10 kHz MAS was chosen, which involved single excitation 90° pulse of 2.1 μs followed by acquisition of ^{29}Si data accompanied by continuous wave (CW) decoupling of ^{1}H nuclei at 65 kHz rf power. Typically 270 repetitions were completed using pulse delay of 300 s. For additional evidence of presence of T^n groups, ^{1}H→^{29}Si CPMAS spectra were recorded under similar experimental conditions as ^{1}H→^{13}C CPMAS data, but contact time of 10 ms and 2K accumulations. Specifically the silicone groups were found at positions: -56 (T^2), -67 (T^3), -92 (Q^2), -101 (Q^3), and -110 ppm (Q^4).

3.2. Quantification of silicon groups

Quantitative measurements of various T^n and Q^n silicon groups could be achieved only by ^{29}Si DPMAS experiment. Although T_1 of ^{29}Si is typically in order of minutes, pulse delay of 300 s was chosen to assure restoration up to 99% of initial magnetization. Indeed saturation recovery experiment, completed for allyl- and 3-isocyanatopropyl- functionalized MCM-41 samples, revealed that values of T_1 relaxation time are in the order of 50 to 65 s for T^n groups and of 30 to 45 s for Q^n groups. Hence integrals of those groups, obtained from ^{29}Si DPMAS spectra, were achieved with 3 % accuracy. Following are relative concentrations, molecular formulas and molar concentration of organic moieties (± 0.05 mmol/g accuracy) in AEP-MP and CP-MP attained from ^{29}Si DPMAS experiment.

	Relative concentration of silicon groups [%]					Molecular Formula	Molar concentration of organic group [mmol/g]
	T^2	T^3	Q^2	Q^3	Q^4		
AEP-MP	1	6	3	35	55	$(SiO_2)_{100}(H_2O)_{17.5}(C_7H_{19}N_3)_7$	0.95
CP-MP	2	8	2	29	59	$(SiO_2)_{100}(H_2O)_{12.5}(C_4H_7N)_{10}$	1.44

3.4. Quantification of functional groups in bifunctionalized samples

It is noted that direct (single pulse) ^{13}C polarization is often the preferred method in applications involving quantitative measurements. We initially tried to use this method, but chose the cross-polarization (CPMAS) experiment for three reasons. First, the relaxation delays required for direct excitation were prohibitively long, on the order of several minutes. In addition, the delays would have to be measured in several samples to assure quantitative accuracy. Second, all NMR probes used in our laboratory have some level of ^{13}C

background, which interfered with the signals of interest to this study. Since most of the background originated from parts of the probe made of teflon, these unwanted signals were completely 'invisible' under the ^{1}H→^{13}C cross polarization. Another important benefit of using the CPMAS method was the observation of very different dynamic properties of AEP and CP, as described below. This discovery would not have been possible without the measurements of CPMAS dynamics.

The time evolution of each carbon magnetization during the CPMAS experiment is a result of complicated interplay between the spin-lattice relaxation processes in the rotating frame, described by relaxation time $T_{1\rho}{}^H$, and cross polarization kinetics.[4] The CP kinetics, in turn, is further influenced by sample spinning, molecular motions and sample heterogeneity. In the simplest case, for each resonance the time dependence of the ^{13}C magnetization $M_{xy}(\tau)$ during the cross-polarization contact is given by

$$M_{xy}(\tau) = M_0 \lambda^{-1} \left(1 - \exp\left[-\lambda \frac{\tau}{\tau_{CH}} \right] \right) \times \exp\left(-\frac{\tau}{T_{1\rho}^H} \right) \tag{1}$$

where M_0 is the carbon equilibrium magnetization, τ is the CP contact time, τ_{CH} is the time CP constant for a given species and of $\lambda = 1 - \tau_{CH}/T_{1\rho}{}^H$. In general, a wide range of τ_{CH} and $T_{1\rho}{}^H$ times can exist in molecular systems with different ^{13}C-^{1}H distances and/or in the presence of internal motion. MAS introduces additional time dependencies to homo- and heteronuclear dipolar Hamiltonians and further complicates the polarization transfer.

---

[4] M. Mehring, *'Principles of High Resolution NMR in Solids'*, 2nd edn., Springer, Berlin, 1983, Chapter 4.

In this study, we measured separately the 'build-up' of a carbon magnetization during spin-lock for the mesoporous materials mono-functionalized with AEPTMS and CPTES. By fitting the experimental data using equation (1), we obtained the values of M_0, as well as the $T_{1\rho}^H$ and τ_{CH} times for all carbons in these samples. The results of Table S1 show that the values of τ_{CH} found for CH_2 groups in AEP-MP are on the order of 60 μs, which is consistent with the literature data for such groups in rigid molecules. A similar time constant has been found for the C1 carbon in CP-MP. However, the evolution of resonance at 19 ppm in this sample involved two time constants of approximately 100 and 700 μs. This result shows that the C2-H_2 and C3-H_2 groups in CP-MP experience increasing mobility, which weakens the dipolar coupling between ^1H and ^{13}C nuclei and inhibits the CP process. The τ_{CH} value of 5 ms observed for carbon C4 is consistent with the nitrile end of CPTES being the most mobile.

The standard strategy for measuring the relative concentrations using CPMAS involves fitting the build-up curves to obtain the values of M_0 for different ^{13}C resonance lines. However, our measurements showed that in the bifunctionalized AEP/CP-MP samples studied in this work the relaxation parameters were the same, within the experimental error, as for the corresponding carbon species in the samples containing only one type of moieties. This allowed us to avoid measuring the build-up curves. Instead, we prepared the physical mixture of AEP-MP with CP-MP in a known molar ratio of 6.9:3.1, and used it as intensity standard for the bifunctionalized samples, which were measured under identical conditions. The studies were performed using resonances at 48 and 120 ppm for AEP-MP and CP-MP, because they were easily distinguishable in the corresponding spectra. Due to significant

differences in the polarization dynamics between these two resonances (see **Fig. S4**), the spectra were collected using two different contact times of 0.4 and 2 ms, which favored one of the species involved at a time, and added before the final analysis. The resonances of our interest were then integrated and referred to the known standard in order to obtain the relative concentration of each species (see **Table S2**).

Fig. S1. Pulse scheme used in the $^1H \rightarrow ^{13}C$ variable amplitude cross polarization (CP) experiment.
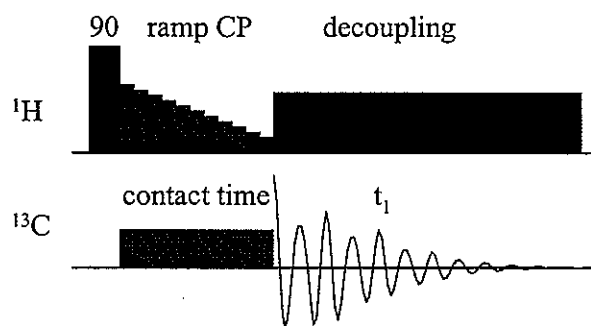
Fig. S2. $^1H \rightarrow ^{13}C$ CPMAS spectra obtained for functionalized mesoporous materials with AEPTMS (a) and CPTES (b) using CP contact times 0.2 and 5 ms, respectively.
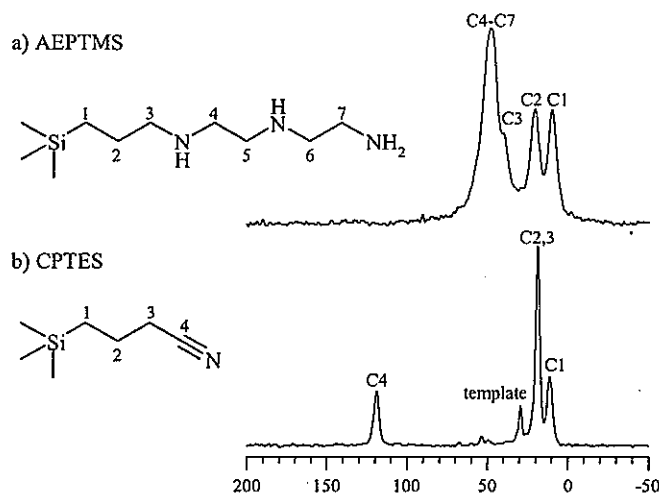
Fig. S3. ^{29}Si DPMAS (left column) and ^{1}H→^{29}Si CPMAS (right column) spectra obtained for functionalized mesoporous materials with AEPTMS (a) and CPTES (b).
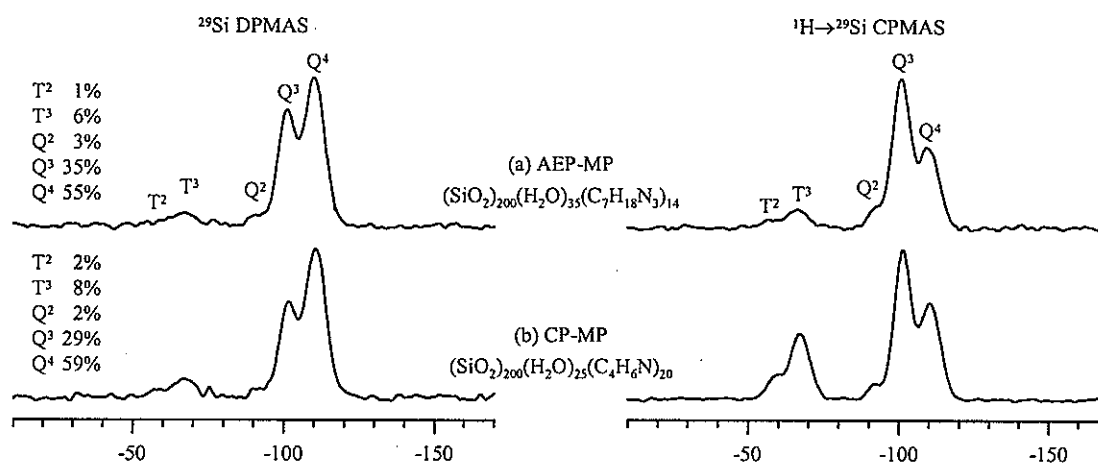
Table S1. Values of T_{CP} and $T_{1\rho}^{H}$ obtained for functionalized mesoporous samples from the analysis of ^{13}C cross polarization 'build-up' curves.

	AEPTMS				CPTES			
Peak [ppm]	48	39	20	9	119	19	19	11
τ_{CH} [µs]	50	110	60	45	5000	700	100	60
$T_{1\rho}^{H}$ [ms]	0.9	0.4	0.9	1.1	5.8	4	48	20

Fig. S4. 'Build-up' of carbon magnetization during spin-locking for the resonance lines at 48 ppm in AEP-MP (◊) and 119 ppm in CP-MP (O) fitted using equation 1 (solid lines). Dashed lines reveal contact times selected for the quantitative measurements (see text).
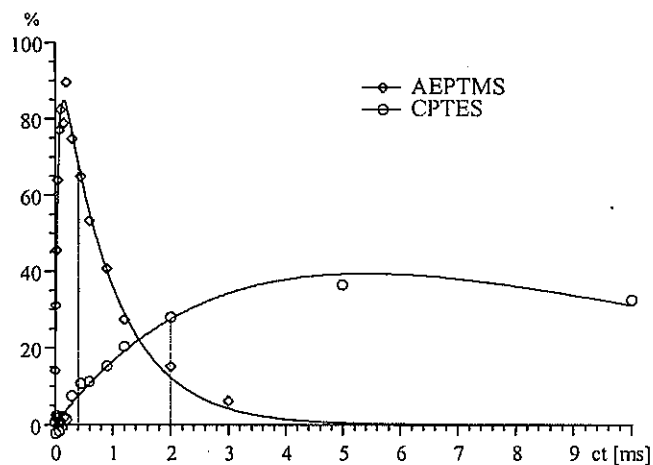
Table S2. Molar ratios of two components used for preparation of AEP/CP-MP materials and the relative concentrations of both moieties obtained from ^{13}C CPMAS spectra.

AEPTMS:CPTES	
prep.	NMR
1:9	1.1:8.9
2:8	2.0:8.0
3:7	2.9:7.1
4:6	4.7:5.3
5:5	5.0:5.0

Fig. S5. FE-SEM images of monofunctional materials (Hitachi S4700).

(a) AEP-MP
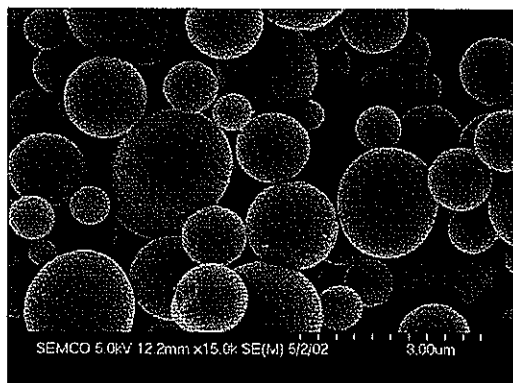
(b) CP-MP
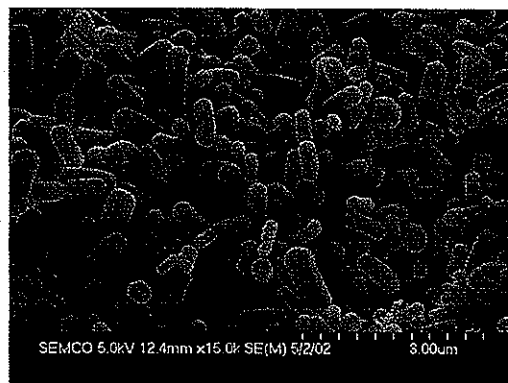
Fig. S6. FE-SEM images of bifunctional materials (Hitachi S4700).

(a) 5/5 AEP/CP-MP
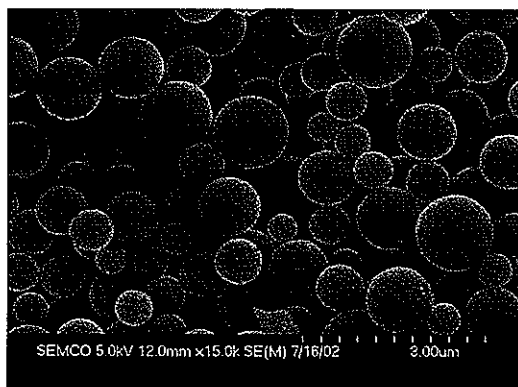
(b) 4/6 AEP/CP-MP
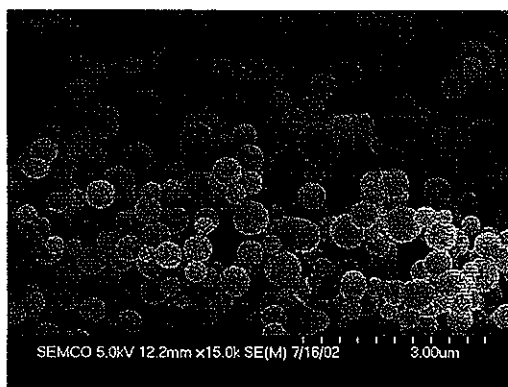
(c) 3/7 AEP/CP-MP
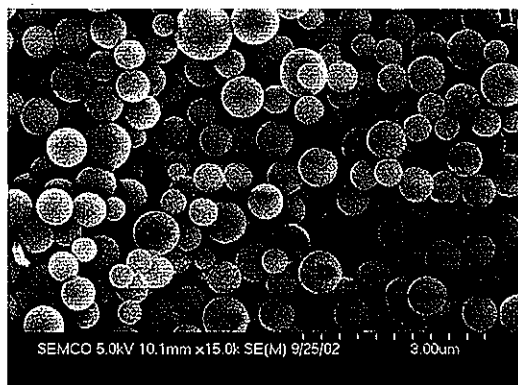
(d) 2/8 AEP/CP-MP
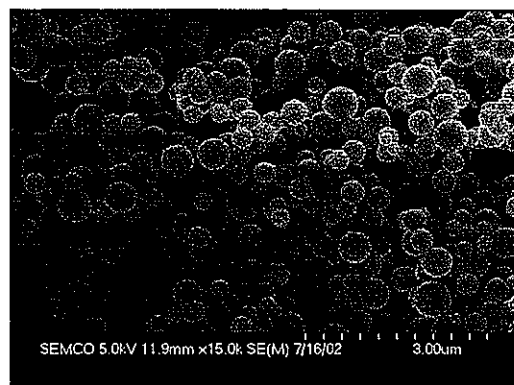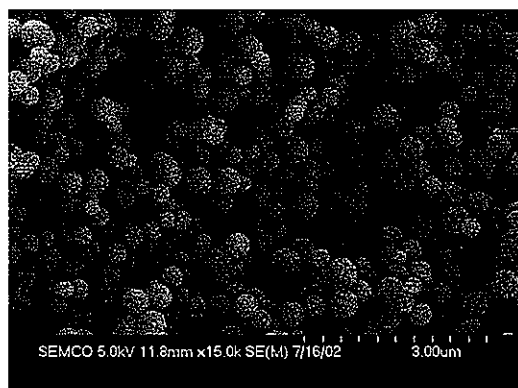
(e) 1/9 AEP/CP-MP

(f) Pure MCM-41
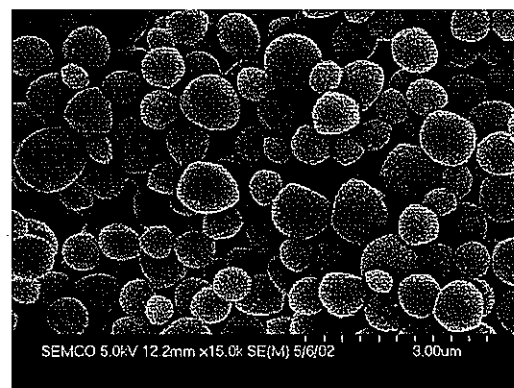
Fig. S7. TEM images of the selected materials.

(a) AEP-MP (Ultramicrotomed)
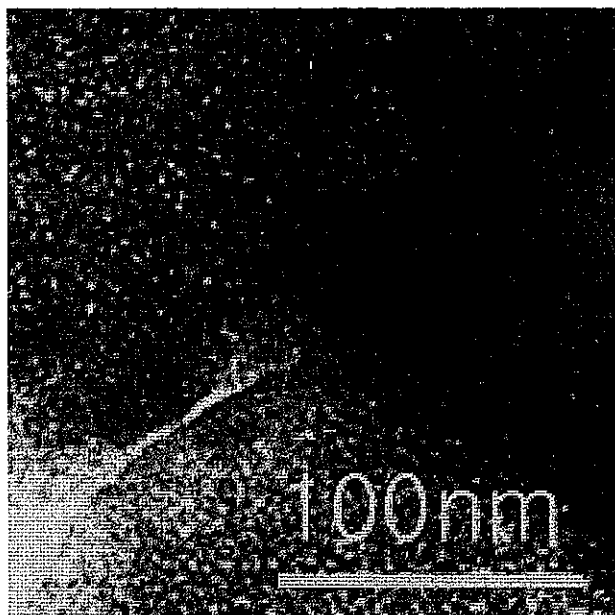
(b) CP-MP
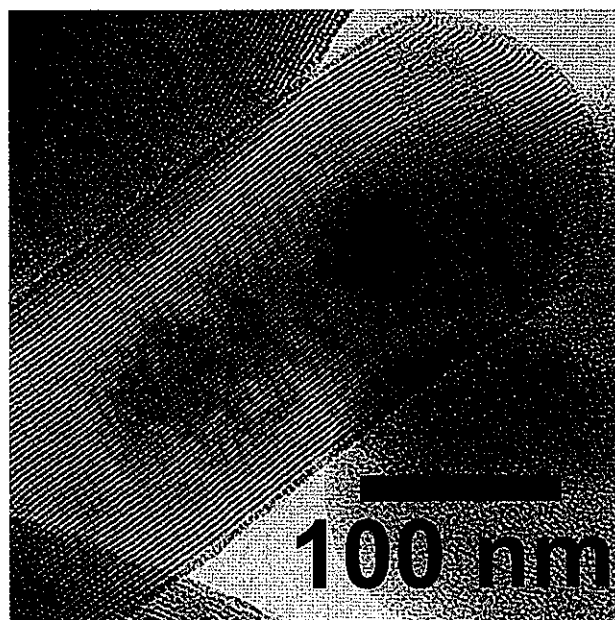
(c) 5/5 AEP/CP-MP (Ultramicrotomed)
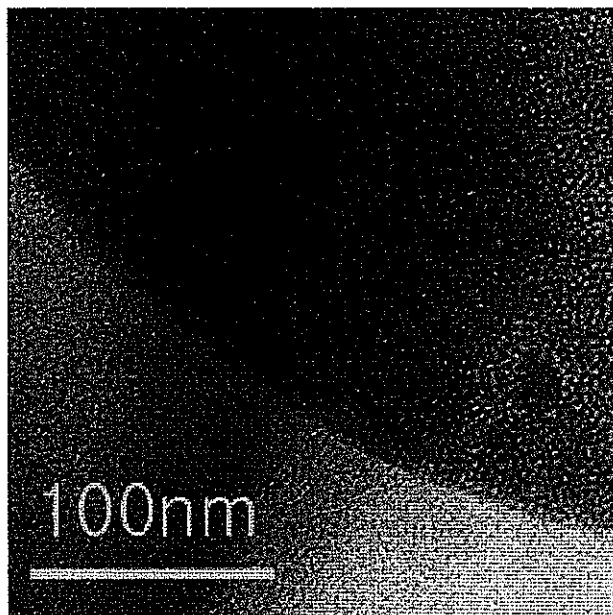
(d) 1/9 AEP/CP-MP (Ultramicrotomed)
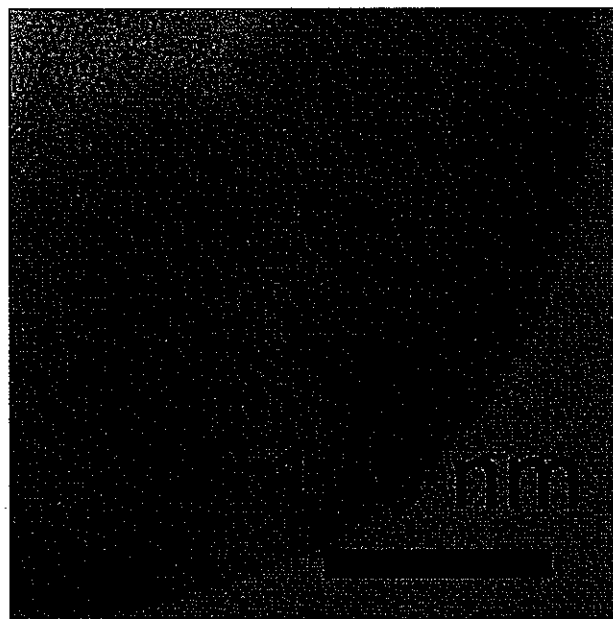
Table S3. Textural properties of the surfactant-free materials.

Sample	d_{100} (Å)	a_0 (Å)	S_{BET} (m^2/g)	V_p (cm^3/g)	W_{BJH} (Å)	$d_{pore\ wall}$ (Å)
5/5 AEP/CP-MP	37.1	42.9	722.2	0.38	-	-
4/6 AEP/CP-MP	42.1	48.6	822.6	0.51	26.4	22.2
3/7 AEP/CP-MP	38.1	44.0	980.8	0.56	26.4	17.6
2/8 AEP/CP-MP	37.4	43.2	801.4	0.43	20.5	22.7
1/9 AEP/CP-MP	36.5	42.2	966.6	0.51	20.7	21.5

Fig. S8. PXRD data of as-made materials.
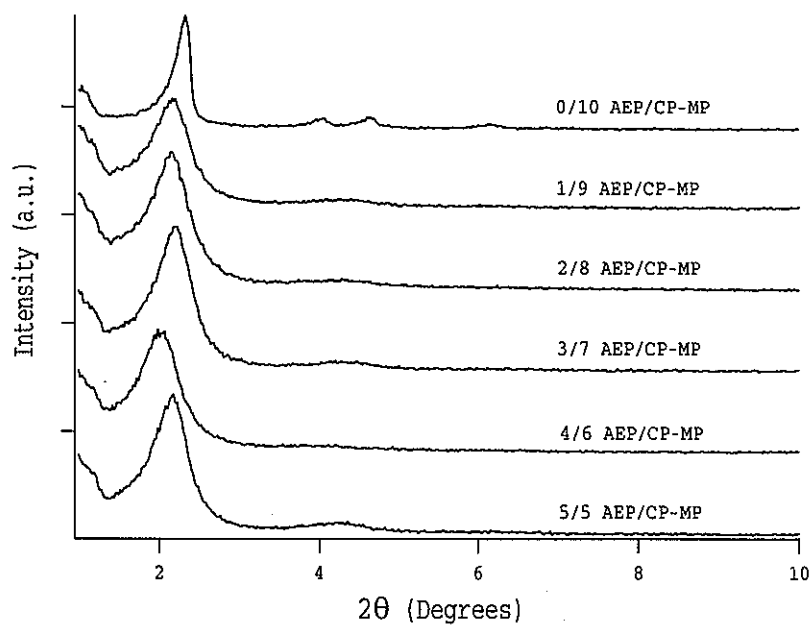
Fig. S9. BET isotherms and pore size distribution curves.

(a) 5/5 AEP/CP-MP
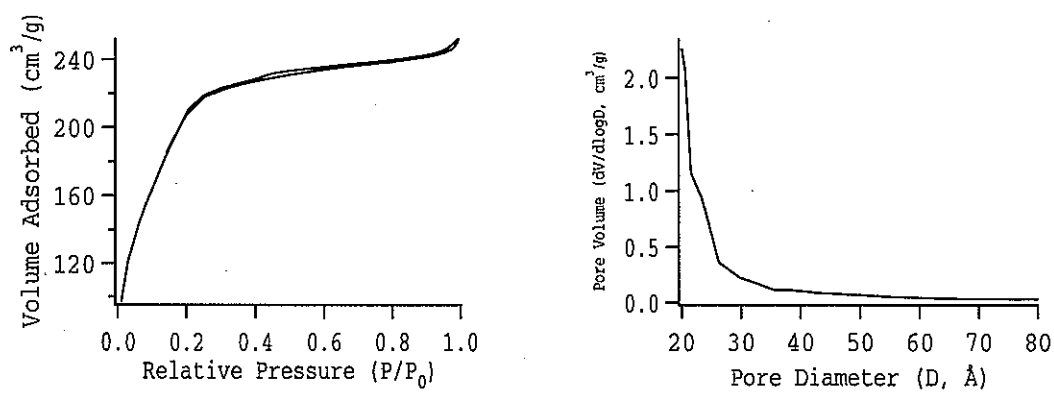
(b) 4/6 AEP/CP-MP
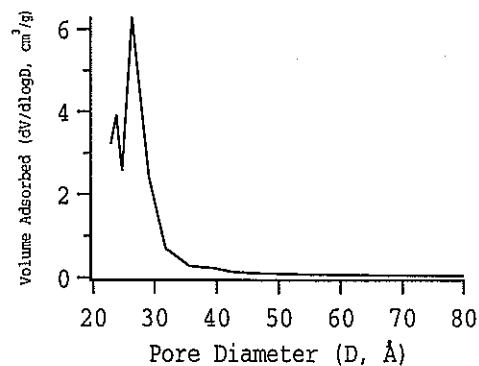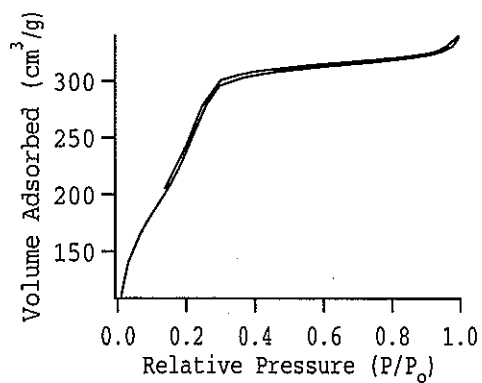
(c) 3/7 AEP/CP-MP
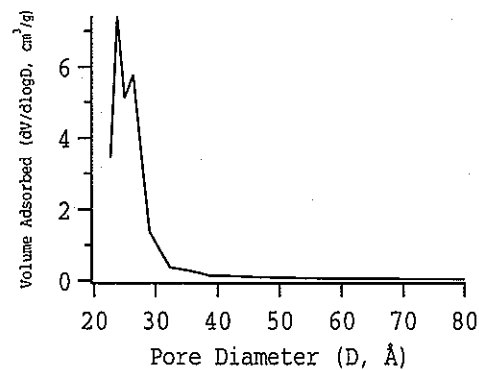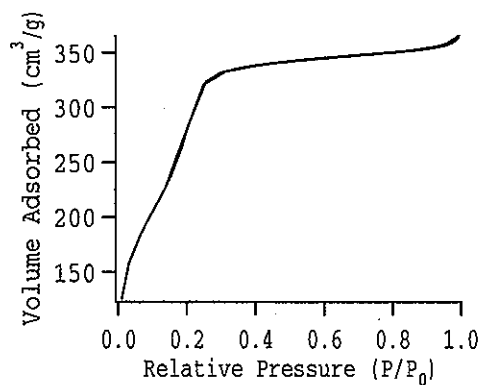
(d) 2/8 AEP/CP-MP
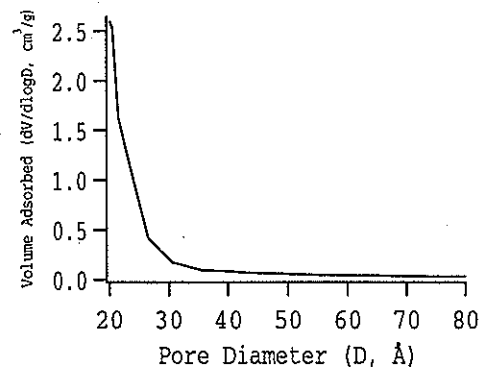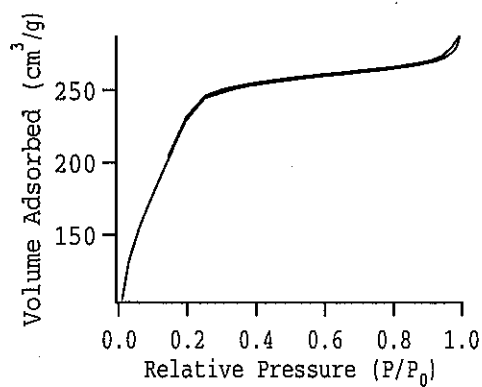
(e) 1/9 AEP/CP-MP
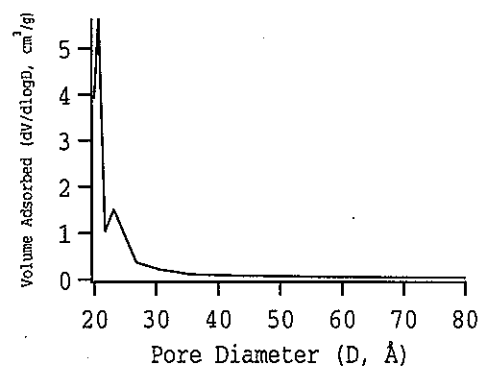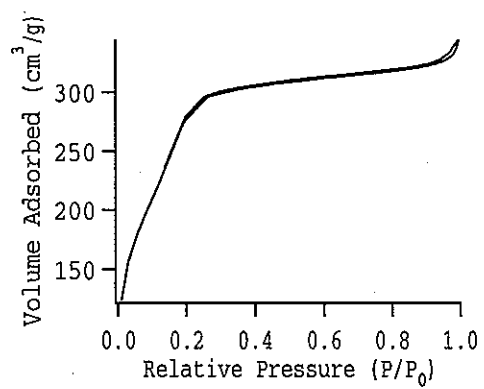
CHAPTER 4. CONTROLLING THE SELECTIVITY OF COMPETITIVE NITROALDOL CONDENSATION BY USING A BIFUNCTIONALIZED MESOPOROUS SILICA NANOSPHERE-BASED CATALYTIC SYSTEM

A paper published in *Journal of the American Chemical Society*[1]

Seong Huh, Hung-Ting Chen, Jerzy W. Wiench, Marek Pruski and Victor S. –Y. Lin

Abstract

A series of bifunctionalized mesoporous silica nanosphere-based (MSN) heterogeneouscatalysts for the nitroaldol (Henry) reaction have been synthesized. A common 3-[2-(2-aminoethylamino)ethylamino]propyl (AEP) primary group and three different secondary groups, ureidopropyl (UDP), mercaptopropyl (MP), and allyl (AL) functionalities, were incorporated to these mesoporous silica materials by introducing equal amts. of AEP-trimethoxysilane with UDP-, MP-, or AL-trialkoxysilane precursors to our previously reported co-condensation reaction. Nanospheres were prepd. by mixing the corresponding reactants in the presence of CTAB, NaOH, and H_2O and heating to 80° for 30 min; an example compound thus prepared was N-(2-aminoethyl)-N'-[3-(trimethoxysilyl)propyl]-1,2-ethanediamine polymer with silicic acid (H_4SiO_4) tetraethyl ester and [3-(trimethoxysilyl)propyl]urea. Structures and relative concentrations of the functional groups were detailed by solid-state NMR and other spectroscopic techniques. The AEP group served as a catalyst, and the other secondary groups provided different noncovalent interactions to

---

reactants and thereby controlled the reaction selectivity. By varying the secondary group in these bifunctionalized MSN catalysts, the selectivity of a nitroaldol reaction of two competing benzaldehydes reacting with nitromethane was investigated by measuring the molar ratio of the nitroalkene products. The selectivity of the bifunctionalized MSN catalysts could be systematically tuned simply by varying the physicochemical properties of the pore surface-bound secondary groups, i.e., polarity and hydrophobicity.

Introduction

Recent progress in functionalization of MCM and SBA types of mesoporous silicas with catalytically active groups has highlighted the potential of utilizing these structurally uniform materials as a new generation of heterogeneous catalysts with high selectivity. Several previous studies[1] involved immobilization of single-site catalysts, such as transition metal complexes and Lewis or Brönsted acids and bases, onto the mesopore surfaces. However, in contrast to zeolite-based catalysts, which utilize the "shape/size selective cavity effect",[2] the selectivity of mesoporous silica-based systems was mainly controlled by the intrinsic coordination environment of the heterogenized catalytic group. The mesoporous silica itself served only as an inert supporting matrix with large surface area, whose chemical and geometric properties were often not utilized.[1a,c,g,3]

We recently reported a new synthetic method based on co-condensation, which allowed us to functionalize mesoporous silica materials with multiple organic groups.[4] By using this method, not only the loading of functional groups, but also the particle size and shape of the resulting mesoporous silicas could be controlled.[4] Herein we apply the same principle to synthesize a class of bifunctionalized mesoporous silica nanosphere (MSN)

materials, where one common functional group (primary group) served as a catalyst and the other functionality (secondary group) provided different non-covalent interactions to reactants and thereby controlled the reaction selectivity. By varying the secondary group in these bifunctionalized MSN catalysts, we investigated the selectivity of a nitroaldol (Henry) reaction of two competing benzaldehydes reacting with nitromethane by measuring the molar ratio of the nitroalkene products as depicted in Figure 1. To the best of our knowledge, this is the first demonstration of utilizing multi-functionalized mesoporous silicas as heterogeneous catalysts to control the selectivity of a competitive organic reaction.

Experimental Section

The bifunctionalized MSN materials with a common 3-[2-(2-aminoethylamino)ethylamino]propyl (AEP) group and three different secondary groups, ureidopropyl (UDP), mercaptopropyl (MP), and allyl (AL) functionalities, were synthesized by introducing equal amounts of AEP-trimethoxysilane with UDP-, MP- or AL-trialkoxysilane precursors to our co-condensation reaction.[4a,b] A monofunctionalized MSN with only AEP group incorporated inside the mesoporous silica framework was also synthesized via the same method.[4a]

Results and Discussion

Despite of a variation in the particle sizes, all of the organically functionalized MSNs exhibited the same spherical particle shape (Figure 2). The XRD measurements showed large (100) peaks and broad higher diffraction patterns in all samples, typical of disordered porous structure.[5] The observed d_{100} values ranged between 38.4 Å for sample AEP/AL-MSN and

41.7 Å for sample AEP/UDP-MSN. The TEM study of these materials further confirmed their disordered channel structure (Figure 2e).[5]

The N_2 surface sorption analyses of these mono- and bi-functionalized MSNs showed typical type IV BET isotherms.[5] The measured BET surface areas of AEP-MSN, AEP/UDP-MSN, AEP/MP-MSN, and AEP/AL-MSN are 805.8, 759.6, 778.7 and 703.5 m^2/g, respectively. Interestingly, the BJH pore distributions of the MSNs functionalized with hydrophilic organic groups, i.e., AEP-MSN and AEP/UDP-MSN, displayed average pore diameters of 26.0 and 22.9 Å, respectively, whereas functionalization with the hydrophobic functional groups (AEP/MP-MSN and AEP/AL-MSN) resulted in smaller mean pore diameters of ca. 15 Å, as evidenced by the TEM images.[5]

The structures of organic functional groups in the mesopores, their relative concentrations, and the overall surface coverages were scrutinized by ^{29}Si MAS, ^{29}Si CPMAS and ^{13}C CPMAS solid-state NMR spectroscopy.[5] The ^{29}Si and ^{13}C NMR spectra confirmed the successful functionalization of MSNs. The resulting materials were surfactant-free. The ^{29}Si resonances were observed at positions typical of silicon groups Q^n (($\equiv$SiO)$_n$Si(OH)$_{4-n}$, where n is 2, 3, or 4) and T^n (($\equiv$SiO)$_n$Si(OH)$_{4-n}$R, where n is 2 or 3).[5,6] The ^{13}C peaks (Figure 3) were assigned based on the solution spectra of the corresponding precursors and on our earlier study of AEP-, AL- and UDP-MSN's.[4a] Also detailed in the Supporting Information are the quantitative ^{13}C and ^{29}Si measurements, which showed that all MSNs contained approximately equal total amounts of organic functional groups (1.0 mmol/g in AEP/UDP-MSN, 1.4 mmol/g in AEP/MP-MSN and 1.3 mmol/g in AEP/AL-MSN). This corresponded to 15%, 25% and 23%, respectively, of surface silicon atoms being involved in Si-C bonds. Furthermore, the relative molar concentrations between AEP and the

secondary groups were very similar (1.17, 1.04 and 1.13 for AEP/UDP-MSN, AEP/MP-MSN and AEP/AL-MSN).[5]

As demonstrated in recent literature reports,[7] MCM-41 silicas grafted with amines or polyamines could effectively catalyze nitroaldol reactions to produce nitroalkenes in high yields, whereas the pure inorganic MCM-41 silica gave rise to only small amounts of β-nitroalcohol intermediates. To investigate how the secondary functional groups of our bifunctionalized MSN catalysts could influence the reaction selectivity, three series of competitive nitroaldol reactions were performed by introducing equal molars of 4-hydroxybenzaldehyde (1) and one of the three different alkoxybenzaldehydes (2, 3 and 4) to nitromethane solutions of a chosen bifunctional MSN. By analyzing the molar ratios between products (10/9, 11/9, and 12/9), we observed that the mono-functionalized AEP-MSN and the hydrophilic bi-functionalized AEP/UDP-MSN catalysts did not show any reaction selectivity for all three combinations of the reactants as shown in Figure 4 and the Supporting Information. However, an increase of reaction selectivity towards the nonpolar and more hydrophobic alkoxybenzaldehyde reactants (2, 3, and 4) was clearly observed in the cases of AEP/MP-MSN and AEP/AL-MSN catalysts, where the catalytic AEP groups are situated in mesopores decorated with hydrophobic groups. The hydrophobic nature of MP and AL is corroborated by the low dielectric constants of propanethiol (5.94) and propene (2.14) around room temperature.[5] The AEP/AL-MSN displayed the highest reactant selectivity toward alkoxybenzaldehydes. For example, a molar product ratio (12/9) of 2.58 (Figure 4) was reached when 4-n-octyloxybenzaldehyde (4) was used in competition with 4-hydroxybenzaldehyde (1) indicating the high selectivity of AEP/AL-MSN catalyst toward the nonpolar reactant. The results suggested that the hydrophobic secondary groups (MP and

AL) played a significant role in preferentially allowing the more hydrophobic reactants to penetrate into the mesopores and react with the AEP functionality. To demonstrate this hydrophobic solvation effect, 1 mmol of reactants 1 and 4 were introduced to 1 mL of propanethiol to simulate the penetration/dissolution of these substituted benzaldehydes with different polarities[5] into the mercaptopropyl-functionalized mesopores. The fact that the more polar reactant 1 was insoluble in propanethiol, whereas compound 4 was completely miscible with propanethiol, indicated that the selectivity of our catalysts most likely originated from the variation of the physicochemical properties of the bifunctionalized mesopores, *i.e.* polarity and hydrophobicity.

Figure 1. Competitive nitroaldol reaction. Reaction condition: 50 mg MSN catalyst, 10 mL CH_3NO_2, 5.0 mmol aldehydes, 263 K for 24 h.

$R = -CH_2CH_2CH_2NHCONH_2$ (UDP)
$-CH_2CH_2CH_2SH$ (MP)
$-CH_2CH=CH_2$ (AL)
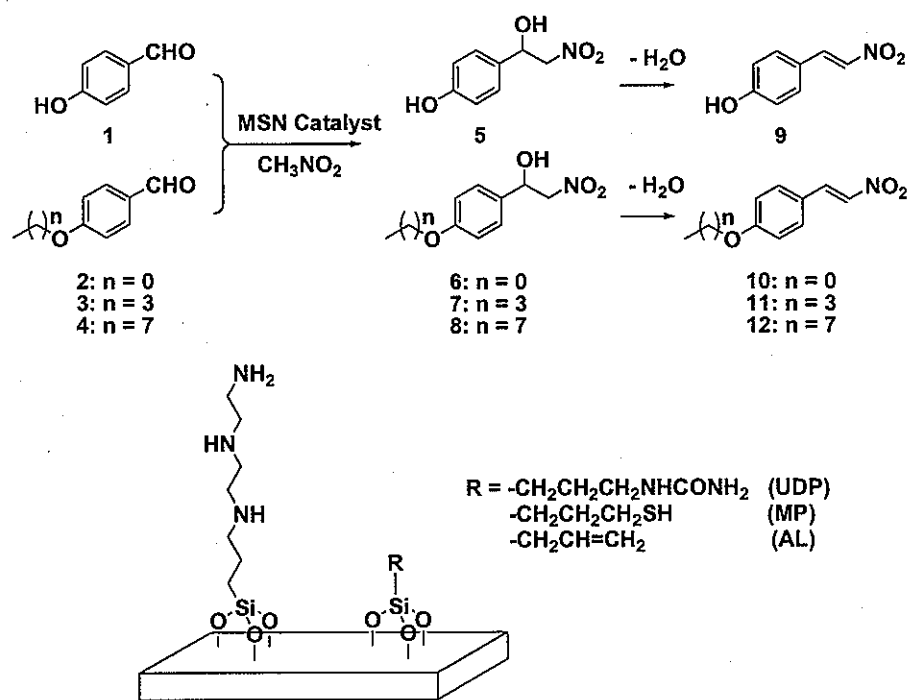
Figure 2. FE-SEM images of (a) AEP/UDP-MSN (0.7~1.3 µm), (b) AEP/MP-MSN (0.7~1.6 µm), (c) AEP/AL-MSN (0.2~0.7 µm), and (d) AEP-MSN (0.8~2.1 µm). TEM micrograph of the ultramicrotomed sample (60 to 90 nm thickness) of AEP/AL-MSN (e). Scale bar is 3 µm for the (a-d) micrographs and 100 nm for the (e) micrograph.
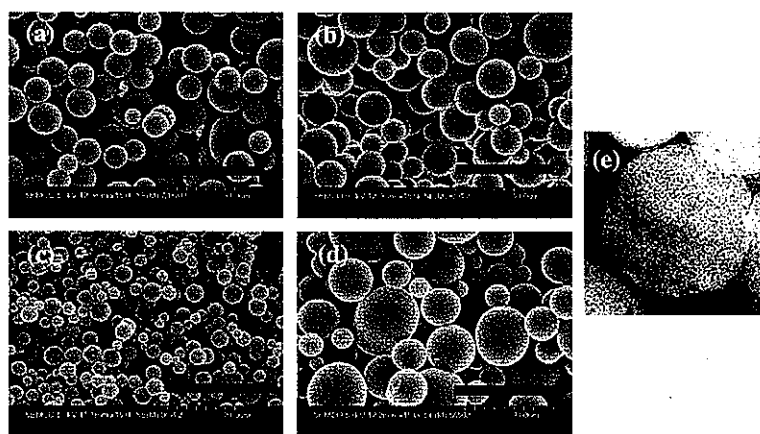
Figure 3. ^{13}C CPMAS spectra of (a) AEP, (b) AEP/UDP, (c) AEP/MP, (d) AEP/AL-MSN. Only the resonances due to secondary groups are marked in spectra (b)-(d).
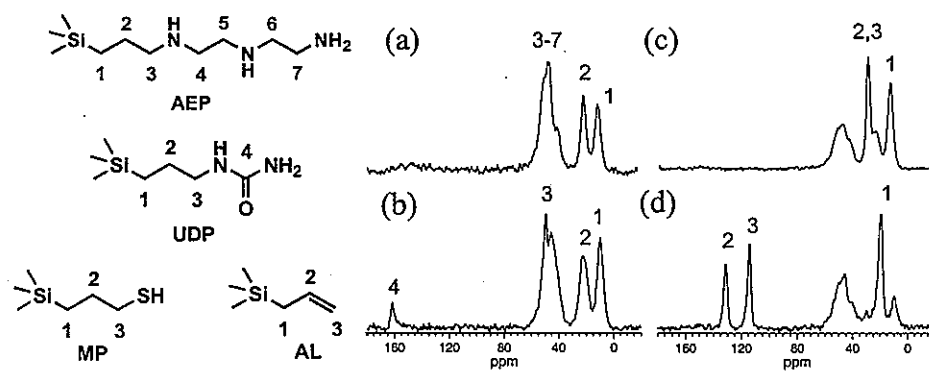
Figure 4. Histogram of the competitive nitroaldol reactions. Blue bars: Yield of **9** (mmol); Red bars: Yield of **10, 11,** or **12** (mmol); White bars: Molar ratio of products (**10/9, 11/9,** or **12/9**). Series 1, 2, and 3 are experiments conducted with reactants **1 & 2, 1 & 3,** and **1 & 4,** respectively.
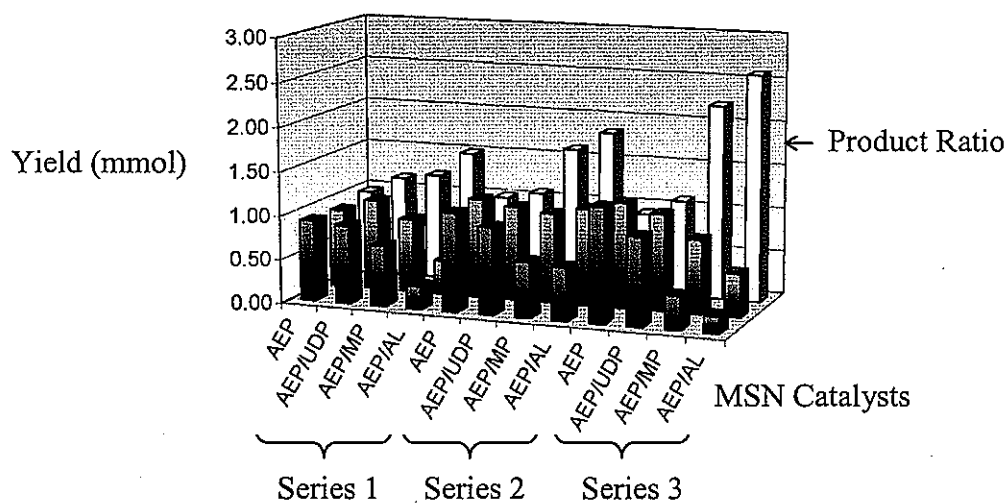
References

1. (a) Clark, J. H. *Acc. Chem. Res.* **2002**, *35*, 791-797. (b) Davis, M. E. *Nature (London)* **2002**, *417*, 813-821. (c) Corma, A.; Garcia, H. *Chem. Rev.* **2003**, *103*, 4307-4365. (d) Ying, J. Y.; Mehnert, C. P.; Wong, M. S. *Angew. Chem., Int. Ed. Engl.* **1999**, *38*, 56-77. (e) Mehnert, C. P.; Weaver, D. W.; Ying, J. Y. *J. Am. Chem. Soc.* **1998**, *120*, 12289-12296. (f) Liu, Y.; Pinnavaia, T. J. *J. Am. Chem. Soc.* **2003**, *125*, 2376-2377, and the references therein.

2. (a) Flanigen, E. M.; Bennett, J. M.; Grose, R. W.; Cohen, J. P.; Patton, R. L.; Kirchner, R. M.; Smith, J. V. *Nature (London)* **1978**, *271*, 512-516. (b) Dubbeldam, D.; Calero, S.; Maesen, T. L. M.; Smit, B. *Angew. Chem., Int. Ed. Engl.* **2003**, *42*, 3624-3626.

3. (a) Jones, M. D.; Raja, R.; Thomas, J. M.; Johnson, B. F. G.; Lewis, D. W.; Rouzaud, J.; Harris, K. D. M. *Angew. Chem., Int. Ed. Engl.* **2003**, *42*, 4326-4331. (b) Kageyama, K.; Tamazawa, J.-I.; Aida, T. *Science (Washington, D. C.)* **1999**, *285*, 2113-2115.

4. (a) Huh, S.; Wiench, J. W.; Yoo, J.-C.; Pruski, M.; Lin, V. S. Y. *Chem. Mater.* **2003**, *15*, 4247-4256. (b) Huh, S.; Wiench, J. W.; Trewyn, B. G.; Song, S.; Pruski, M.; Lin, V. S. Y. *Chem. Commun.* **2003**, 2364-2365. (c) Lai, C.-Y.; Trewyn, B. G.; Jeftinija, D. M.; Jeftinija, K.; Xu, S.; Jeftinija, S.; Lin, V. S. Y. *J. Am. Chem. Soc.* **2003**, *125*, 4451-4459. (d) Lin, V. S. Y.; Radu, D. R.; Han, M.-K.; Deng, W.; Kuroki, S.; Shanks, B. H.; Pruski, M. *J. Am. Chem. Soc.* **2002**, *124*, 9040-9041. (e) Lin, V. S. Y.; Lai, C.-Y.; Huang, J.; Song, S.-A.; Xu, S. *J. Am. Chem. Soc.* **2001**, *123*, 11510-11511.

5. See Supporting Information for details.

6. Maciel, G. E. In *Encyclopedia of Nuclear Magnetic Resonance*; Grant, D. M., Harris, R. K., Eds.; John Wiley & Sons Ltd: Chichester, 1996; Vol. 7, pp 4370-4386.

7. (a) Kantam, M. L.; Sreekanth, P. *Catal. Lett.* **1999**, *57*, 227-231. (b) Demicheli, G.; Maggi, R.; Mazzacani, A.; Righi, P.; Sartori, G.; Bigi, F. *Tetrahedron Lett.* **2001**, *42*, 2401-2403.

1. Synthesis of mono- and bi-functionalized MSN materials
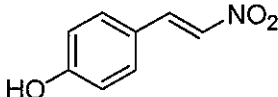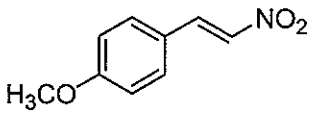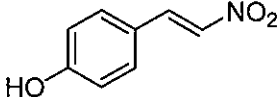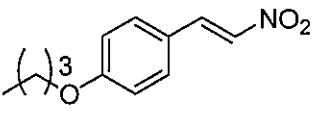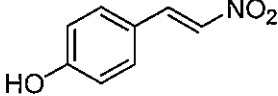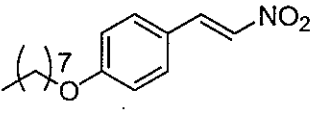
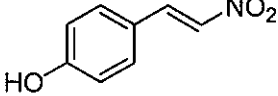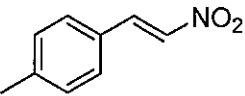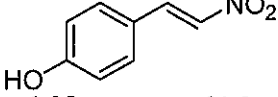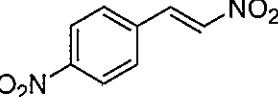The functionalized materials were synthesized via the previously described co-condensation reaction.[1,2] An example of the specific procedure, used for preparation of bifunctionalized MSN materials, such as AEP/UDP-MSN material which has equimolar ratio of 3-[2-(2-aminoethylamino)ethylamino]propyl (AEP) and 3-ureidopropyl (UDP) groups, is given below. A mixture of CTAB (2.0 g, 5.49 mmol), 2.0 M of NaOH (aq) (7.0 mL, 14.0 mmol) and H_2O (480 g, 26.67 mol) was heated at 80 °C for 30 min. To this clear solution, TEOS (9.34 g, 44.8 mmol), AEPTMS (0.76 g, 2.88 mmol), and UDPTMS (0.64 g, 2.88 mmol) were added rapidly and sequentially via injection, yielding an opaque reaction mixture. The white solid products of synthesis were observed after vigorous (550 rpm) stirring of the mixture for ~2 min. The as-synthesized bifunctionalized mesoporous materials were obtained after additional 2 hours of heating at 80 °C, followed by hot filtration, washing with copious amount of water and methanol, and drying under vacuum. An acid extraction of the CTAB surfactant was performed at 50 °C, by placing 1.0 g of the as-synthesized material in a mixture of methanol (100 mL) and hydrochloric acid (0.3 ~ 0.5 mL) for 1.5 ~ 2 h. The resulting surfactant-removed solid products were filtered and washed with water and methanol and then dried under vacuum for 3 h at 90 °C.

2. Competitive catalytic nitroaldol reactions

All the chemicals were purchased from Aldrich and used without further purification. The reaction was performed in the presence of equimolar ratio amounts of two different

aldehydes in a capped vial. Reagent grade nitromethane was used without any purification.

For example, the reaction mixture consisting of 50 mg of the mesoporous silica catalyst,

0.300 g (2.5 mmol) of p-tolualdehyde and 0.305 g (2.5 mmol) of p-hydroxybenzaldehyde in

10 mL of nitromethane, was heated at 90 °C with a constant stirring for 24 h. The reaction

mixture was filtered on a glass frit and the solids were washed with chloroform. The resultant

filtrate was evaporated on a rotary evaporator. The residue was completely dissolved in a

sufficient amount of acetone-d_6. An internal standard, THF (*ca.* 10 mmol), was added into

the acetone-d_6 solution. Analysis of the product was performed by measuring ^{1}H NMR

spectra on a Bruker DRX400 NMR spectrometer. All combinations of two different sets of

products gave distinctive vinylic proton chemical shifts for the integrations. Assignments of

the peaks were performed by comparing the chemical shifts of the products with the

authentic samples, which were independently prepared using AEP/UDP-MSN material under

the similar reaction condition and purified by silica gel column chromatography.

Table S1. Results of competitive nitroaldol reactions by mono- and bi-functionalized MSN catalysts.

Catalyst	Product A		Product B		Product Ratio B/A
	Yield, mmol	Turnover[a]	Yield, mmol	Turnover[a]	
Series 1	(HO–C6H4–CH=CH–NO2)		(H3CO–C6H4–CH=CH–NO2)		
AEP	0.92	18.4	0.89	17.8	0.97
AEP/UDP	0.89	33.0	1.03	38.1	1.16
AEP/MP	0.69	18.9	0.84	23.0	1.22
AEP/AL	0.26	7.5	0.39	11.3	1.50
Series 2	(HO–C6H4–CH=CH–NO2)		(C3H7O–C6H4–CH=CH–NO2)		
AEP	1.12	22.4	1.13	22.6	1.01
AEP/UDP	0.99	36.7	1.07	39.6	1.08
AEP/MP	0.63	17.3	1.02	27.9	1.62
AEP/AL	0.60	17.4	1.10	31.9	1.83
Series 3	(HO–C6H4–CH=CH–NO2)		(C7H15O–C6H4–CH=CH–NO2)		
AEP	1.30	26.0	1.20	24.0	0.92
AEP/UDP	1.00	37.0	1.10	40.7	1.10
AEP/MP	0.38	10.4	0.84	23.0	2.21
AEP/AL	0.19	5.5	0.49	14.2	2.58
Series 4	(HO–C6H4–CH=CH–NO2)		(CH3–C6H4–CH=CH–NO2)		
AEP	1.37	27.4	1.08	21.6	0.79
AEP/UDP	1.11	41.1	1.03	38.1	0.93
AEP/MP	0.89	24.4	0.89	24.4	1.00
AEP/AL	0.32	9.3	0.37	10.7	1.16
Series 5	(HO–C6H4–CH=CH–NO2)		(O2N–C6H4–CH=CH–NO2)		
AEP	1.05	21.0	0.92	18.4	0.88
AEP/UDP	0.97	35.9	0.89	33.0	0.91
AEP/MP	0.65	17.8	0.69	18.9	1.06
AEP/AL	0.57	16.5	0.88	25.5	1.54

[a] Turnover = mmol product / mmol catalyst during 24 h of reaction time.

3. Summary of solid-state NMR measurements

3. 1. Experimental

Solid-state NMR spectra were obtained at 100.59 (^{13}C) and 79.47 MHz (^{29}Si) on a Varian/Chemagnetics Infinity spectrometer, equipped with a doubly tuned, 5 mm magic angle spinning (MAS) probe. Direct polarization (DP) and variable amplitude cross polarization (CP) methods were used under the conditions described earlier.[1,2] These measurements provided quantitative evidence for functionalization of the mesopores with the organic moieties and confirmed their structure. For AEP-, UDP-, AL-, AEP/UDP- and AEP/AL-MSN's, the assignments of ^{29}Si and ^{13}C NMR spectra were made following our earlier study (see Figures S1 and S2).[2] The interpretation of ^{13}C spectra of samples containing mercaptopropyl (MP-MSN and AEP/MP-MSN) was also straightforward (see Figure S1 c). We note the presence of small concentration of methoxy groups in the MP-MSN sample. Similar spectrum of MP-functionalized silica was earlier reported by Maciel et al.[3] The methods used for quantitative measurements of ^{29}Si and ^{13}C intensities are detailed in Sections 3.2 and 3.3 below. All NMR results are summarized in Table 1, which contains the relative concentrations of T^n and Q^n groups, the molar concentrations of organic functional groups and the corresponding average molecular formulae.

3.2. Quantification of silicon groups

Relative concentrations of T^n and Q^n silicon groups[4] were obtained from the analysis of ^{29}Si DPMAS spectra. In agreement with our earlier results, the measurements of T_1 relaxation in AL-MSN and 3-cyanopropyl-MSN (CP-MSN) systems, yielded T_1 values on

the order of 50 to 65 s for T^n groups and 30 to 45 s for Q^n groups.[2] Therefore, a delay of 300

s between scans has been used during the acquisition of ^{29}Si NMR spectra. The accumulation

of 270 scans yielded intensities that were accurate within ±5%.

3.3. Quantification of functional groups in bifunctionalized samples using ^{13}C NMR

Although direct polarization is the preferred method for quantitative measurements,

^{13}C intensities were compared using a CPMAS-based method. The following strategy, which

proved reliable in our earlier study,[1] was developed in order to speed up the measurements

and eliminate the probe background. In short, the time evolution of each carbon

magnetization during the CPMAS experiment is a result of complicated interplay between

the spin-lattice relaxation processes in the rotating frame, described by relaxation time $T_{1\rho}{}^{H}$,

and cross polarization kinetics described by cross polarization time τ_{CH}. For example, the

cross polarization kinetics for AEP-MSN and CP-MSN revealed different values of $T_{1\rho}{}^{H}$ and

τ_{CH} times.[1] The AEP moieties were rigidly bound with τ_{CH} values on the order of 60 μs for

all carbons. For the CP groups, τ_{CH} values increased from 60 μs at the point of attachment to

the surface (carbon C1) to 5 ms for the nitrile carbon (C4), which reflected increasing

mobility toward the end of the chain. Other samples, AL-MSN, UDP-MSN, and MP-MSN,

exhibited τ_{CH} time constants between 60 μs and 2 ms. Our measurements also showed that in

the bifunctionalized samples the relaxation parameters were the same, within the

experimental error, as for the corresponding carbon species in the samples containing only

one type of moieties. Thus, by properly measuring the spectra of known physical mixtures of

mono-functionalized samples as intensity standards, the bifunctionalized samples could be

quantitatively characterized without the tedious measurements of the ^{13}C build-up curves.[1] In case of AEP/CP-MSN, the studies were performed using resonances at 48 ppm (AEP) and 120 ppm (CP), because they were easily distinguishable in the corresponding spectra. Similar method was used in current report for AEP/UDP-, AEP/MP-, and AEP/AL-MSN systems.

Table S2. Relative concentrations of T^n and Q^n silicon groups (in %), surface coverage (*SC*, in %), molecular concentrations of organic functionalities (*MC*, in mmol/g), molecular formulae (*MF*), molar ratios in bifunctional samples, and amounts (in mmol/g) of each organic functionality derived from solid state ^{13}C CPMAS and ^{29}Si DPMAS NMR data.

Functionality	T^2	T^3	Q^2	Q^3	Q^4	*SC*	*MC*	*MF*	Ratios	Amounts
AEP [a]	1	6	3	35	55	16	1.0	$(SiO_2)_{100}(H_2O)_{17.5}(ORG)_7$ [b]		
AL [a]	3	8	1	24	64	31	1.7	$(SiO_2)_{100}(H_2O)_9(ORG)_{11}$		
MP	3	9	3	28	57	26	1.6	$(SiO_2)_{100}(H_2O)_{12.5}(ORG)_{12}$		
UDP [a]	2	4	4	38	52	13	0.9	$(SiO_2)_{100}(H_2O)_{21}(ORG)_6$		
AEP/UDP	2	5	3	36	54	15	1.0	$(SiO_2)_{100}(H_2O)_{18.5}(ORG)_7$	5.4:4.6	AEP: 0.54 UDP: 0.46
AEP/MP	2	8	2	28	60	25	1.4	$(SiO_2)_{100}(H_2O)_{12}(ORG)_{10}$	5.1:4.9	AEP: 0.71 MP: 0.69
AEP/AL	2	7	2	28	61	23	1.3	$(SiO_2)_{100}(H_2O)_{12.5}(ORG)_9$	5.3:4.7	AEP: 0.69 AL: 0.61

(a) Data taken from ref 2. (b) 'ORG' denotes the concentration of the corresponding organic moieties in each sample.

Figure S1. ^{29}Si DPMAS (left column), ^{1}H→^{29}Si CPMAS (middle column), and ^{1}H→^{13}C CPMAS (right column) spectra obtained for monofunctionalized mesoporous materials: AEP-MSN (a), AL-MSN (b), MP-MSN (c), and UDP-MSN (d).
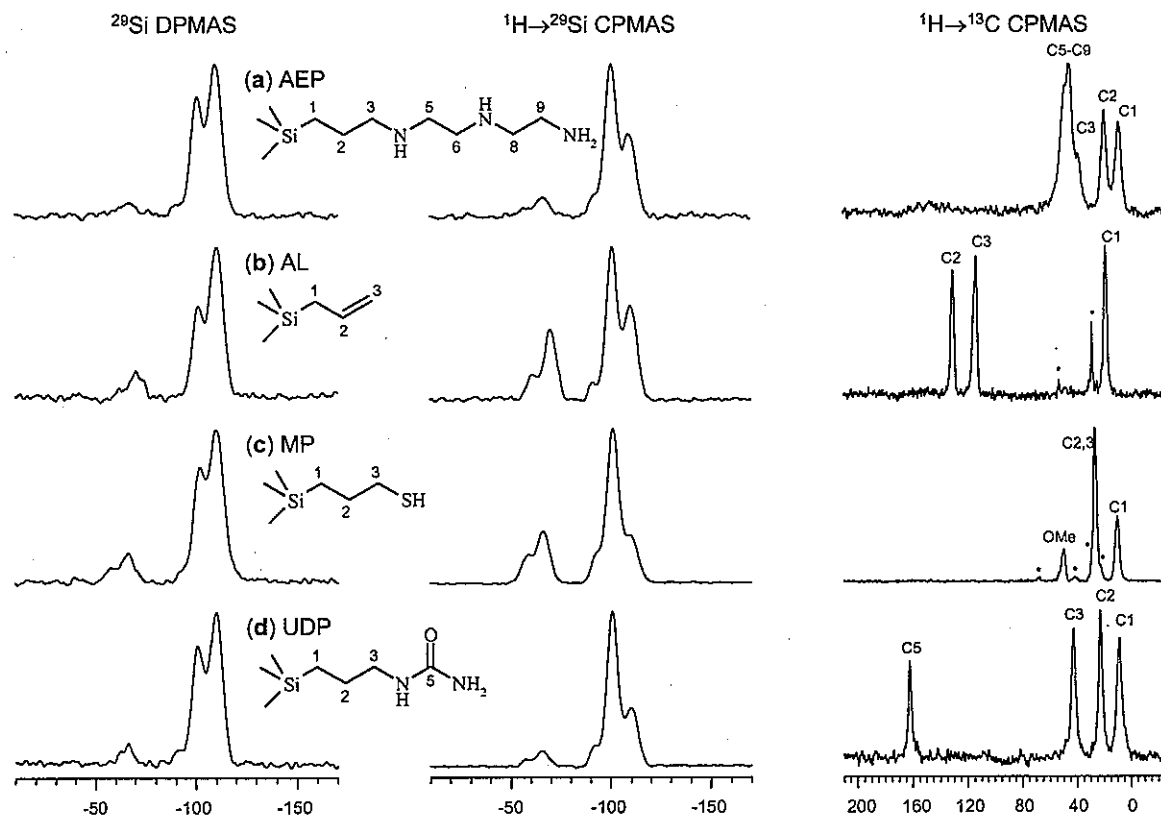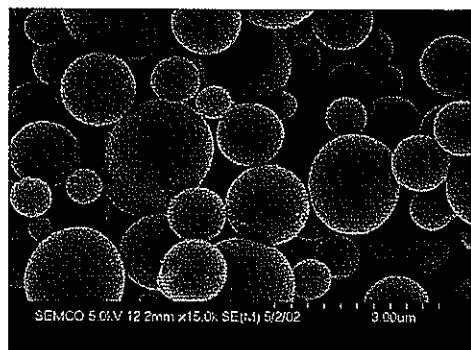
Figure S2. ^{29}Si DPMAS (left column), ^{1}H→^{29}Si CPMAS (middle column), and ^{1}H→^{13}C CPMAS (right column) spectra obtained for bifunctionalized mesoporous silica materials: AEP/AL-MSN (a), AEP/MP-MSN (b), and AEP/UDP-MSN (c).
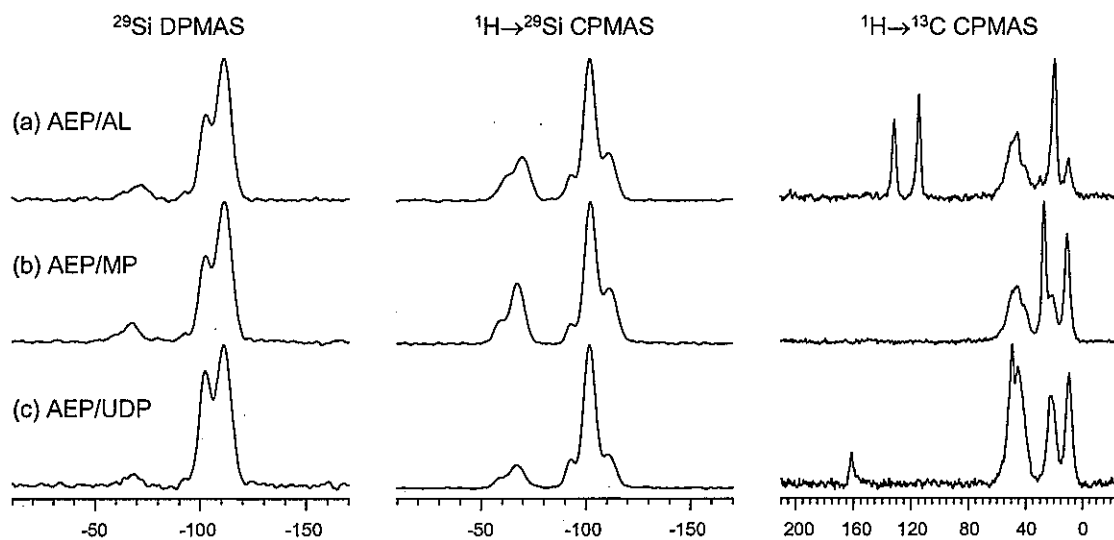
Figure S3. FE-SEM images of MSN materials (Hitachi S4700).

(a) AEP-MSN

(b) AEP/UDP-MSN
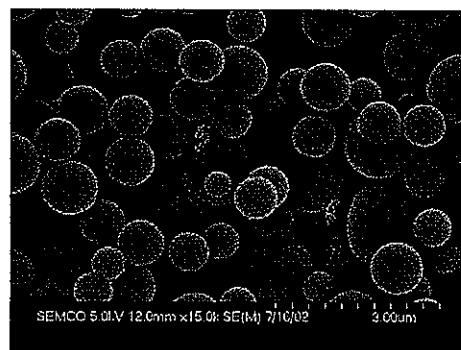
(c) AEP/MP-MSN
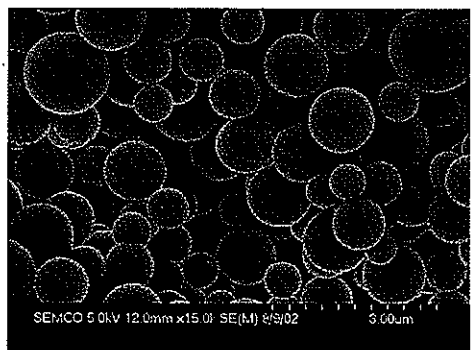
(d) AEP/AL-MSN
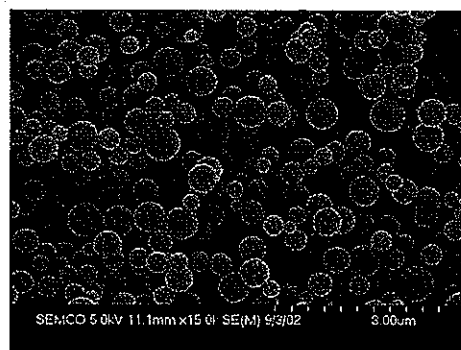
Figure S4. TEM micrographs of ultramicrotomed MSN materials (300 kV).

(a) AEP-MSN
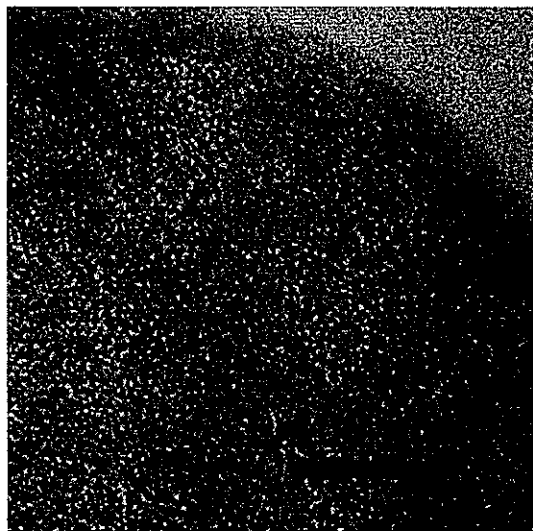
(b) AEP/AL-MSN
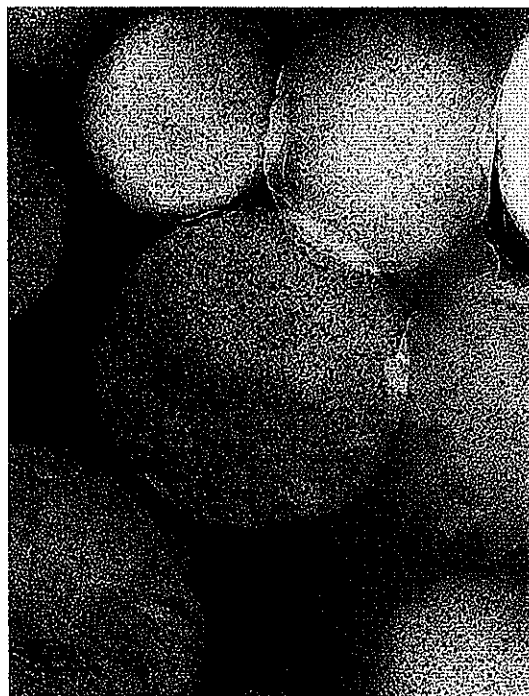
Table S3. Structural properties of the surfactant-free MSN materials.[a]

Samples	d_{100} (Å)	a_0 (Å)	S_{BET} (m^2/g)	V_p (cm^3/g)	W_{BJH} (Å)	$d_{pore\ wall}$ (Å)
AEP-MSN	38.4	44.4	805.8	0.57	26.0	18.4
AEP/UDP-MSN	41.7	48.2	759.6	0.47	22.9	25.3
AEP/MP-MSN	39.1	45.1	778.7	0.39	-	-
AEP/AL-MSN	38.4	44.4	703.5	0.40	-	-

[a] The BET surface area (S_{BET}), the mesopore volume (V_p), and the mean mesopore size (W_{BJH}) were obtained from the nitrogen adsorption/desorption data. The d_{100} numbers represent the d-spacing corresponding to the main (100) XRD peak. The unit cell size (a_0) is calculated from the d_{100} data using $a_0 = 2d_{100}/3^{1/2}$. The pore wall thickness ($d_{pore\ wall} = a_0 - W_{BJH}$).
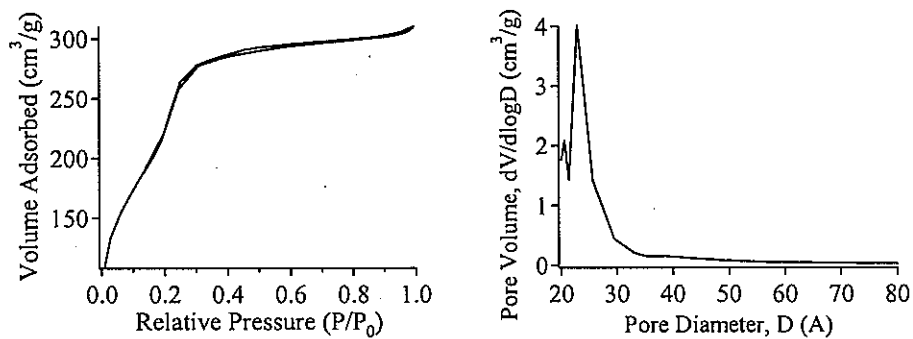
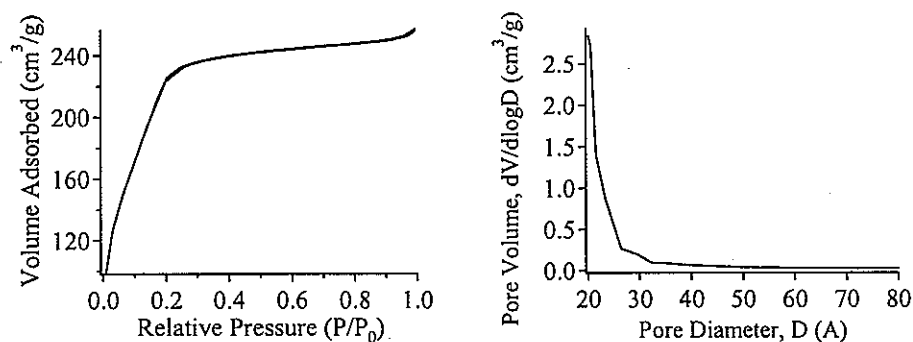**Figure S5.** Powder XRD data of the MSN materials: (a) AEP-, (b) AEP/UDP-, (c) AEP/MP-, (d) AEP/AL-MSN.
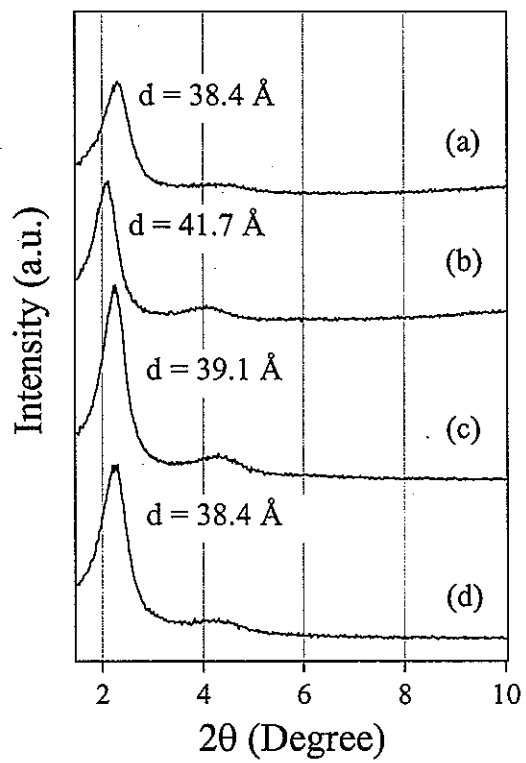
Figure S6. BET isotherms and BJH pore size distribution curves of the MSN materials.
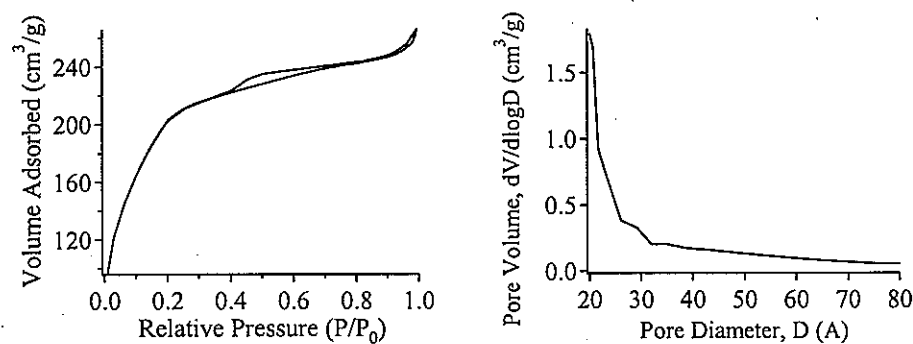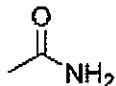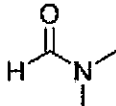
(a) AEP/UDP-MSN

(b) AEP/MP-MSN

(c) AEP/AL-MSN
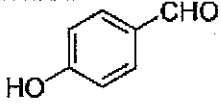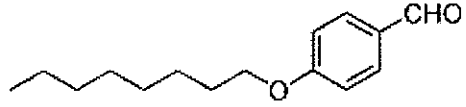
Table S4. Dielectric constants of various organic compounds [a].

Compound	Dielectric Constant	Temp. (K)
H_2O	80.10	293.2
	67.60	363.7
	38.25	293.2
CH_3NO_2	37.27	293.2
SH	5.94	288.2
	2.14	220.0

[a] Data taken from "CRC Handbook of Chemistry and Physics" 84th ed., CRC Press. The dipole moment of 4-methoxybenzaldehyde is 3.85×10^{-18} esu (*J. Phys. Chem.*, **1935**, *39*, 1005).

Table S5. Solubility tests of two different aldehydes in 1-propanethiol.

Compound	Solubility in 1 mL of 1-propanethiol
	< 13.9 µmol
	Completely miscible

References

1. Huh, S.; Wiench, J. W.; Trewyn, B. G.; Song, S.; Pruski, M.; Lin, V. S. Y. *Chem. Commun.* **2003**, 2364.

2. Huh, S.; Wiench, J. W.; Yoo, J. C.; Pruski, M.; Lin, V. S. Y. *Chem. Mater.* **2003**, *15,* 4247.

3. Maciel, G. E.; Sindorf, D. W.; Bartuska, V. J. *J. Chromatogr.* **1981**, *205*, 438.

4. Maciel, G. E. In *Encyclopedia of Nuclear Magnetic Resonance*; Grant, D. M., Harris, R. K., Eds.; John Wiley & Sons Ltd: Chichester, 1996; Vol. 7, pp 4370.

CHAPTER 5. COOPERATIVE CATALYSIS BY GENERAL ACID AND BASE BIFUNCTIONALIZED MESOPOROUS SILICA NANOSPHERE CATALYSTS

A paper submitted to *Angew. Chem. Int. Ed.*

Seong Huh, Hung-Ting Chen, Jerzy W. Wiench, Marek Pruski and Victor S. –Y. Lin

Abstract

We synthesized and characterized a new cooperative catalytic system comprised of a series of bifunctionalized mesoporous silica nanosphere (MSN) materials with various relative concentrations of a general acid, ureidopropyl (UDP) group, and a base, 3-[2-(2-aminoethylamino)ethylamino]propyl (AEP) group. Three bifunctional AEP/UDP-MSN materials with different relative ratios (AEP/UDP = 2/8, 5/5, and 8/2) were employed as catalysts for aldol, Henry and cyanosilylation reactions. A common electrophile, 4-nitrobenzaldehyde, and different nucleophiles, acetone, nitromethane and trimethylsilyl cyanide (TMSCN), were used as reactants. The turnover numbers (TONs) of these reactions indicated that the UDP groups could cooperatively activate substrates with the AEP groups in catalyzing reactions that involve carbonyl activation. By fine-tuning the relative concentrations and proper spatial arrangements of different cooperative functional groups, we envision that our multifunctionalized MSNs could serve as new selective catalysts for many important reactions.

Introduction

Enzymes engaged in carbonyl chemistry often employ both general acid and base catalytic residues in the active sites to cooperatively activate specific subtrates.[1] Recently, several synthetic catalytic systems have utilized the double hydrogen bonding capability of urea or thiourea functionality as a general acid catalyst to activate carbonyl compounds in homogeneous reactions.[2] However, to our knowledge, the cooperativity between general acid and base groups is yet to be demonstrated in any synthetic heterogeneous catalyst. Clearly, an important prerequisite for the construction of such a cooperative catalytic system would be to multifunctionalize a solid support with control of the relative concentrations and proper spatial arrangements between these functional groups. In contrast to many recently reported monofunctionalized mesoporous silica catalysts,[3] we and others focused on *multifunctionalized* mesoporous catalysts.[4] Herein, we report a new cooperative catalytic system comprised of a series of bifunctionalized mesoporous silica nanosphere (MSN) materials with various relative concentrations of a general acid, ureidopropyl (UDP) group, and a base, 3-[2-(2-aminoethylamino)ethylamino]propyl (AEP) group (Figure 1).

Results and Discussion

Three bifunctional AEP/UDP-MSN catalysts with the initial molar ratio of the organosilane precursors, AEP/UDP = 2/8, 5/5, and 8/2, were synthesized via our previously reported cocondensation method.[5,6] The syntheses and characterizations of the monofunctionalized MSNs with either AEP or UDP functionality were reported previously.[5a] All of the mono- and bi-functionalized MSNs exhibited spherical particle shapes with similar particle sizes (1 μm).[5a,6] The actual concentrations of the two functional groups (AEP and

UDP) were measured using the previously described solid state ^{13}C CPMAS and ^{29}Si MAS NMR methods.[5b,6] The total surface concentrations of the organic functional groups (AEP + UDP) in the 2/8, 5/5, and 8/2 AEP/UDP-MSNs were determined to be 1.3, 1.0, and 1.5 mmol/g, and the concentration ratios of AEP/UDP were 2.5/7.5, 5.4/4.6, and 6.7/3.3, respectively.[6] The XRD measurements of these materials showed large (100) peaks and broad higher diffraction patterns, typical of disordered pore structure.[5] The observed d_{100} values ranged between 37.8, 41.7, and 38.1 Å for sample 2/8, 5/5, and 8/2 AEP/UDP-MSNs. The TEM micrographs of these materials also confirmed their disordered pore structure.[6] The N_2 surface sorption analyses of these bifunctionalized MSNs revealed typical type IV BET isotherms. The measured BET surface areas of 2/8, 5/5, and 8/2 AEP/UDP-MSNs are 938.7, 759.6, and 830.4 m^2/g, respectively. The corresponding BJH average pore diameters of these MSNs are 27.8, 22.9, and 25.9 Å.

To investigate how UDP and AEP could cooperatively catalyze different reactions involving carbonyl activation, the aforementioned AEP/UDP-MSN materials were employed as catalysts for aldol, Henry and cyanosilylation reactions. As shown in Figure 2, a common electrophile, 4-nitrobenzaldehyde, and different nucleophiles, acetone, nitromethane and trimethylsilyl cyanide (TMSCN), were used as reactants. In these reactions, the secondary amines of the AEP group were demonstrated in the literature to be responsible for the enamine formation with acetone (aldol reaction),[7] the deprotonation of CH_3NO_2 (Henry reaction),[4] and the generation of a potential nucleophile of TMSCN through a hypervalent silicate formation (cyanosilylation).[8] On the other hand, a general acid group (UDP) could activate (through double hydrogen bonding) the carbonyl group of 4-nitrobenzaldehyde for nucleophilic attacks.[2] Therefore, the presence of both AEP and UDP groups in a close

proximity could cooperatively activate the electrophile and nucleophile to enhance the reaction rates of the desired catalytic reactions (Scheme 1). Indeed, the observed turnover numbers (TONs) of these reactions (Table 1) are consistent with this hypothesis. In the case of aldol reaction, the monofunctionalized AEP-MSN catalyzed the conversion of 4-nitrobenzaldehyde (0.5 mmol) to compound **1** (0.091 mmol) and a small amount of the dehydrated product, compound **2** (0.018 mmol), in the presence of acetone (10 mL). In contrast, the UDP-MSN did not show any catalytic activity under the same reaction condition. The result suggested that the presence of AEP functionality is crucial for converting acetone solvent molecules to the active enamine species.[7] However, a synergistic effect between AEP and UDP groups was observed in the case of the bifunctionalized AEP/UDP-MSN catalysts. As shown in Table 1 and Figure 3, the TONs of all three AEP/UDP-MSNs are higher than that of AEP-MSN. It is noteworthy that the TON (6.4) of a 1:1 mixture of the monofunctionalized AEP-MSN and UDP-MSN was clearly lower than that of the 5/5 AEP/UDP-MSN (11.9). Furthermore, the TONs of the bifunctionalized MSNs significantly increased as the actual ratio of surface concentrations between AEP and UDP groups decreased from 2.5/7.5 to 5.4/4.6, and 6.7/3.3. According to our solid state NMR data, the total numbers of organic functional groups (AEP + UDP) in these bifunctionalized MSNs are similar, only the relative concentrations between the AEP and UDP groups were varied. To examine whether this activity enhancement was due to the "surface dilution effect" of the AEP group, we investigated the catalytic performance of two bifunctional MSN materials (2/8 and 5/5 AEP/CP-MSNs) that have the AEP group and a cyanopropyl (CP) functionality, which cannot activate the electrophiles through the double hydrogen bonding interaction. The synthesis and characterizations of these two materials have been previously reported.[5b] As

shown in Table 1, the TONs of the 2/8 and 5/5 AEP/CP-MSNs are 12.4 and 9.3, respectively. Indeed, the TON increased slightly as the AEP/CP ratio decreased. However, the large difference in TONs between the AEP/CP-MSNs and the AEP/UDP-MSN catalysts that have the similar surface concentrations of the AEP group cannot be explained by the surface dilution effect. These results strongly indicated that the rate of aldol reaction was accelerated as the surface concentration of UDP groups increased. Given that the UDP group can only activate the electrophile, the observed rate acceleration in the UDP abundant MSN catalysts suggested that the activation of the carbonyl group of 4-nitrobenzaldehyde might be the rate-determining step in our cooperative catalysts. Such a "cooperative dual catalysis" effect in homogeneous system where one catalyst activates the nucleophile and the other catalyst is responsible for the activation of the electrophile has been reported recently by Jacobsen and co-workers.[9] In their study, the best mol ratio between the two catalysts was 0.67 and not 1, which indicated that the best ratio between the cooperative catalytic groups greatly depends on the kinetic nature of the reaction of interest. Similar trend of catalytic reactivity was also observed in the cases of Henry and cyanosilylation reactions. A pronounced cooperativity effect was manifested by a two-fold increase of TONs between 8/2 and 2/8 AEP/UDP-MSNs in both reactions (Table 1). Since the surface concentration of the primary catalytic group (AEP) in the 2/8 AEP/UDP-MSN (AEP = 0.32 mmol/g) is only 1/3 of that of 8/2 AEP/UDP-MSN (AEP = 1.00 mmol/g), these unusual catalytic enhancements are strong indications of the existence of cooperativity between the general acid (UDP) and base (AEP) groups in our system.

Conclusions

In conclusion, we have demonstrated that a general acid group, UDP, could cooperatively activate substrates with a base group, AEP, in catalyzing various reactions that involve carbonyl activation. By fine-tuning the relative concentrations and proper spatial arrangements of different cooperative functional groups, we envision that our multifunctionalized MSNs could serve as new selective catalysts for many important reactions.
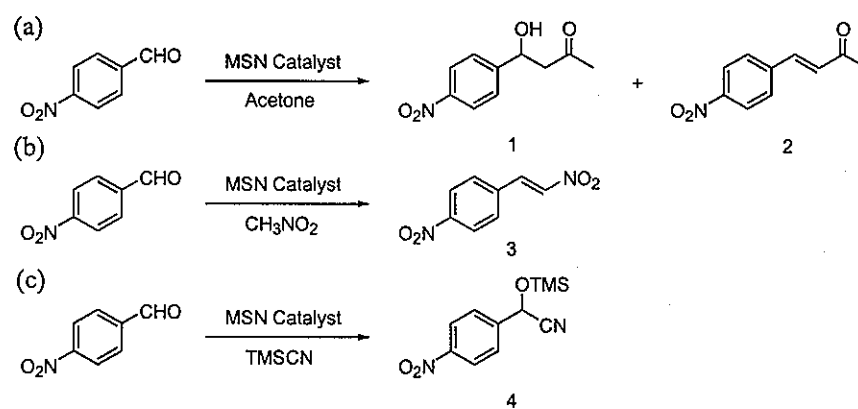
Acknowledgement

Figure 1. Scanning electron micrographs (SEM, above) and schematic drawings (below) of the bifunctional MSNs: (a) 2/8 AEP/UDP-MSN, (b) 5/5 AEP/UDP-MSN and (c) 8/2 AEP/UDP-MSN. Scale bar = 2.0 μm.
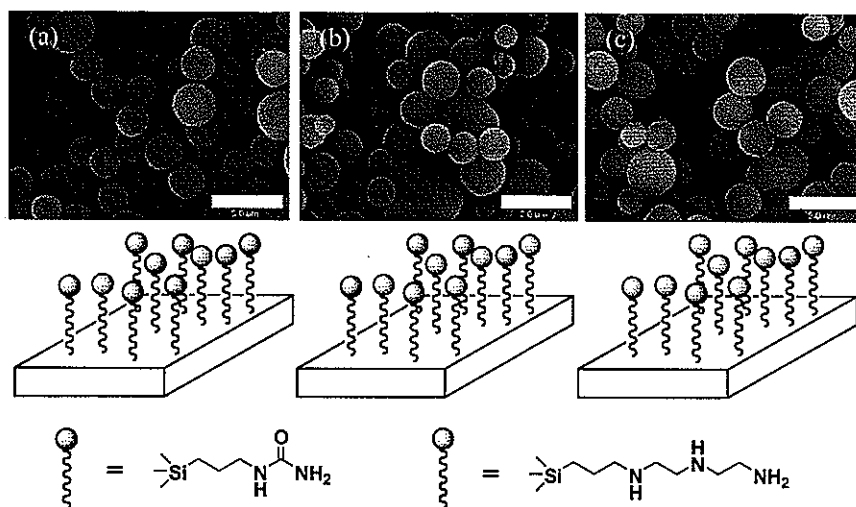
Figure 2. Three model reactions catalyzed by the MSN catalysts: aldol reaction (a), Henry reaction (b) and cyanosilylation (c).

Figure 3. Diagram showing the TONs for the aldol reaction: 2/8 AEP/UDP-MSN (1), 5/5 AEP/UDP-MSN (2), 8/2 AEP/UDP-MSN (3), AEP-MSN (4), physical mixture of AEP-MSN and UDP-MSN (5) and UDP-MSN (6). Product alcohol is 1 and alkene is 2.
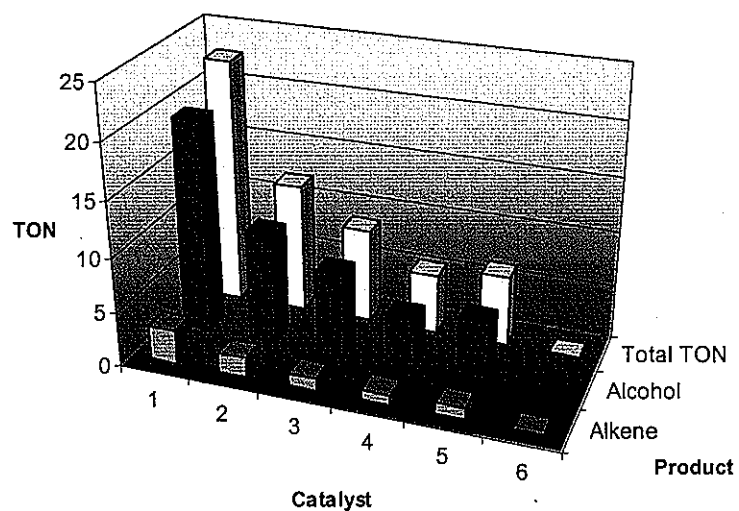
Table 1. TONs of the MSN-catalyzed Reactions[a]

Reaction	MSN Catalyst	Temp °C	Product	TON
Aldol	2/8 AEP/UDP	50	1, 2	22.6
	5/5 AEP/UDP	50	1, 2	11.9
	8/2 AEP/UDP	50	1, 2	8.6
	AEP	50	1, 2	5.4
	physical mixture[b]	50	1, 2	6.4
	UDP	50	1, 2	0.0
	2/8 AEP/CP	50	1, 2	12.4
	5/5 AEP/CP	50	1, 2	9.3
Henry	2/8 AEP/UDP	90	3	125.0
	5/5 AEP/UDP	90	3	91.1
	8/2 AEP/UDP	90	3	65.8
	AEP	90	3	55.9
	physical mixture[b]	90	3	79.2
	UDP	90	3	5.8
	2/8 AEP/CP	90	3	78.0
	5/5 AEP/CP	90	3	71.0
Cyanosilylation	2/8 AEP/UDP	50	4	276.1
	5/5 AEP/UDP	50	4	170.5
	8/2 AEP/UDP	50	4	109.4
	AEP	50	4	111.4
	physical mixture[b]	50	4	126.9
	UDP	50	4	45.9

[a]TON = mmol product/mmol catalyst during 20 h of reaction time for aldol and Henry reactions and 24 h for cyanosilylation reaction using 20 mg of MSN. [b]Physical mixture = 20 mg of AEP-MSN + 20 mg of UDP-MSN.

Scheme 1

Aldol Reaction **Henry Reaction** **Cyanosilylation**
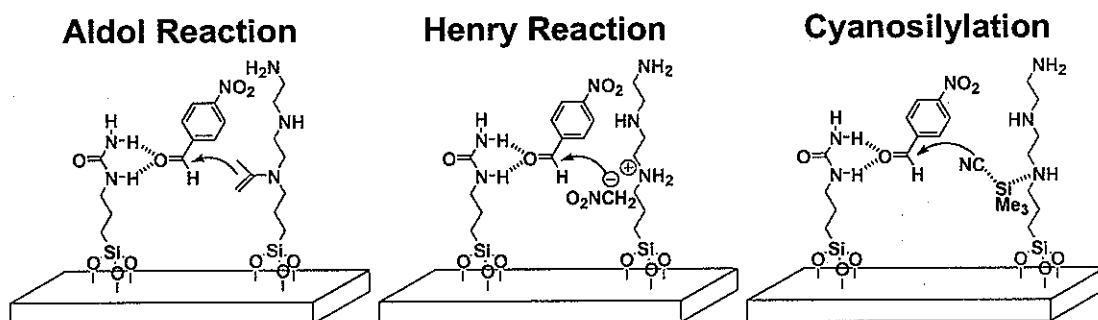
References

1. For review: Nakayama, T.; Suzuki, H.; Nishino, T. *J. Mol. Catal. B* **2003**, *23*, 117-132.

2. For review: Pihko, P. M. *Angew. Chem, Int. Ed.* **2004**, *43*, 2062-2064.

3. (a) Wight, A. P.; Davis, M. E. *Chem. Rev.* **2002**, *102*, 3589-3613. (b) Lindner, E.; Schneller, T.; Auer, F.; Mayer, H. A. *Angew. Chem. Int. Ed.* **1999**, *38*, 2155-2174. (c) Corma, A. *Chem. Rev.* **1997**, *97*, 2373-2419.

4. (a) Huh, S.; Chen, H.-T.; Wiench, J. W.; Pruski, M.; Lin, V. S. Y. *J. Am. Chem. Soc.* **2004**, *126*, 1010-1011. (b) Liu, J.; Shin, Y.; Nie, Z.; Chang, J. H.; Wang, L.-Q.; Fryxell, G. E.; Samuels, W. D.; Exarhos, G. J. *J. Phys. Chem. A* **2000**, *104*, 8328-8339.

5. (a) Huh, S.; Wiench, J. W.; Yoo, J.-C.; Pruski, M.; Lin, V. S. Y. *Chem. Mater.* **2003**, *15*, 4247-4256. (b) Huh, S.; Wiench, J. W.; Trewyn, B. G.; Song, S.; Pruski, M.; Lin, V. S. Y. *Chem. Commun.* **2003**, 2364-2365.

6. See Supporting Information for details.

7. (a) Kubota, Y.; Goto, K.; Miyata, S.; Goto, Y.; Fukushima, Y.; Sugi, Y. *Chem. Lett.* **2003**, *32*, 234-235. (b) List, B. *Acc. Chem. Res.* **2004**, *37*, 548-557.

8. Kantam, M. L.; Sreekanth, P.; Santhi, P. L. *Green Chem.* **2000**, *2*, 47-48.

9. Sammis, G. M.; Danjo, H.; Jacobsen, E. N. *J. Am. Chem. Soc.* **2004**, *126*, 9928-9929.

Supporting Information

1. Synthesis of mono- and bi-functionalized MSN materials

The functionalized materials were synthesized via the previously described co-condensation reaction.[5] For example, the preparation of 2/8 AEP/UDP-MSN is as follows. A mixture of cetyltrimethylammonium bromide, CTAB (2.0 g, 5.49 mmol), 2.0 M of NaOH(aq) (7.0 mL, 14.00 mmol) and H_2O (480 g, 26.67 mol) was heated to 80 °C for 30 min. To this solution, tetraethoxysilane, TEOS (9.34 g, 44.8 mmol), 3-[2-(2-aminoethylamino)ethylamino]propyltrimethoxysilane, AEPTMS (0.305 g, 1.15 mmol), and ureidopropyltrimethoxysilane, UDPTMS (1.023 g, 4.60 mmol) were rapidly and sequentially added via injection, yielding an opaque reaction mixture. White precipitates were observed after vigorous (550 rpm) stirring of the reaction mixture for ~2 min. After additional 2 h of heating at 80 °C, the as-synthesized bifunctionalized 2/8 AEP/UDP-MSN material was isolated by hot filtration, washed with copious water and methanol, and dried under vacuum. An acid extraction of The CTAB surfactant molecules were extracted out of the mesopores of the MSN by placing 1.0 g of the as-synthesized material in a mixture of methanol (100 mL) and hydrochloric acid (0.6 mL) for 2.5 h at 60 °C. The resulting surfactant-removed solid product was filtered and washed with water and methanol and then dried under vacuum for 3 h at 90 °C.

---

[5]. (a) Huh, S.; Wiench, J. W.; Trewyn, B. G.; Song, S.; Pruski, M.; Lin, V. S. Y. *Chem. Commun.* **2003**, 2364-2365. (b) Huh, S.; Wiench, J. W.; Yoo, J.-C.; Pruski, M.; Lin, V. S. Y. *Chem. Mater.* **2003**, *15*, 4247-4256.

2. Bifunctionalized MSN-catalyzed aldol reaction of 4-nitrobenzaldehyde with acetone

All chemicals were purchased from Aldrich and used without further purification.

Reagent grade acetone was used without any purification. For example, a reaction mixture

consisted of 20 mg of the MSN catalyst and 0.076 g (0.5 mmol) of 4-nitrobenzaldehyde in 10

mL of acetone, was heated at 50 °C with a constant stirring for 20 h. The reaction mixture

was filtered on a glass frit and the solids were washed with chloroform and acetone. The

resulting filtrate was evaporated on a rotary evaporator and dried under high vacuum. The

residue was completely dissolved in a sufficient amount of $CDCl_3$. Analysis of the product

was performed by measuring ^1H NMR spectra on a Bruker DRX400 NMR spectrometer. The

resulting two products gave distinctive proton chemical shifts for the integrations.

Assignments of the peaks were performed by comparing the chemical shifts of the products
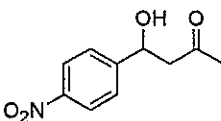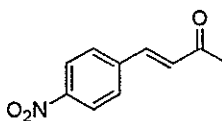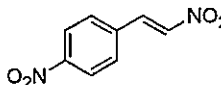
with the literature values.[6,7]

3. Bifunctionalized MSN-catalyzed Henry (Nitroaldol) reaction of 4-nitrobenzaldehyde with nitromethane

Reagent grade nitromethane was used without any purification. For example, a

reaction mixture consisted of 20 mg of the MSN catalyst and 0.453 g (3.0 mmol) of 4-

nitrobenzaldehyde in 10 mL of nitromethane, was heated at 90 °C with a constant stirring for

20 h. The reaction mixture was filtered on a glass frit and the solids were washed with

chloroform and acetone. The resulting filtrate was evaporated on a rotary evaporator and

dried under high vacuum. The residue was completely dissolved in 10 mL of acetone-d_6.

Analysis of the product was performed by measuring ^1H NMR spectra on a Bruker DRX400

---

[6]. Shokat, K.; Uno, T.; Schultz, P. G. *J. Am. Chem. Soc.* **1994**, *116*, 2261-2270.

[7]. Sakthivel, K.; Notz, W.; Bui, T.; Barbas, C. F. III. *J. Am. Chem. Soc.* **2001**, *123*, 5260-5267.

NMR spectrometer. The resulting product gave distinctive vinylic proton chemical shifts for the integrations. Assignments of the peaks were performed by comparing the chemical shifts of the products with the literature values.[8]
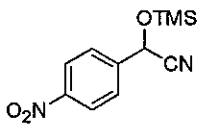
4. Bifunctionalized MSN-catalyzed cyanosilylation of 4-nitrobenzaldehyde with TMSCN

All chemicals were purchased from Aldrich and used without further purification. For example, a reaction mixture consisted of 20 mg of the MSN catalyst, 0.453 g (3.0 mmol) of 4-nitrobenzaldehyde, and 0.298 g (3.0 mmol) of TMSCN in 10 mL of dry toluene was heated at 50 °C with a constant stirring for 24 h. The reaction mixture was filtered on a glass frit and the solids were washed with chloroform and acetone. The resulting filtrate was evaporated on a rotary evaporator and dried under high vacuum. The residue was completely dissolved in CDCl$_3$. Analysis of the product was performed by measuring ^{1}H NMR spectra on a Bruker DRX400 NMR spectrometer. The resulting silylether product gave a distinctive proton chemical shift at 5.6 ppm for the integrations. Assignments of the peaks were performed by comparing the chemical shifts of the products with the literature values.[9]

[8]. Huh, S.; Chen, H.-T.; Wiench, J. W.; Pruski, M.; Lin, V. S. Y. *J. Am. Chem. Soc.* **2004**, *126*, 1010-1011.
[9]. Deuchert, K.; Hertenstein, U.; Huenig, S.; Wehner, G. *Chem. Ber.* **1979**, *112*, 2045-2061.

Table S1. Turnover numbers (TONs) of the MSN-catalyzed reactions.

Catalyst	Product		Total TON
	Turnover[a]	Turnover[a]	(Yield in mmol)
Aldol Reaction			
2/8 AEP/UDP	19	3	22 (0.14)
5/5 AEP/UDP	10	2	12 (0.13)
8/2 AEP/UDP	7	1	8 (0.17)
AEP	5	1	6 (0.11)
Physical mixture	5	1	6 (0.13)
UDP	0	0	0 (0.00)
Henry reaction			
2/8 AEP/UDP	125		125 (0.80)
5/5 AEP/UDP	91		91 (0.98)
8/2 AEP/UDP	66		66 (1.32)
AEP	56		56 (1.12)
Physical mixture	79		79 (1.58)
UDP	6		6 (0.12)
Cyanosilylation			
2/8 AEP/UDP	276		276 (1.77)
5/5 AEP/UDP	170		170 (1.84)
8/2 AEP/UDP	109		109 (2.19)
AEP	111		111 (2.23)
Physical mixture	127		127 (2.54)
UDP	46		46 (0.92)

[a] Turnover = mmol product / mmol catalyst during 20 h for aldol and Henry reactions and 24 h for cyanosilylation.

5. Summary of solid-state NMR measurements

5.1. Experimental

Solid-state NMR spectra were obtained at 100.59 (^{13}C) and 79.47 MHz (^{29}Si) on a Varian/Chemagnetics Infinity spectrometer, equipped with a doubly tuned, 5 mm magic angle spinning (MAS) probe. Direct polarization (DP) and variable amplitude cross polarization (CP) methods were used under the conditions described earlier.[1,4] These measurements provided quantitative evidence for functionalization of the mesopores with the organic moieties and confirmed their structure. For AEP-, UDP-, and AEP/UDP-MSN's, the assignments of ^{29}Si and ^{13}C NMR spectra were made following our earlier study (see Figure S1).[1b,4] The methods used for quantitative measurements of ^{29}Si and ^{13}C intensities are detailed in Sections 5.2 and 5.3 below. All NMR results are summarized in Table 1, which contains the relative concentrations of T^n and Q^n groups, the molar concentrations of organic functional groups and the corresponding average molecular formulae.

5.2. Quantification of silicon groups

Relative concentrations of T^n and Q^n silicon groups[10] were obtained from the analysis of ^{29}Si DPMAS spectra. In agreement with our earlier results,[1b] the measurements of T_1 relaxation in functionalized MSN's yielded T_1 values on the order of 50 to 65 s for T^n groups and 30 to 45 s for Q^n groups. Therefore, a delay of 300 s between scans has been used during the acquisition of ^{29}Si NMR spectra. The accumulation of 270 scans yielded intensities that were accurate within ±10%.

---

[10]. Maciel, G. E. In *Encyclopedia of Nuclear Magnetic Resonance*; Grant, D. M., Harris, R. K., Eds.; John Wiley & Sons Ltd: Chichester, 1996; Vol. 7, pp 4370-4386.

## 5.3. Quantification of functional groups in bifunctionalized samples using ^{13}C NMR

Although direct polarization is the preferred method for quantitative measurements, relative ^{13}C intensities were measured using a CPMAS-based method. The strategy, developed in our earlier study,[1a] was also successfully used for AEP/UDP-MSN system in our previous report.[4] The procedure utilizes differences in values of $T_{1\rho}{}^{H}$ and τ_{CH} times between AEP and UDP.[1a] The bifunctionalized samples could be quantitatively characterized without the tedious measurements of the ^{13}C build-up curves[1a,4] by properly measuring and processing the CPMAS spectra with two different contact times (i.e. 0.4 and 1.5 ms), using known physical mixtures of mono-functionalized samples as intensity standards.[1a,4]

Table S2. Relative concentrations of T^n and Q^n silicon groups (in %), surface coverage (*SC*, in %), molecular concentrations of organic functionalities (*MC*, in mmol/g), molecular formulae (*MF*), molar ratios in bifunctional samples, and concentrations (in mmol/g) of each organic functionality derived from solid state ^{13}C CPMAS and ^{29}Si DPMAS NMR data.

| Functionality	T^2	T^3	Q^2	Q^3	Q^4	*SC*	*MC*	*MF*	Molar ratio	Concentr.
AEP [a]	1	6	3	35	55	16	1.0	$(SiO_2)_{100}(H_2O)_{17.5}(ORG)_7$[c]		
UDP [a]	2	4	4	38	52	13	0.9	$(SiO_2)_{100}(H_2O)_{21}(ORG)_6$		
2/8 AEP/UDP	4	5	1	35	55		1.3	$(SiO_2)_{100}(H_2O)_{16}(ORG)_9$	2.5:7.5	AEP: 0.32 UDP: 0.98
5/5 AEP/UDP [b]	2	5	3	36	54	15	1.0	$(SiO_2)_{100}(H_2O)_{18.5}(ORG)_7$	5.4:4.6	AEP: 0.54 UDP: 0.46
8/2 AEP/UDP	3	3	4	30	60		1.5	$(SiO_2)_{100}(H_2O)_{12.5}(ORG)_{12}$	6.7:3.3	AEP: 1.00 UDP: 0.50

(a), (b) Data taken from ref 1b and ref. 4. (c) 'ORG' denotes the organic functional groups (AEP and UDP).

Figure S1. ^{1}H→^{13}C CPMAS (top) and ^{29}Si DPMAS (bottom) spectra obtained for 2/8 AEP/UDP-MSN (left column) and 8/2 AEP/UDP-MSN (right column). Locations of carbon resonances in UDP and AEP are marked separately on the left top and the right top spectra.
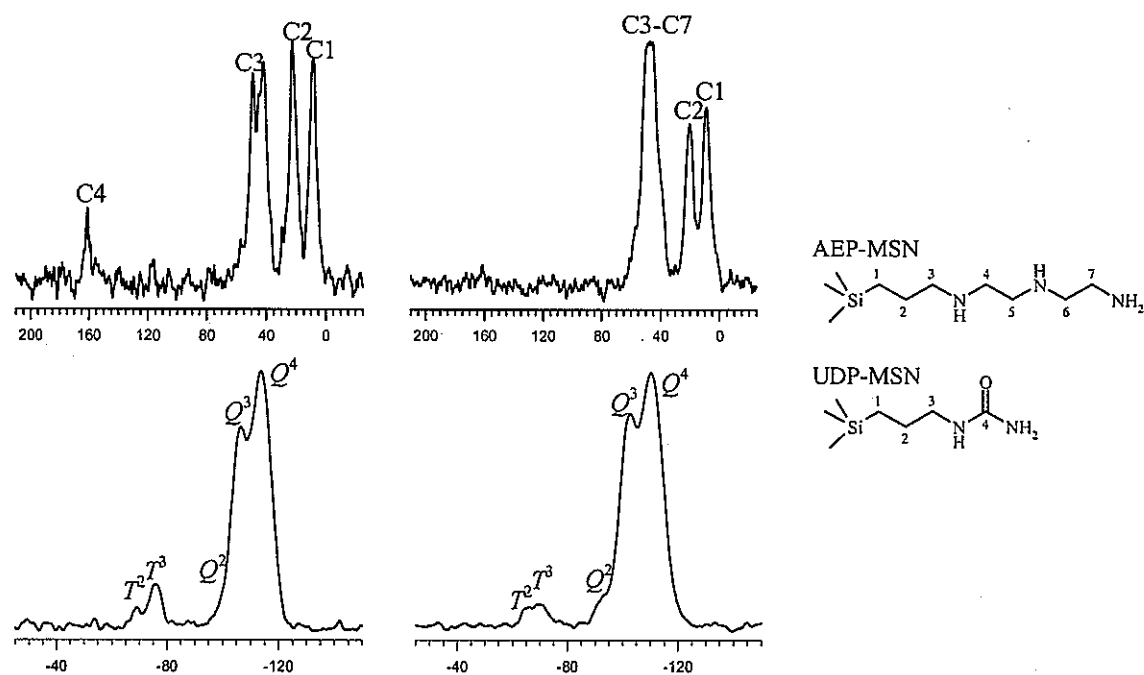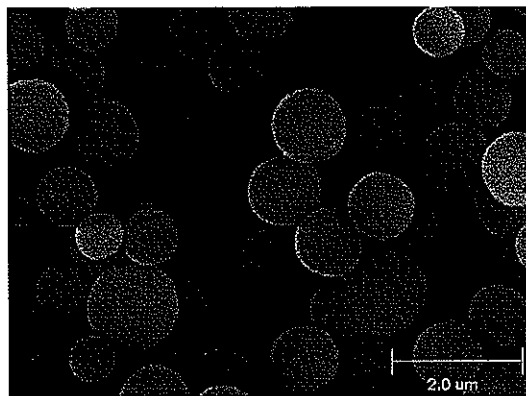
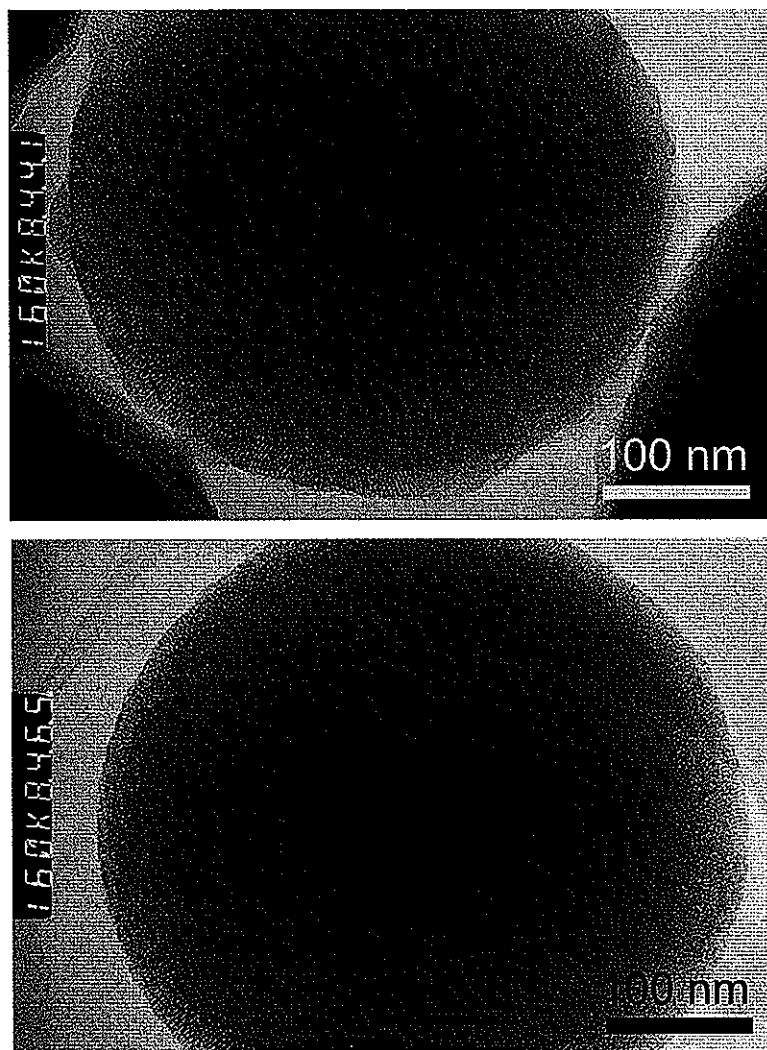**Figure S3.** SEM images of MSN materials (JEOL 840A).

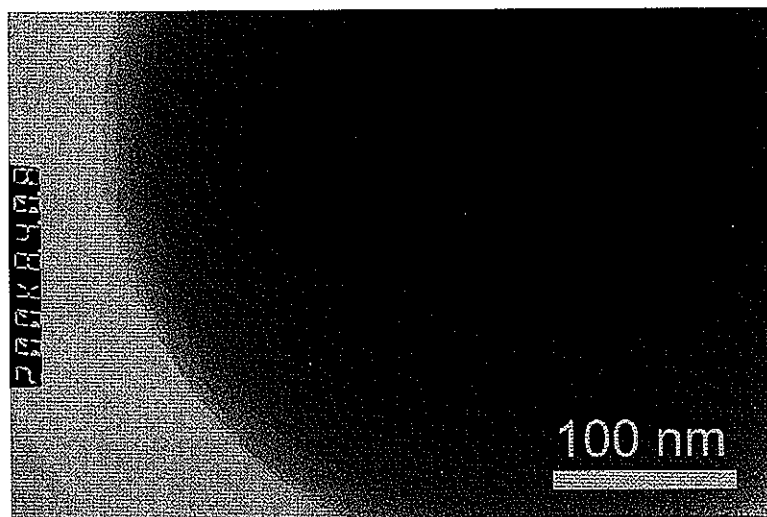(a) 2/8 AEP/UDP-MSN (0.74~1.56 μm)
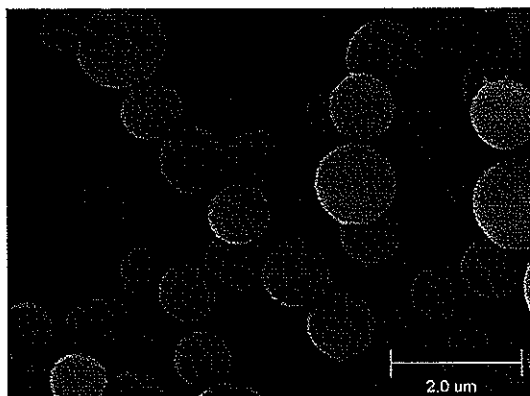
(b) 8/2 AEP/UDP-MSN (0.74~1.43 μm)

Figure S4. TEM micrographs of 2/8 AEP/UDP-MSN (top) and 8/2 AEP/UDP-MSN (bottom) materials (Philips CM-30 at 300 kV).

Figure S5. TEM micrograph of 2/8 AEP/UDP-MSN (top) after aldol reaction (Philips CM-30 at 300 kV).


Table S3. Structural properties of the surfactant-free MSN materials.[a]

| Samples	d_{100} (Å)	a_0 (Å)	S_{BET} (m²/g)	V_p (cm³/g)	W_{BJH} (Å)	$d_{pore\ wall}$ (Å)
2/8 AEP/UDP-MSN	37.8	43.6	938.7	0.77	27.8	15.8
5/5 AEP/UDP-MSN	41.7	48.2	759.6	0.47	22.9	25.3
8/2 AEP/UDP-MSN	38.1	44.0	830.4	0.60	25.9	18.1

[a] The BET surface area (S_{BET}), the mesopore volume (V_p), and the mean mesopore size (W_{BJH}) were obtained from the nitrogen adsorption/desorption data. The d_{100} numbers represent the d-spacing corresponding to the main (100) XRD peak. The unit cell size (a_0) is calculated from the d_{100} data using $a_0 = 2d_{100}/3^{1/2}$. The pore wall thickness ($d_{pore\ wall} = a_0 - W_{BJH}$).

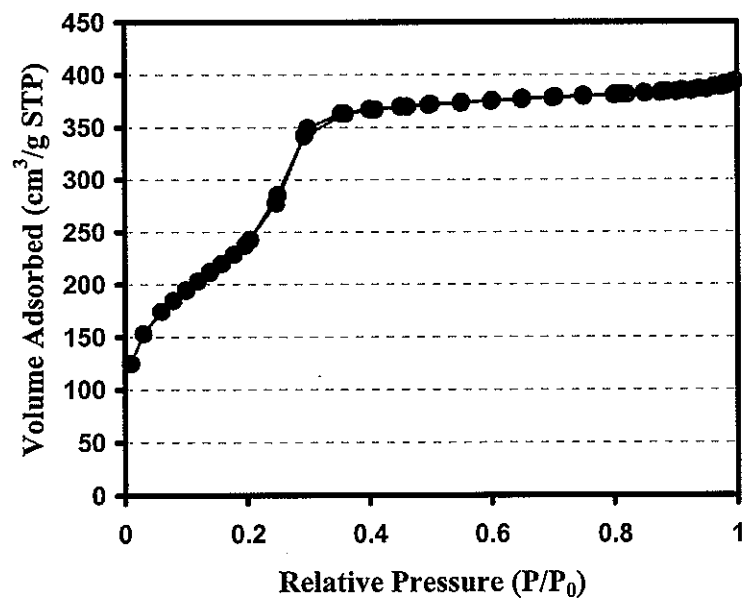**Figure S6.** Powder XRD data of the MSN materials: 2/8 AEP/UDP-MSN (blue) and 8/2 AEP/UDP-MSN (red).
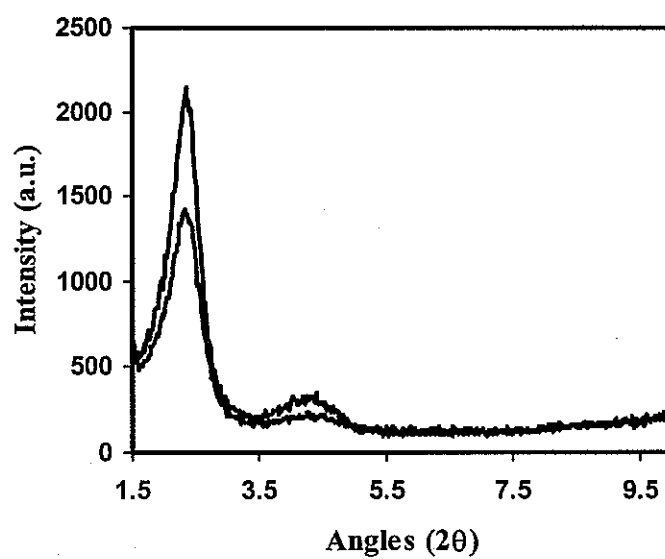
Figure S7. BET isotherms of the bifunctionalized MSN materials (ASAP 2000).

(a) 2/8 AEP/UDP-MSN
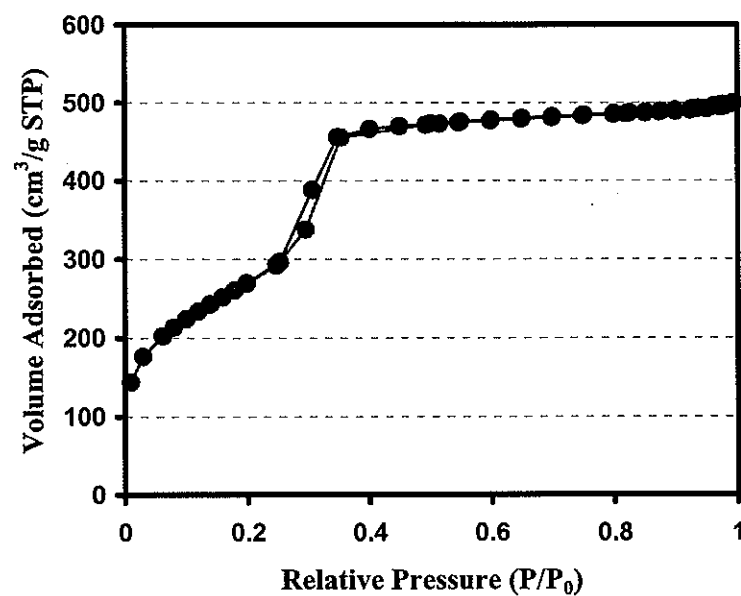
(b) 8/2 AEP/UDP-MSN

CHAPTER 6. GENERAL CONCLUSIONS

My original goal to prepare shape-controlled hybrid mesoporous silica nanoparticles has been successfully achieved. A series of new mesoporous silica materials with MCM-41 type of structure containing a homogeneous layer of organic functional groups inside the pores was prepared using a co-condensation method under low surfactant concentration condition. This reproducible synthetic approach resulted in high surface coverage with several functional groups such as a primary amine, secondary amine, urea, isocyanate, vinyl, and nitrile. In addition, I found that the presence of organoalkoxysilane precursors during the base catalyzed condensation greatly influenced the final particle shape. By simply changing the precursor or its concentration, the particle morphology was fine-tuned in a predictable way to various shapes, including spheres, tubes, and rods of various dimensions. The mechanism of this unprecedented synthetic procedure that gave rise to the specific particle morphologies was investigated. The structure and functionality of these novel materials were fully characterized by the field-emission scanning electron microscopy, transmission scanning microscopy, solid state NMR spectroscopy, thermogravimetric analysis, and nitrogen adsorption and desorption studies.

In addition, I have developed another important synthetic method has been developed for the first time that can control both multifunctionalization and morphology of the mesoporous organic/inorganic hybrid materials. The method involved the introduction of different molar ratios of organoalkoxysilane precursors to a base-catalyzed co-condensation of silicate. Bifunctional mesoporous silica nanosphere (MSN) materials containing various

ratios of two different organic groups were obtained. They exhibited characteristic Cu^{2+}

sorption behaviours depending of the physicochemical nature of the mesopore surface.

I also succeeded in preparing a series of bifunctionalized MSN-based heterogeneous

catalysts for the nitroaldol (Henry) reaction. A common 3-[2-(2-

aminoethylamino)ethylamino]propyl (AEP) primary group and three different secondary

groups, ureidopropyl (UDP), mercaptopropyl (MP), and allyl (AL) functionalities, were

incorporated to these mesoporous silica materials by introducing equal amounts of AEP-

trimethoxysilane with UDP-, MP-, or AL-trialkoxysilane precursors to our co-condensation

reaction. The AEP group served as a catalyst, and the other secondary groups provided

different noncovalent interactions to reactants and thereby controlled the reaction selectivity.

By varying the secondary group in these bifunctionalized MSN catalysts, the selectivity of a

nitroaldol reaction of two competing benzaldehydes reacting with nitromethane was

controlled depending on the surface characteristics. The selectivity of the bifunctionalized

MSN catalysts could be systematically tuned simply by varying the physicochemical nature

of the pore surface-bound secondary groups, i.e., polarity and hydrophobicity unlike the well

known size selection in zeolite catalysis.

Furthermore, I synthesized and characterized a new cooperative catalytic system

comprised of a series of bifunctional MSN materials with various relative concentrations of a

general acid, ureidopropyl (UDP) group, and a base, 3-[2-(2-

aminoethylamino)ethylamino]propyl (AEP) group. Three bifunctional AEP/UDP-MSN

materials with different relative ratios (AEP/UDP = 2/8, 5/5, and 8/2) were employed as

catalysts for aldol, Henry and cyanosilylation reactions. A common electrophile, 4-

nitrobenzaldehyde, and different nucleophiles, acetone, nitromethane and trimethylsilyl cyanide (TMSCN), were used as reactants. The turnover numbers (TONs) of these reactions suggested that the UDP groups cooperatively activate substrates with the AEP groups in catalyzing reactions that involve carbonyl activation. By fine-tuning the relative concentrations and proper spatial arrangements of different cooperative functional groups, we envision that our multifunctionalized MSNs could serve as new selective catalysts for many other important reactions.

I have also involved in other research areas including the preparation of monodisperse MSNs with a variety of organic functional groups and chiral catalysis and chiral separation using predefined arrays of chiral mesopores.

ACKNOWLEDGEMENTS